END

MICROCOPY RESOLUTION TEST CHART
NATIONAL BUREAU OF STANDARDS-1963-A

TAMPERE UNIVERSITY OF TECHNOLOGY

DTIC
ELECTE
NOV 0 5 1986
S D
D

Tampere, September 26, 1986

FINAL REPORT

We have studied the applicability of the Atomic Layer Epitaxy (ALE, see Ref. 1) and Molecular Beam Epitaxy (MBE) to growth of $Hg_xCd_{1-x}Te$ thin-films throughout the composition range $0 \leq x \leq 0.8$. The progress of the Contract has been reported periodically in five interim reports. This final Report summarizes the whole work.

In addition, four CdTe overlayers grown on GaAs substrates by ALE and MBE, together with X-ray diffractographs and Nomarsky micrographs taken for these samples have been mailed under a separate cover to The United States Army Research, Development and Standardization Group, London, England.

The objective of our work has been to study *alternatives* to the conventional MBE growth of HgCdTe. We have applied ALE as one possibility and an ionized Hg technique as another. The results may be summarized as follows.

1) Mercury has a small sticking coefficient (of the order of 10^{-4}) at growth temperatures, T, from 180 to 200 C. It was found that for this reason the mole fraction of Hg always remained below 0.1 in ALE growth, even if the recovery time between the successive pulses was shortened to a minimum (below 1 sec). On the other hand, the MBE method used under closely similar growth conditions at practically same Hg, Cd and Te fluxes (from separate sources) yielded films with high x values. On the grounds of these observations we do not find ALE suitable for growth of HgCdTe.

2) ALE can be used to grow CdTe. However, the ideal ALE model (M. Pessa et al., J. Appl. Phys. 54, 6047 (1983); J. Crystal Growth 67, 255 (1984)) may not be applied. This is due to the fact that the CdTe ALE growth is a complex process which requires a careful optimization of the growth parameters. As discussed in Ref. 2, the Cd-Te bonds are weaker in the outermost atomic layer than those in the bulk and, thus, relatively

unstable at growth temperatures ranging from 260 to 320 C. This instability is related to the absence of the double-layer zincblende structure for the surface layer. Re-evaporation of Te (from a Cd terminated CdTe (111)A surface underneath) continues during the recovery time, before the next Cd pulse arrives, until all loosely bound Te atoms are removed and a persistent submonolayer coverage of about 0.7 monolayer (ML) is left behind. Similarly, the outermost Cd layer (with a complete Te monolayer underneath) continues to desorb during the recovery time until a rather stationary state of the surface with a Cd coverage of roughly 0.3 ML is reached. These processes at the growing front of CdTe make the ALE method remarkably complex. The timing and dose of the sequential pulses influence the structural quality of CdTe; as opposed to the prediction of the ideal ALE model. Apparently, it is more difficult and much slower (by a factor of 3 to 5) to grow CdTe by ALE than by MBE with similar structural qualities from the elemental source materials. Growth from chemical compounds via surface exchange reactions, e.g. chloride epitaxy, has not been tried.

3) Attempts have been made to increase condensation of Hg by ionizing the flux in a "Kaufman-type" one-cm ion source (manufactured by Commonwealth Scientific Corp., Aleksandria, VI, USA). A neutral Hg flux from a reservoir placed outside the growth chamber was allowed to flow through the ion source which was installed close to the substrate in the growth chamber. Although the ion source worked very well for an Ar beam in test measurements it was hard to get any stable Hg flux through the ion source at reasonably high intensity. We would like to emphasize, however, that our experiments have been preliminary. It is conceivable that by modifying the present source configuration one might overcome these problems. Apparently, a greater sticking coefficient would reduce the consumption of Hg from its present level of about 1 kg per 70- μm $Hg_{0.8}Cd_{0.2}Te$ film in our reactor and lower the growth temperature. We intend to continue experiments on ionized Hg in the near future.

4) $Hg_xCd_{1-x}Te$ overlayers with $0 \lesssim x \lesssim 0.8$ have also been prepared by conventional MBE. In most experiments GaAs (100) substrates, oriented 2° towards (110) to cause layer-by-layer growth on terraces, were used. In a few cases CdTe (111)B substrates were also used. The molecular beams were produced either from separate Cd and Te cells or from CdTe and Te cells.

The films have been characterized by using single-crystal X-ray diffractometry, Nomarsky microscopy, Auger and ESCA spectroscopy, Rutherford backscattering and Hall mobility measurements. This characterization has shown that in its present form the reactor cannot grow reproducibly device

quality material with a desired mole fraction and structural perfection sufficient for use in infra-red detector structures (see, e.g., Ref. 3). These are quite typical problems encountered in any MBE growth of HgCdTe. To improve the quality of the films we are planning to modify the growth chamber and build a new Hg (ion) source.

Yours faithfully

Markus Pessa

Accesion For		
NTIS CRA&I	☑	
DTIC TAB	☐	
Unannounced	☐	
Justification		
By		
Distribution /		
Availability Codes		
Dist	Avail and/or Special	
A-1		

3

Atomic layer epitaxy

Colin H. L. Goodman

Standard Telecommunication Laboratories, Harlow, Essex, England

Markus V. Pessa

Department of Physics, Tampere University of Technology, SF-33101 Tampere, Finland

Atomic layer epitaxy (ALE) is not so much a new technique for the preparation of thin films as a novel modification to existing methods of vapor-phase epitaxy, whether physical [e.g., evaporation, at one limit molecular-beam epitaxy (MBE)] or chemical [e.g., chloride epitaxy or metalorganic chemical vapor deposition (MOCVD)]. It is a self-regulatory process which, in its simplest form, produces one complete molecular layer of a compound per operational cycle, with a greater thickness being obtained by repeated cycling. There is no growth *rate* in ALE as in other crystal growth processes. So far ALE has been applied to rather few materials, but, in principle, it could have a quite general application. It has been used to prepare single-crystal overlayers of CdTe, (Cd,Mn)Te, GaAs and AlAs, a number of polycrystalline films and highly efficient electroluminescent thin-film displays based on ZnS:Mn. It could also offer particular advantages for the preparation of ultrathin films of precisely controlled thickness in the nanometer range and thus may have a special value for growing low-dimensional structures.

TABLE OF CONTENTS

I. INTRODUCTION

Thin films are of the greatest technological importance, and range widely in application: the active layers in semiconductor devices as well as the dielectrics in them or in electrolytic capacitors, the transparent conductors in liquid-crystal displays or on aircraft windshields, the luminescent and protective layers in electroluminescent (EL) thin-film displays, etc. More recently ultrathin films of uniform and precisely controlled thickness in the range 1–10 nm have come to be of the greatest importance both scientifically in the branch of solid-state physics termed "low-dimensional," as well as technologically in integrated circuits and optoelectronic devices.

In this general context little attention was initially paid to a patent of Finnish origin taken out in 1977[1] which described a novel mode of evaporation deposition, atomic layer epitaxy (ALE), for preparing thin films of zinc sulfide. This originated from the Lohja Corporation but was probably too unorthodox and seemingly restricted in application to make much impact. By 1980, however, it was being used to make remarkably good large-area thin-film EL displays based on ZnS:Mn (Refs. 2 and 3), and in 1982 still better displays from Lohja won, against strong U.S. and Japan competition, the prize of the Society of Information Display for the greatest advance in the display field during the preceeding year. ALE began to attract considerable attention as a method for *producing thin films of high quality*. More recently still, with the epitaxial film work of Pessa's group at Tampere University of Technology, Finland, on II-VI compounds, and of Nishizawa's group at Tohoku University, Japan, on gallium arsenide, as well as works of Usui *et al.* at Nippon Electric Corporation and Bedair *et al.* at North Carolina State University, on GaAs, the promise of ALE for growing low-dimensional structures has generated much interest.

II. FILM GROWTH BY ATOMIC LAYER EPITAXY

A particularly simple way to describe the ALE approach is to say that it makes use of the difference between chemical absorption and physical adsorption. When the first layer of atoms or molecules of a reactive species reaches a solid surface there is usually a strong interaction (chemisorption); subsequent layers tend to interact much less strongly (physisorption). If the initial substrate surface is heated sufficiently one can achieve a condition such that only the chemisorbed layer remains attached. In the earliest and perhaps simplest example of ALE, viz., the growth of ZnS by evaporation in a vacuum, Zn vapor was allowed to impinge on the heated glass. Evaporation was then stopped and if physisorbed Zn were present because of the impinging flux, it would reevaporate. The process was then repeated with sulfur, the first layer of which would chemisorb on the initial Zn layer; any subsequent physisorbed sulfur would gradually come away from the heated substrate when the
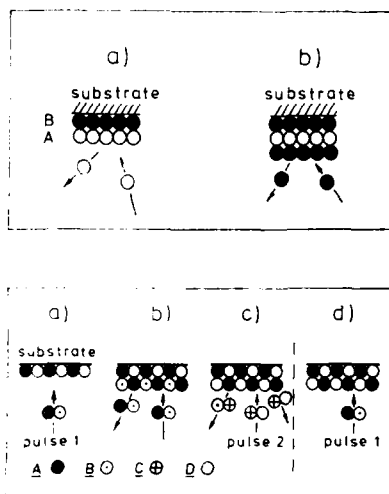
FIG. 1. Film growth by ALE. Upper panel: growth from elemental source materials [variant (i)]. Lower panel: growth from compound source materials via surface exchange reactions [variant (ii)].

Some confusion appears to have been generated because the ALE-grown materials actually used by Lohja in their displays were polycrystalline or amorphous. Also it was not easy from what was published to deduce experimental conditions. It was only later that the first controlled experiments in a laboratory environment[4,5] were carried out at the Tampere University of Technology in 1979–80, and provided confirmation of the general correctness of the ideas developed by Suntola at Lohja. These were followed by further experiments involving deposition onto single-crystal substrates, discussed later in Sec. IV. These experiments showed that the idealized ALE picture, of one complete double layer being grown per cycle, could be an oversimplification. As discussed subsequently, incomplete layer growth occurs in many cases.

To sum up the present situation: the ALE mode of deposition has so far only been applied to a rather small number of materials, listed in detail in Sec. IV. These materials are of considerable scientific and technological interest. It seems highly probable, though yet unproved, that a very much wider range of materials could be handled. One particularly remarkable feature claimed for the ALE approach is that it automatically gives an absolute control of deposit thickness in terms of the number of cycles employed. However, although the general conditions under which ALE would be possible seem reasonable clear, each material will have its own specific requirements regarding the operational conditions under which deposits of high perfection and purity could be obtained—while in some cases ALE might turn out not to be applicable.

sulfur flux was cut off, leaving one (double) layer of ZnS. This complete cycle could be repeated indefinitely, the number of layers grown being determined solely by the number of cycles [see Fig. 1(a)]. This cyclic vacuum evaporation was described in the original Lohja patent.[1]

It has been shown by straightforward measurements[4] that chemical vapor deposition (CVD) of ZnS from $ZnCl_2$ and H_2S could also be operated in an ALE mode, the cycle being somewhat more complex [Fig. 1(b)] in that a chemisorbed $ZnCl_2$ monolayer loses its chlorine to the hydrogen of the later-arriving H_2S molecules, forming HCl, and again resulting in a (double) layer of ZnS. The importance of this CVD variant is that it enables ALE to be applied to compounds with one or more involatile constituents for which the evaporative approach would clearly not be viable.

One can thus arrive at a definition of ALE: it is based on chemical reactions at the solid surface of a substrate, to which the reactants are transported alternately as pulses of neutral molecules or atoms, either as chopped beams in high vacuum, or as switched streams of vapor possibly on an inert carrier gas. The incident pulse reacts directly and chemically only with the outermost atomic layer of the substrate. The film therefore grows stepwise—a single monolayer per pulse—provided that at least one complete monolayer coverage of a constituent element, or of a chemical compound containing it, is formed before the next pulse is allowed to react with the surface. Given that, any excess incident molecules or atoms impinging on the film do not stick if the substrate temperature T_{gr} is properly chosen, and one therefore obtains precisely a monolayer coverage in each cycle.

The formation of a "layer per cycle" is the specific feature that conceptually distinguishes the ALE mode from other modes of vapor phase deposition; the latter all give a growth rate, ALE gives a growth per cycle.

III. THEORETICAL ASPECTS

A. Growth models

As already indicated ALE in its basic form operates by growing complete atomic layers on top of each other, there being two basic variants based on (i) evaporative deposition [with as one extreme, molecular-beam epitaxy (MBE)], relying on heated elemental source materials, or (ii) chemical vapor deposition (CVD), relying on sequential surface exchange reactions between compound reactants.

ALE, therefore, is not so much an entirely new method of crystal growth as a special mode of these well-established growth techniques.

Both ALE variants, illustrated in Fig. 1, assume that at the substrate temperature the vapor pressures of the source materials as solid phases are much larger, perhaps by several orders of magnitude, than those of the compound films eventually formed from them. This requirement is usually met in the case of II-VI materials and can hold reasonably well in many other cases.

The precaution must be taken to turn off the source beam for a sufficiently long time (of the order of 1 s) after each deposition pulse. In this way the surface is allowed to approach thermodynamic equilibrium at the end of each reaction step—a growth condition that is not usually met in other techniques of deposition by evaporation. It is then clear that the fluid dynamics are entirely eliminated from the growth problem. We should also note that a low net growth

rate, a characteristic of ALE, can be partly compensated by designing reactors properly to allow for depositing several large-area samples simultaneously (such a reactor is illustrated in Fig. 4; see Sec. IV).

In ALE variant (i), element A and element B are alternately deposited onto the substrate at temperature T_{gr}. The number of monolayers produced by one pulse can be calculated from

$$\theta = (I_i - I_e)t_i/\theta_i.$$

Here θ_i is the atomic density for one monolayer coverage ($\theta = 1$), I_i the number of atoms per second impinging on the substrate of unit area, I_e the number of atoms per second reevaporated from the substrate during deposition, and t_i the duration of the pulse. As θ reaches unity the sticking coefficient abruptly changes from unity to zero; i.e., I_e becomes equal to I_i. Only a monolayer of element A held by strong B–A bonds is left behind after reevaporation of those atoms (or molecules) that are present in excess. Next, the surface is subjected to a pulse of B. Once all possible A-B bonds have formed, no further B will stick. The process is repeated with alternate pulses of A and B until the desired film thickness is achieved, one monolayer at a time.

Such behavior can be termed the ideal ALE mode.[6] Experiments, however, indicate that this model is oversimplified because it does not take into account the fact that perfect layer-by-layer growth does not always take place, even if an optimum value of T_{gr} is chosen. A detailed study of growth of CdTe epilayers on CdTe (111) substrates has shown[7] that the sticking coefficients of Cd and Te are less than unity at T_{gr}. The persistent coverages left behind after reevaporation are measured to be only 35% of a monolayer for Cd on CdTe (111)B and 72% for Te on CdTe(111)A. Such coverages have structural implications—see the discussion in Sec. III B.

A generalized model has been suggested[7] for growth of an AB compound by ALE variant (i) which involves (a) the existence of weakly bound states of both reactants in the vicinity of the interface and (b) partial reevaporation of the first elemental monolayer deposited. According to this model, the timing and dose of the sequential pulses of elemental A and B should be carefully related to each other. This, of course, represents a considerable departure from the ideal ALE model but does retain the basic growth per cycle that is *the* distinctive feature of ALE.

In the case of ALE variant (ii), sequential surface exchange reactions are used to grow a film of a compound AD [see Fig. 1(b)]. During the first phase of a deposition cycle incident molecules AB are adsorbed by the surface layer. AB remains on the surface until a pulse of CD molecules arrives. At a properly chosen T_{gr} the surface reaction AB + CD →BC + AD then occurs. This releases B and C (usually as a compound BC) and results in the formation of a layer of AD. As with ALE variant (i), the growth proceeds stepwise, and is independent of the size of a reactant pulse, provided that it exceeds the minimum amount of material required to form the appropriate adsorbed monolayer. It nonetheless appears probable that, as noted for variant (i), the timing

and dose of sequential pulses would need to be related to each other.

Comprehensive theoretical quantum chemical studies of the growth of a ZnS surface by ALE variant (ii) using the first of these reactions have been carried out by Pakkanen *et al.*[8] These studies showed that the growth process, which involves several reaction steps, again is not so simple as the ideal ALE reaction scheme shown in Fig. 1b. The calculations were based on *ab initio* Hartree–Fock theory for atoms and molecules. They showed that the formation of a complete ZnS overlayer does not occur in a single ALE cycle.

The calculations suggest that two different growth mechanisms could occur involving ALE-type cyclic reaction with molecules of $ZnCl_2$ and H_2S. These mechanisms might operate simultaneously at different sites of the real ZnS surface. In the first of these mechanisms surface chains are formed, the first step in this chain process being the chemisorption of $ZnCl_2$ which produces a chlorine-bridged $ZnCl_2$ overlayer with a maximum surface coverage of 0.5. Subsequent H_2S adsorbates react with the $ZnCl_2$ chains releasing HCl and creating ZnS chains with the S atoms at the top. $ZnCl_2$ molecules of the next pulse bind to the S atoms and again form a chlorine-bridged $ZnCl_2$ overlayer with a surface coverage of 0.5. The second H_2S pulse completes the new ZnS layer. This complete layer is identical to the bulk structure. On this basis, the maximum growth rate is one new layer per two cycles of $ZnCl_2 + H_2S$. In the second mechanism, an alternative, somewhat similar set of reactions was proposed for the formation of $ZnCl_2$-ring overlayers. The initial surface coverage would now be 0.33 and the maximum growth rate would therefore become one ZnS layer per three cycles of $ZnCl_2 + H_2S$.

Deviations from the simple model of ALE growth discussed so far have all indicated a reduction of the thickness grown per cycle. However, some recently published work[9,10] on GaAs grown by ALE variant (ii), and discussed in Section IV A 3, indicates that growth can proceed in a complete layer-by-layer fashion; in some circumstances there can even be an increase of the thickness per cycle.[11]

B. Kinetic effects

Several factors must be satisfied for ALE growth to be possible. ALE implies the need for (a) a flat perfect substrate surface and (b) equally strong adsorption of the two vapor species taking part in the cycle, and equally easy desorption of any reaction products in the case of ALE variant (ii). It does not as yet appear possible to calculate *accurately* to what extent these requirements will be met by a specific material, simply because not enough is known about the effects due to surface adsorption of impurities (including adsorption of excess of constituent elements). There are, however, some useful guidelines.

The flatness/perfection of a low-energy (close-packed) surface of a crystalline material depends on the energy required to form defects in it. Some insights into this can be obtained from Jackson's model[12] which demonstrates a close relationship between surface roughness during growth and entropy for transformation (i.e., volatilization in the case of vapor growth, fusion for growth from the liquid). A
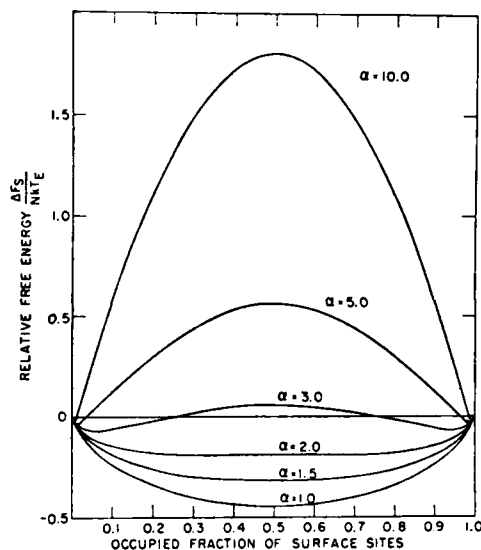
FIG. 2. Free energy of an interface vs occupied fraction of surface sites.[12]

variation of Jackson's factor α, proportional to this entropy of transformation, gives rise to marked changes in the free-energy gain or penalty that arises from surface roughness. This is shown in Fig. 2 which plots as a function of α the contribution to free energy due to surface site occupancy, that is the fraction of empty surface sites in a nearly completed layer, or of occupied sites in a layer beginning to grow (which together constitute a simple index of surface roughness). For values of α less than about 1.5 there is a minimum in this contribution at an occupancy of 0.5; in such cases the surface is always rough, giving ready nucleation and indicating that ALE would not be possible. As α increases above a value of about 2 the minimum free-energy condition rapidly moves towards a situation of extremely small occupancy or vacancy (Fig. 2). As a consequence, an increasingly smooth and perfect surface results. Since vapor–solid entropy changes are usually large this approach suggests that most vapor-grown materials should facet.

Although Jackson's model only refers to the incorporation of a single species at a growing surface, and does not appear to have been extended to more complex situations, some of its features should still be relevant. For example, the observation of marked facetting during growth is direct evidence for smooth surfaces that do not give easy nucleation; that, in turn, implies that a facetting orientation will be a requirement for the occurrence of layer-by-layer growth by ALE.

Hartmann's concept of the periodic bond chain[13] can explain many of the observed details of facetting in terms of the arrangement of chemical bonds within the material and how these intersect the surface. This idealized approach refers to a clean surface at equilibrium; the complexity of real surfaces during growth is likely to involve significant depar-

tures from that. For example, in the case of GaAs, which can give what to the eye are mirror facets on (100), Däweritz[14] has found reason for suggesting that under near-equilibrium conditions a clean but As-rich (100) surface forms minifacets bounded by a variety of planes, mainly [111]. This reduces the number of dangling bonds. It also gives a surface roughness several atomic layers in height. It is interesting to note that Theeten et al.[15] deduced from a simple (PBC) approach assuming atomically flat surfaces that [100] should be relatively fast growing surfaces and therefore probably nonfacetting. They also predicted that [111] surfaces of GaAs should be very slow growing, i.e., facetting, because of the difficulty of nucleation, and [110] and [113] relatively slow growing.

Experimentally the vapor growth of GaAs by the chloride technique[15] is found to be yet more complicated than would be predicted on the PBC approach modified to take into account some surface reconstruction. This is dramatically illustrated[16] in Fig. 3. Here the slowest growing orientations would be expected to be favorable for ALE. Part of the complication of this growth plot arises from the polar nature of GaAs, in which ($\bar{1}11$) and ($1\bar{1}\bar{1}$) orientations are not equivalent. In addition it has been suggested[15] that the adsorption of molecules from the gas phase (e.g., complexes containing chlorine) would be expected to mouify the conclusions of a straightforward PBC approach. Such an argument, while relevant to ALE variant (ii), might not be expected to hold for variant (i). However, even with variant (i) excess of a constituent can be adsorbed on the growing surface, and so modify behavior, and, via the minifacetting mentioned previously, affect surface coverage and surface roughness. The occurrence of some kind of minifacetting may explain the abnormally small thickness increment per cycle found earlier under certain ALE growth conditions. Whether or not one can suitably modify the PBC approach into an accurate predictive tool, there is strong evidence that the kind of orientation dependent growth rate curve of Fig. 3
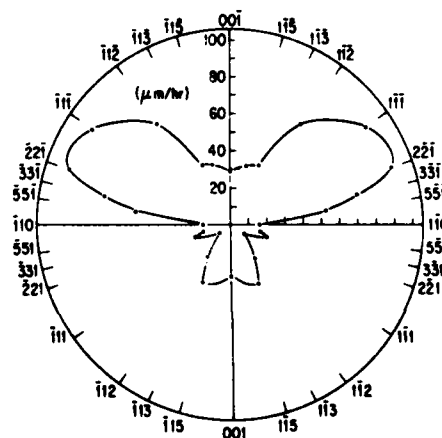

FIG. 3. Polar diagram of GaAs deposition rate vs crystallographic orientation.[16]

directly reflects the surface kinetics that govern the adsorption and incorporation of Ga and As into the growing crystal.

Considerable effort has been expended in trying to understand the detailed adsorption kinetics for GaAs surfaces, see, e.g., Refs. 16–19. However, although qualitative agreement with experiment has been obtained, as for example in Ref. 18, which deals with the effects of adsorption on the vapor growth of GaAs, it should be noted that even for such a well-characterized material as GaAs various assumptions had to be made, while some of the relevant parameters had to be plausibly estimated. It thus seems unlikely that it will be possible in the near future to predict the orientation-dependent behavior of the vapor growth of any less well-understood material. At least for the present time, therefore, whether or not a particular material might be grown by ALE must be judged semiempirically.

IV. GROWTH BY ATOMIC LAYER EPITAXY—EXPERIMENT

The cycle of alternate pulses in ALE may be repeated every 1–3 s, which yields a net growth rate of about 0.3–0.6 μm/h. Considerably longer cycle times, and hence slower growth rate, can also be used, but any significant reduction in cycle time below 1 s is unlikely, due to limited pump capacity. As already mentioned in Sec. III, the small net deposition rate may be compensated by simultaneously growing many films. An ALE reactor capable of handling a batch of substrates is illustrated in Fig. 4. Here the separation of reaction steps is accomplished by a gas flow over immobile substrates. The reactants are alternately injected into the growth chamber, and, following each reaction, are purged away by a carrier gas flow.

A. Monocrystalline deposits

The first detailed investigation of atomic layer epitaxy on single-crystal substrates was carried out at the Tampere University of Technology.[20] This employed an ultrahigh vacuum apparatus of the kind used for MBE. In order to maintain the vacuum of 10^{-7} Pa during growth limited pump capacity made it necessary to use a relatively long cycle time. The final result was a net growth rate of 0.1–0.3 μm/h. Later work[6,7,21,22] employed a new and improved MBE/ALE system, illustrated schematically in Fig. 5, and enabled faster growth to be achieved. The growth chamber incorporates three Knudsen-type effusion furnaces manufactured by Kryovak Ltd. for operation in the ALE mode (i) (and in the usual MBE mode) and two gas inlets for applying ALE variant (ii). This is built onto a VG ADES-400 electron spectrometer capable of x-ray photoelectron
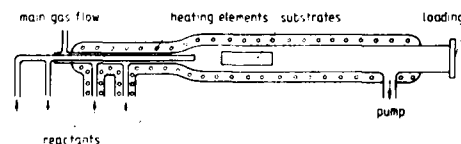
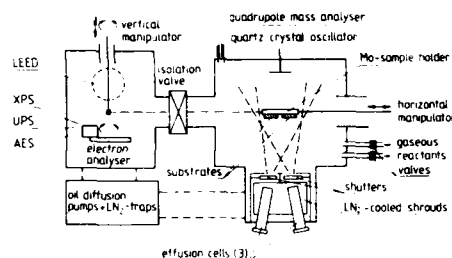FIG. 4. Schematic diagram of a gas-flow-type ALE reactor.

FIG. 5. Layout of an ultrahigh vacuum reactor chamber capable of ALE and MBE growth by evaporation from Knudsen-type effusion cells or by surface exchange reactions of gases from vapor sources, built on a multitechnique electron spectrometer for in situ characterization of films.

(XPS), Auger electron (AES), angle-resolved UV photoemission (UPS), and low-energy electron diffraction (LEED) measurements.

1. Cadmium telluride

The first material to be investigated was CdTe.[20] ALE variant (i) was used because of the rather high vapor pressures of elemental Cd and Te at elevated temperatures where the dissociative evaporation of CdTe itself would be negligibly small.[23] We note parenthetically that it might also prove possible to use ALE variant (ii), for example, with dimethyl cadmium and diethyl telluride as reactants, because these compounds have been used to grow CdTe epilayers by metal organic CVD.[24] CdTe was also chosen for investigation because of its potential importance in the areas of optoelectronics, integrated optics, and solar energy conversion. It is already used as a substrate material for Cd_1 $_x Hg_x$ Te solid solutions and as a constituent of CdTe-HgTe superlattices, which make excellent infrared detectors for the 8–14 μm atmospheric window.[25,26]

It should be noted in passing that CdTe single-crystal substrates of high structural perfection are difficult to obtain. Other substrates, such as GaAs (100), lattice-matching InSb (100),[27,28] and (111),[27] sapphire (0001),[29] and Si (111),[30] all of which have been employed in the MBE growth of CdTe, offer viable alternatives to CdTe substrates for growth of CdTe epilayers.

ALE experiments with nonpolar (110) CdTe substrates,[20] polar (111) A and (111)B substrates,[7,21,22] as well as GaAs (100)[31] have been carried out. In order to determine an appropriate growth temperature, an amorphous Te overlayer about 1 nm thick was deposited onto the substrate at room temperature.[20] The substrate was then gradually heated to 800 K while observing the Te $M_{4,5}N_{4,5}N_{4,5}$ Auger signal at 485 eV. The intensity of this signal decreased with increasing temperature up to 540 K (see Fig. 6), above which it leveled off. This change was due to the desorption of loosely bound Te atoms in the deposit, and the constant signal in the range 550–750 K corresponded to the stable surface. Similar results were obtained for Cd. These and other similar experiments indicated that at 540 K thick amorphous deposits reevaporated at the rate of roughly 300 nm/s
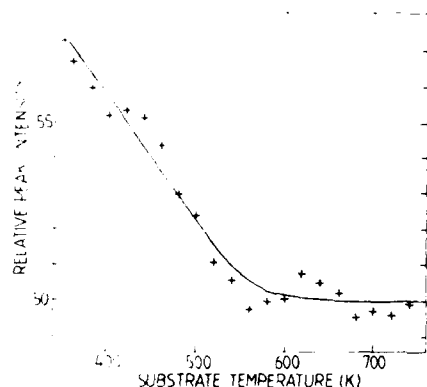
FIG. 5 Peak-to-peak height of the 485-eV Auger signal of Te for a Te deposit on a CdTe (110) substrate as a function of substrate temperature. Loosely bound Te atoms desorb at high temperature. Fluctuations in the AES peak intensities are mainly due to quick recording of the signals at short intervals while heating the sample.

for Te and $27\,\mu$m/s for Cd, confirming that ALE variant (i) was indeed operative.

With the substrate at 540 K, Cd and Te were alternately deposited as molecular beam pulses of Cd and Te_2. The deposition rate was varied from 0.01 to 0.08 nm/s, as monitored by a quartz crystal oscillator. In order to obtain a rough estimate of actual growth per cycle, films were deposited onto small pieces of molybdenum at 540 K. The Auger signals from Cd, Te, and Mo were recorded as a function of the number of ALE cycles. After 10 cycles it was found that the Mo MNN Auger line could no longer be detected. From this it was deduced that a film of thickness between 2 and 2.5 nm must have grown, in good agreement with the expected growth per cycle of 0.229 nm, the (110) interplanar spacing.

LEED patterns of the (110) face of the grown films showed a simple (1×1) surface unit cell. (This does not preclude reconstruction; see Ref. 32). From LEED patterns and AES and XPS spectra clean and stoichiometric single-crystal films could be obtained for T_{gr} of 480 K and above. At lower temperatures, e.g., 390 K, diffuse LEED spots suggested poor crystal structure and, usually, deviations from stoichiometry. This result was expected because the vapor pressures of elemental Cd and Te are about 10^{-4} and 10^{-8} Pa, respectively, so that some trapping of excess Te may have occurred.

It is thought that the ideal ALE model cannot fully account for LEED observations which indicate that a growing film may possess better crystal structure than the CdTe substrate.[5,21] It was partly as a consequence of these findings that an intermediate surface adsorbed layer was suggested to be present during deposition. Based on experimental studies[7] of isothermal reevaporation rates of elemental Cd and Te deposits, it was estimated that reevaporation rates of Cd and Te of this near-interface region were less than one tenth those for thick amorphous deposits of these elements. This conclusion led to a revised schematic model for the ALE process, sketched in Fig. 7. Here, the weakly bound layers
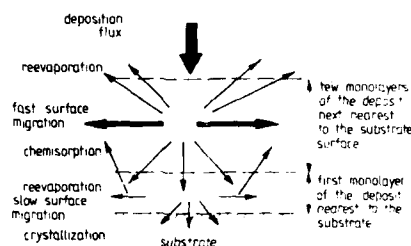

FIG. 7. Schematic illustration of the key conceptual steps associated with growth of CdTe overlayers.

just above the substrate would allow ready migration and mixing of atoms and molecules. The activation energies for reevaporation of this near-interface region were measured to be 1.5 eV for Te on CdTe (111)A and 0.5 eV for Cd on CdTe (111)B. Because the activation energies for surface diffusion are only about one-third of the bond energies,[15] i.e., 0.5 and 0.17 eV for Te and Cd, respectively, migration of the adsorbed atoms and molecules should, indeed, take place effectively in the near-interface region.

In order to study the interrelation of timing and dose of the pulses, growth experiments on CdTe were performed by varying the beam fluxes, lengths of duration of the pulses and time windows while maintaining $T_{gr} = 553$ K constant.[7] After each growth, the surface morphology was studied by a scanning electron microscope. The smoothest surface was obtained when the growth parameters were "optimized." As an example of this optimization at a relatively low net growth rate the following set of parameters may be chosen:

(a) growth rate of 0.12 nm/s of the Cd and Te deposits,
(b) length of duration of pulses from 2.5 to 2.8 s;
(c) delay times (windows) 0.5 s for the Te_2 pulse incident on CdTe (111)A and 1.0 s for the Cd pulse incident on (111) B.

In an experiment, these parameters yielded growth of a monomolecular layer of 0.37 nm per cycle in 7 s, corresponding to a net deposition rate of 190–200 nm/h.

Angle-resolved UPS, which is very sensitive to surface crystal structure and contamination, gave further information.[20] The emission peaks were sharper and of higher intensity for ALE-grown films than for the original substrate, suggesting improved quality and, probably, a smoother surface. In addition, the films grown under optimal conditions showed features that are not observed with bulk CdTe(110) unless it is cleaved in vacuum. These features of the electronic band structure were interpreted as due to the presence of occupied surface states caused by surface reconstruction.[32] They could not be seen in films grown at temperatures giving diffuse LEED spots, nor for those exposed to air, so that they were definitely associated with a rather perfect surface.

CdTe overlayers on CdTe (111)B are often better in crystal structure than those on CdTe (111)A, or on CdTe (110), as deduced from LEED. It is also noted that the sharpness of LEED patterns improves as films grew thicker,
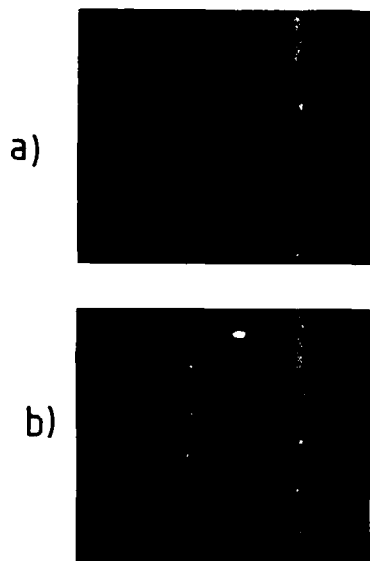
FIG. 8. LEED patterns (a) for a CdTe (111) B substrate (cleaned by Ar ion sputtering then annealing at 470 K) and (b) for a 37-nm CdTe (111)A film grown on this substrate by ALE at 540 K.
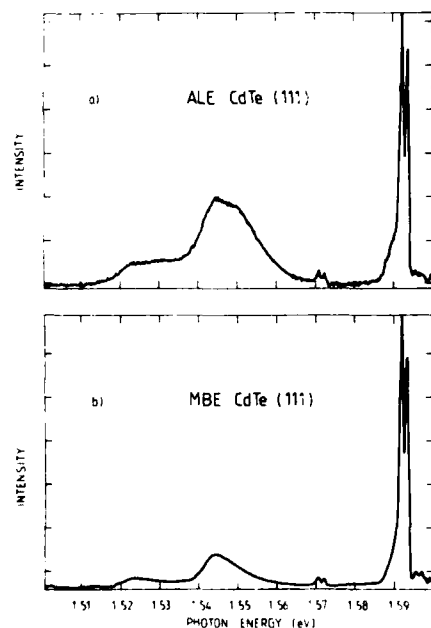
FIG 9 Photoluminescence spectra taken at 2 K from (a) an ALE-grown CdTe/CdTe (111) sample and (b) an MBE-grown CdTe/CdTe (111) sample These films were prepared under closely similar conditions in a CdHgTe MBE reactor at Tampere University of Technology.

at least up to 50 nm. An example of this behavior is given in Fig. 8 for growth on (111)B. However, LEED only samples local order and, therefore, small coherent areas 20–30 nm across may produce reasonably good LEED patterns. LEED is also rather insensitive to nonperiodic surface defects and dislocations. Unfortunately, high-energy electron diffraction measurements (RHEED), capable of probing large areas, have not yet been reported in the literature for ALE-grown films.

Low-temperature photoluminescence (PL) from a few ALE-grown CdTe (111)B overlayers has been measured.[14] Figure 9 shows a 2 K PL spectrum from a 1-μm CdTe film grown at $T_{gr} = 550$ K in a CdHgTe MBE reactor (at Tampere University of Technology, the reactor is not described here). There are two narrow lines just above 1.59 eV, which dominate this spectrum. They are most likely associated with radiative recombination of excitons bound to shallow acceptors (p type).[14] Their strength and sharpness provide evidence that the film is of high electrical quality. We are not able to make a definitive assignment to the broad feature ranging from 1.54 to 1.56 eV, nor to the weak doublet centered at 1.57 eV. However, a possibility arises that the broad feature is due to band-edge emission.[34] For comparison, a PL spectrum from MBE-grown CdTe prepared under closely similar conditions is also shown in Fig. 9. The two spectra are very similar. Perhaps the only difference observed is the intensity of the broad feature which is about three times greater for the ALE-grown film.

In the recent literature much attention has been paid to growth of CdTe on foreign substrates. The major limitations of employing CdTe crystals are due to the high costs and unsatisfactory grain-boundary structures. GaAs is an attractive alternative because large-area wafers of high structural perfection [dislocation densities $\approx (1-5) \times 10^4$ cm^{-2}] are readily available at a modest cost. Despite the fact that CdTe has a large lattice mismatch of 14.6% with GaAs it grows perfectly epitaxially in the (100) (Refs. 35–38) and (111) (Refs. 37, 39–41) directions on GaAs (100). The growth mechanism of CdTe on this substrate has been studied in detail by Otsuka et al.[37] and Datta et al.[42] When CdTe (100) is on GaAs (100), the (7×7) CdTe superlattice cell is almost exactly commensurate with the (8×8) GaAs cell with the two crystals being separated by a thin interfacial oxide layer. If no such oxide layer exists the growth is likely to occur in the (111) direction.[37] Massive dislocations of complex line nesting structure with line densities of 10^{11} cm^{-2} are formed in the CdTe/GaAs interface,[16] due to the lattice mismatch. However, the dislocation line density reduces gradually as the film grows thicker. In the near-surface region (≈ 100 nm) of the overlayer of thickness of a few micrometers the dislocation line density is of the same order of magnitude as in GaAs wafers.

We have grown CdTe overlayers[31] of thicknesses from 2 to 4 μm on n-type GaAs (100) substrates [oriented 2° towards (110)[1]. Since the growth time required for these films would have been discouragingly long by ALE alone a layer of 1–3 μm was first deposited by MBE at the rate of 0.5–1 μm/h, after which the growth was continued by ALE at a net rate of 0.2 μm/h. Figure 10 compares LEED pat-

a)

b)
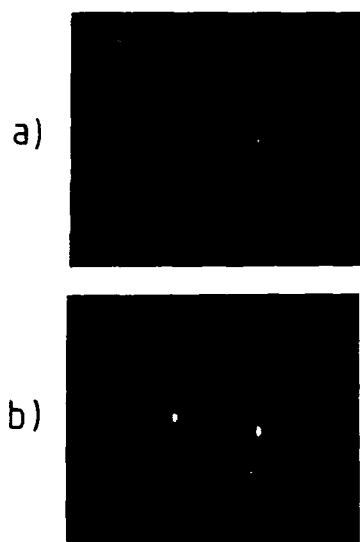
FIG. 10. LEED patterns (a) for a GaAs (100) substrate after heating at 850 K (no Ar⁺ ion bombardment) and (b) for a 3.3-μm CdTe (100) film grown on this substrate at T_{gr} = 570 K Primary beam energy = 45 eV.

terns for a GaAs (100) substrate and a 3.3-μm CdTe overlayer. In this example growth has occurred in the (100) direction, as indicated by LEED and by a x-ray diffraction curve shown in Fig. 11. Furthermore, a scanning electron micrograph (SEM) of the film of Fig. 10 (see Fig. 11) shows that the surface is smooth under medium magnification and comparable to that obtained usually by MBE. A multipoint AES analysis indicates that the film is uniform and stoichiometric all over the film area (of about 0.5 cm²), being reproducible to within a few parts per thousand.

2. Cadmium manganese telluride, Cd₁₋ₓMnₓTe

This solid solution is a diluted magnetic semiconductor, also known as a semimagnetic semiconductor, whose sublattice is partly made up of the substitutional magnetic ions. Its ternary nature permits one to vary the energy gap, the effective mass, the lattice constant, and other physical parameters by alloying Mn.[43-45] It has interesting magnetic, optical, and magneto-optical properties,[46] for example, a giant Zeeman splitting[47] with exotic consequences.[48]

Manganese is an incongruently evaporating element having a low vapor pressure of 1.8×10^{-15} Pa, compared to 1.3 Pa for Cd and 8.3×10^{-2} Pa for Te, at T_{gr} = 540 K. One might therefore expect it to be impossible to make use of ALE variant (i). This problem has been circumvented by

a)

b)

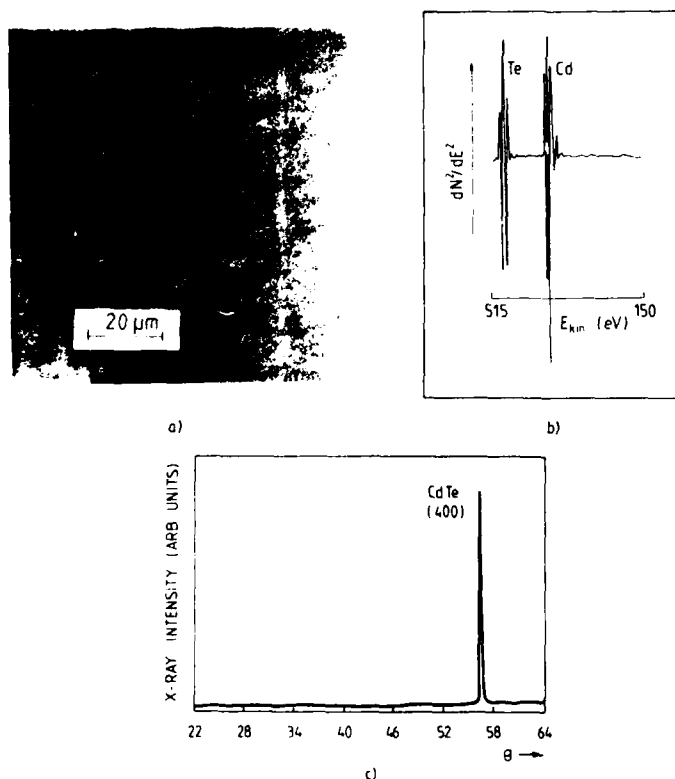FIG. 11. (a) Scanning electron micrograph, (b) AES spectrum, and (c) x-ray diffraction for a 3.3-μm CdTe (100) overlayer on GaAs (100) of Fig. 10
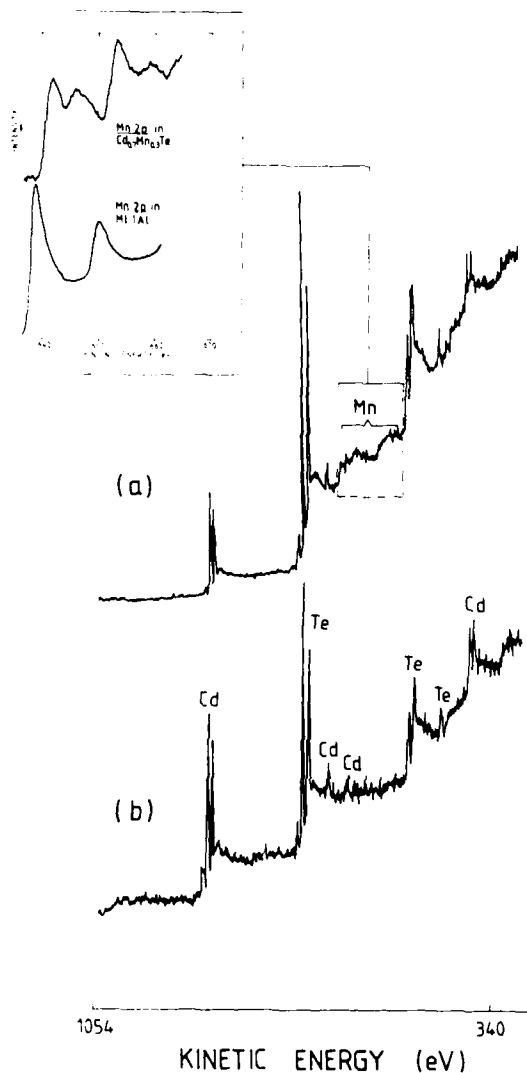

c)

FIG. 12. X-ray photoelectron spectra (a) for a $Cd_{0.7}Mn_{0.3}Te$ (111) overlayer and (b) for a CdTe (111) overlayer. The inset shows precision measurements for the Mn 2p core level emission from $Cd_{0.7}Mn_{0.3}Te$ and from a metallic Mn overlayer grown on this compound.

KINETIC ENERGY (eV)

careful control of the amount of Mn during deposition. Two different methods were used[22]:

(a) The pulsed beams of Cd and Mn were generated simultaneously by opening and closing the effusion cell shutters at the same time, with the relative Cd and Mn beam intensities set at a fixed value (e.g., 10:1);

(b) The beam intensities of Cd and Mn were equalized but the duration of the Cd pulse was made much longer than that of the Mn pulse (e.g., by a factor of 10).

It is then clear that the mole fraction x is determined by the intensity and the length of duration of the Mn pulse. An interesting feature in this stepwise growth is that when the Mn pulse is adjusted to produce a coverage less than one full atomic layer, a fixed value of $x < 1$ is always obtained per cycle; excessively arriving Cd and Te_2 or variations in these fluxes (within certain limits) do not alter x. On the contrary, MBE-type evaporation results in continuous layer growth x being determined by the *relative* concentration of Mn, Cd, and Te_2 in the vapor phase near the sample surface; any variation in the beam fluxes is reflected in x. We should note, however, that this particular ALE variant cannot be used to grow any larger film than that obtained by MBE because the opening of the cones of molecular beams is limited by geometric factors similarly to ALE and MBE.

$Cd_{1-x}Mn_xTe$ films with x ranging from 0 to 0.9 have been successfully grown by ALE on CdTe (111)B substrates

at $T_{gr} = 540$ K.[22] The pulse length was varied in different experiments from 10 to 20 s for Cd and Te_2 and from 2 to 20 s for Mn. The beam intensities were chosen to correspond to the deposition rates of 0.05–0.10 nm/s for Cd and Te_2 and 0.01 -0.04 nm/s for Mn. In all cases less than a monolayer of Mn was deposited in each cycle.

The $Cd_{1-x}Mn_x$Te films were found to retain essentially their zinc-blende structure up to at least $x = 0.9$, in sharp contrast to bulklike crystals. We would like to note in this context that even pure MnTe overlayers of a zinc-blende form, when grown on appropriate substrates, are conceivable. Furdyna[49] suggested that there exist well lattice-matched substrates, such as $Cd_{0.65}Zn_{0.35}$Te and $InSb_{0.77}P_{0.23}$ on which MnTe of the zinc-blende structure might be anchored.

Little work has been done so far on spatial distribution of magnetic ions of semimagnetic semiconductor films. One way of studying this question is to measure x-ray photoelectron spectra of the films. Figure 12 shows $MgK\alpha$-XPS of pure CdTe (111) and $Cd_{0.7}Mn_{0.3}$Te(111) grown on CdTe (111)B. It can be seen that upon alloying Mn a large reduction in relative intensity of the Cd $3e_{3/2, 5/2}$ doublet occurs and the Mn $2p_{1/2, 3/2}$ lines appear. High-precision measurements shown in the inset of Fig. 12, where XPS spectra of the $Cd_{0.7}Mn_{0.3}$Te overlayer and a 2-nm metallic Mn overlayer deposited onto the $Cd_{0.7}Mn_{0.3}$Te are compared with each other, provide closer insight into substitutional disorder of the sublattice. The chemical shift of 2.6 eV of the leading Mn $2p_{5/2}$ peak, the line broadening, the presence of a satellite structure, and the absence of a metallic Mn signal in the compound spectrum provide evidence that manganese is indeed a constituent of random $Cd_{0.7}Mn_{0.3}$Te with no significant metallic clusters.

A LEED pattern for an ALE-grown $Cd_{0.82}Mn_{0.18}$Te (111) epilayer of 30-nm thickness on CdTe (111) is shown in Fig. 13. The surface is well ordered, exhibiting sharp (1×1) LEED spots with low background intensity.

Figure 14 shows a schematic real-space energy band diagram of an ALE-grown unintentionally doped CdTe–$Cd_{0.6}Mn_{0.4}$Te (111) multiquantum-well heterostructure. Electronic valence-band features of these two component layers were studied by measuring angle-resolved UV photoemission. Apart from differences in details of emission from the valence bands no measurable valence-band offset was observed on alloying Mn (for determining band off-sets by electron spectroscopy, see e.g., Ref. 50). Thus the difference
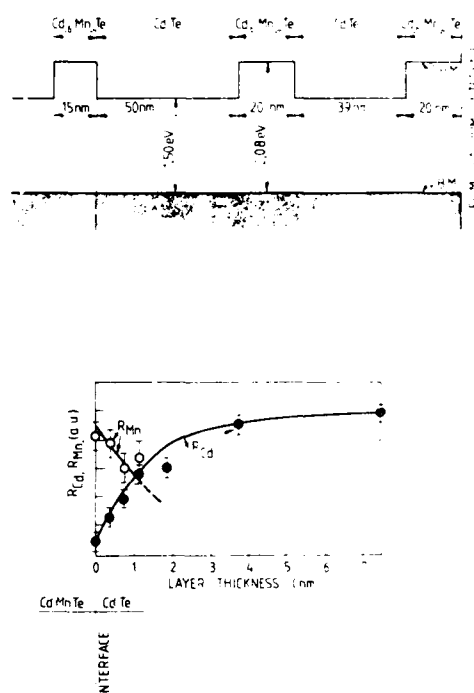

FIG. 14. Schematic real-space energy band diagram of a $Cd_{1-x}Mn_x$Te CdTe multiquantum-well heterostructure grown by ALE (upper panel). The valence-band maximum (VBM) remains unaffected on alloying Mn to within an experimental accuracy of 50 meV investigated by angle-resolved photoemission; the difference in band gaps influences the conduction-band minimum (CBM) alone. The lower panel shows a study of the interface at the position indicated by the vertical line. This study was based on measurements of the peak-to-peak intensity ratios of Cd MNN, Mn LMM, and Te MNN Auger transitions; $r_{Cd} = I_{Cd}/I_{Te}$, and $R_{Mn} = I_{Mn}/I_{Te}$. The solid curves are calculated assuming that the interface is sharp and growth occurs in a layer-by-layer fashion, one molecular layer per cycle.

in the band gap E_g at the interface affects only the conduction-band minimum, as illustrated in Fig. 14.

The CdTe/$Cd_{0.6}Mn_{0.4}$Te (111) interface was studied in a nondestructive way by combining the ALE and AES techniques. Very thin overlayers of CdTe were deposited onto $Cd_{0.6}Mn_{0.4}$Te, and Mn LMM, Cd MNN, and Te MNN AES signals were measured at room as a function of overlayer thickness. The results are shown and compared with theoretical estimates for relative signal intensities in Fig. 14. The solid curves represent the calculated behavior of Cd MNN and Mn LMM peak-to-peak intensities relative to Te MNN peak-to-peak intensity, $R_{Cd} = I_{Cd}/I_{Te}$, and $R_{Mn} = I_{Mn}/I_{Te}$, respectively, on the assumption that the junction is sharp. In other words, no interdiffusion of Mn or other grading effects are assumed to occur in the interface region. Furthermore, the well-known law of exponential decay of low-energy electron signals in solids was applied. The inelastic mean free paths of Cd MNN and Mn LMM electrons were taken to be 1.4 and 1.9 nm, respectively. Judging from the measured and calculated behavior of the intensity

FIG. 13. LEED pattern of a 30-nm $Cd_{0.82}Mn_{0.18}$Te (111) film deposited onto a 37-nm (111) buffer layer on CdTe.

ratios one may conclude that the interface is extremely sharp, possibly of an order of atomic diameter. For comparison, by the standard AES–ion milling technique[51] the interface region of MBE-grown $CdTe/Cd_{1-x}Mn_xTe$ heterojunctions with x ranging from 0.20 to 0.53 has been found to be as large as 10 nm. Such a graded junction is an artifact which arises from an intermixing and cratering of the junction region during ion bombardment.

3. Gallium arsenide, GaAs

Nishizawa et al.[9,11] have described the growth of GaAs using ALE variant (ii). Trimethyl gallium (TMG) and AsH_3 were cycled alternately over a single-crystal substrate, using the reaction

$$Ga(CH_3)_3 + AsH_3 \rightarrow GaAs + 3CH_4.$$

The apparatus used is shown in Fig. 15. Arsine was admitted at a pressure of $10^{-4}-10^{-5}$ Pa for times of 2-200 s, then evacuated. A standard cycle of AsH_3 20s, evacuated for 3s, TMG 4 s, evacuated for 3 s (20, 3, 4, 3) was adopted (see Fig. 16). AsH_3 pressure was usually 7×10^{-3} Pa, TMG admittance was varied. It was found possible to obtain ALE growth at temperatures between 720 and 970 K.

The thickness of deposit grown per cycle d varied quite markedly with the amount of TMG admitted to the apparatus in each cycle. From the initial brief publication[11] d saturated at about 0.55 nm for $T_{gr} = 870$ K, as shown in Fig. 17. This corresponds to about two layers of GaAs per cycle on (100). As would be expected for the ALE mode of growth, d remained constant over large numbers of cycles, as shown in Fig. 18 which corresponds to a TMG dosage of about 10^{-2} Pa 1/s, and a d value of 0.4 nm. While the constancy appears to confirm that ALE does occur, the variation of d with the amount of TMG admitted per cycle must presumably indicate that even an incomplete coverage can lead to growth in the ALE mode, while, as already noted, sufficient TMG can allow up to two GaAs (100) layers to form per cycle even though this is not too readily explained on the simple theory presented in Sec. III. In their later work Nishizawa et al.[9] found much smaller d values by lowering the growth tem-
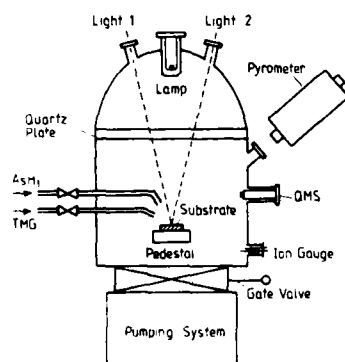
peratures and increasing the TMG dosage. At $T_{gr} = 770$ K, d was found to saturate at a value very slightly below the 0.283-nm characteristic of a true monolayer of GaAs on (100); i.e., the simple ALE growth model was well obeyed.

One problem with the reaction between TMG and AsH_3 is that its rate falls off rapidly below 870 K apparently because of the energy required to dissociate arsine. Nishizawa[52] showed that it was possible to use UV radiation from a high-pressure Hg lamp or an excimer laser to alleviate this source of difficulty. Growth could be obtained down to temperatures as low as 560 K. This appears to be a true enhancement of reaction by the radiation, and not an effect due to heating—any temperature rise of the substrate caused by the radiation would be no more than about 1 K. It was also found that below 870 K the growth thickness per cycle decreased quite sharply for constant TMG dosage. Even at very low d values, however, a constant growth per cycle was maintained.

Some electrical results have been quoted by Nishizawa et al.[9] The films produced at low temperatures, ~620 K, were p type, with hole concentrations of the order of 10^{19} cm^{-3}. This high defect concentration was attributed to the incorporation of carbon. Some improvement on this was obtained by using triethyl gallium, (TEG) which still gave p-type material but with carrier concentration of the order of 10^{18} cm^{-3}. Most recently, Nishizawa[52] reported on carrier concentrations below the 10^{17} cm^{-3} level. No results have

FIG. 16. Gas pressure in growth chamber of Fig. 13 during standard ALE cycles (20, 3, 4, 3 s).

FIG. 15. Schematic drawing of equipment for atomic layer epitaxy of GaAs.[9,11] Lights 1 and 2 are for photoexcitation (see text). The lamp is for heating the substrate (QMS stands for a quadrupole mass spectrometer).
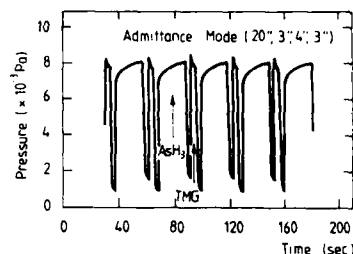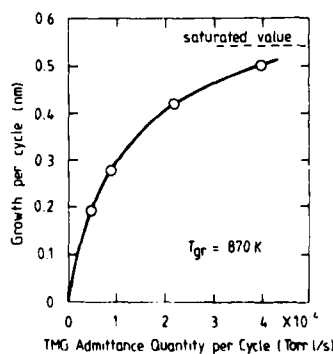

FIG. 17. Thickness per cycle of GaAs as a function of TMG admittance

R75   J. Appl. Phys., Vol. 60, No. 3, 1 August 1986

C. H. L. Goodman and M. V. Pessa   R75
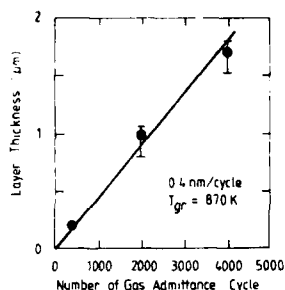
FIG. 18. Thickness of GaAs grown at 870 K vs number of ALE cycles (20, 1, 4, 1 s).

FIG. 20. Growth rate per cycle for GaAs overlayers as a function of flow rate of HCl. T_{gr} = 820 K (figure courtesy of A. Usui).

been reported for material grown at higher temperatures, or from higher alkyls e.g. tri-isobutyl gallium, either (or both) of which might lead to still lower carbon incorporation.

Usui and Sunakawa[10] at Nippon Electric Corp., Japan, have also prepared GaAs by ALE. They employed a dual growth chamber reactor in hydride vapor-phase epitaxy. The principle of his growth system is illustrated in Fig. 19. The substrate was exposed alternately to GaCl and As_4 by switching its position between the two chambers (the AsH_3 vapor stream was interrupted during the substrate transfer). The period of the cycle was 60 s but considerably shorter cycles could also be applied.

The growth thickness per cycle for several substrate surfaces was studied as a function of HCl(Ga) flow rate at T_{gr} of 820 K. The d values thus obtained remained almost constant independent of the flow rate in the range from 1 to 5 cm^3/min and closely corresponded to the thickness of a monolayer on each surface (see Fig. 20).

The films were monocrystalline, as revealed by reflection high-energy electron diffraction (RHEED) measurements, with completely mirrorlike surfaces (Fig. 21). No oval defects typical of MBE-grown GaAs were present. Furthermore, it is believed that ALE growth reduces the number of EL2 deep traps, but this has not yet been demonstrated.

Of particular importance was the observation[10] that selective growth at windows of SiO_2 masks on GaAs did not show any significant enhancement in d. This result implies that ALE might be suitable for selective epitaxy.

It is also interesting to note that preparations for growth of III-V mixed crystals by ALE are under way at NEC. Preliminary results on InGaP have already been obtained. They are found to be very encouraging.[10]

ALE growth of GaAs and AlAs from metalorganic (TMG and TMA, respectively) and hydride sources has

GaAs by ALE

a)

SURFACE PHOTOMICROGRAPH

b)

FIG. 21. (a) Photograph of a GaAs (100) film grown by ALE.[10] (b) Scanning electron micrograph of the film exhibiting no oval defects (figure courtesy of A. Usui).
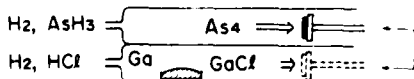

H_2, AsH_3

As_4

H_2, HCl

Ga   GaCl

FIG. 19. Schematic diagram of the dual growth chamber reactor used for ALE growth of GaAs.[10] The substrate is alternately exposed to the two reactants (figure courtesy of A. Usui).
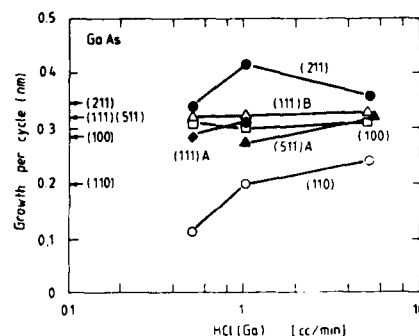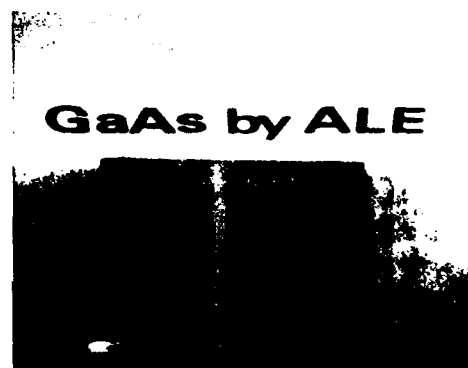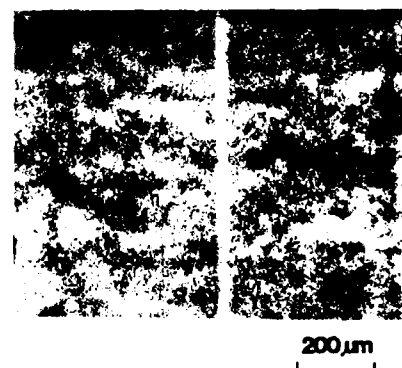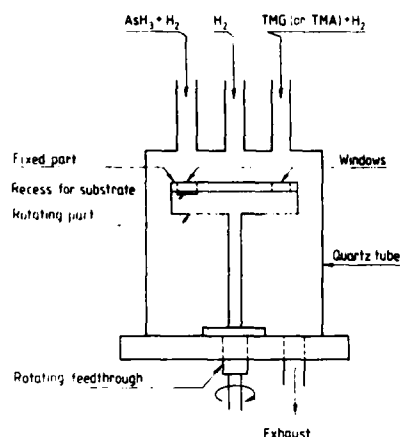
FIG. 22. Schematic diagram of the growth chamber and susceptor of ALE (Ref. 53) for preparing GaAs and AlAs. The susceptor consists of a fixed part, a rotating part, and a recess (in the rotating part) which holds the substrate. The H_2 flow in the middle tube helps prevent mixing of the reactants.

been reported by Bedair et al.[53] Their growth chamber (see Fig. 22) has a simple, ingeniously designed structure which may permit one to grow several samples at the same time in a cyclic fashion. The susceptor incorporates a shuttering action which allows successive exposure to streams of gases from two sources, viz., from $AsH_3 + H_2$ and $TMG + H_2$ for growth of GaAs, or $AsH_3 + H_2$ and $TMA + H_2$ for growth of AlAs. A large flow of H_2 in the middle tube is designed to prevent mixing of the reaction gases from the adjacent tubes. When the substrate is rotated away from the growth (window) position by a rotating part, most of the boundary layer will be sheared off by a fixed plate placed above the rotating part facilitating an almost immediate termination of exposure of the substrate to the input flux. In the experiments, one complete cycle was performed in about 10 s; T_{gr} for growth of GaAs and AlAs was in the range from 830 to 870 K.

The GaAs and AlAs overlayers prepared in this way on GaAs (100) substrates were single crystals, as deduced from transmission electron micrographs. Photoluminescence measured at 77 K of 100 cycles of ALE-grown GaAs sandwiched between layers of MOCVD-grown $GaAs_{0.97}P_{0.03}$ showed a full width at half-maximum of 11 meV, indicating that the sample was of a good electrical quality.

## B. Polycrystalline and amorphous deposits

Most of the published papers on ALE are concerned with polycrystalline and amorphous deposits. These arise mainly from the use of amorphous substrates. In part, poor crystal structure may be due to carrying out deposition at temperatures that are only a small fraction of the absolute melting point of the material concerned, so that surface mobility of adsorbed species would be small or negligible. It is possible that many materials in this section could be grown

as epitaxial layers if single-crystal substrates and higher growth temperatures were used.

The various materials grown as polycrystalline or amorphous films using ALE cycling will be listed in turn.

1. Zinc sulfide

This is the most widely studied material for ac EL thin-film displays. The growth and properties of thin films of ZnS and ZnS:Mn fabricated by ALE variant (ii) have been the subject of many investigations (see, for example, Refs. 2, 54–63. Either zinc chloride and hydrogen sulfide via the sequential exchange reaction:

$$ZnCl_2 + H_2S \rightarrow ZnS + 2HCl (600 < T_{gr} < 800 \text{ K}), \quad (1)$$
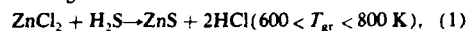
or anhydrous zinc acetate and hydrogen sulfide[54] via the reaction

$$Zn(CH_3COO)_2 + H_2S$$
$$\rightarrow ZnS + 2CH_3COOH (520 < T_{gr} < 620 \text{ K}) \quad (2)$$
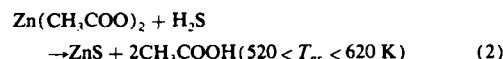
can be used. The occurrence of reaction (1) was demonstrated by straightforward in situ AES measurements[4] (see Fig. 23). The spectra shown were taken for a glass substrate which was exposed alternately to pulses of $ZnCl_2$ and H_2S under UHV conditions. The reactions were found to leave no traces of Cl or other impurities within the detection limit of AES. By contrast, ZnS grown in a gas-flow reactor of Fig. 4 from the same reactants exhibits traces of Cl and C.

Tammenmaa et al.[54] used reaction (2) to grow ZnS on glass. The maximum growth rate achieved was 0.26 nm per cycle, which corresponds to 6/7 of the lattice spacing of 0.312 nm in the preferential (111) growth direction. They proposed that $Zn(CH_3COO)_2$ forms multinuclear compounds in the vapor phase. Chemisorption of these species on the substrate surface leads to high coverages and, accordingly, to the relatively high growth rate observed.
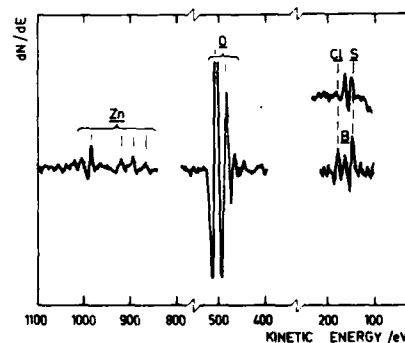

FIG. 23. Auger electron spectra showing an occurrence of stepwise growth of a ZnS film on a glass substrate via surface exchange reactions. The spectra were taken at two successive phases of a deposition cycle. The wide-range scan (100–1100 eV) in the middle was recorded after exposing the substrate to a $ZnCl_2$ pulse; Cl is chemisorbed on the surface as indicated by the appearance of the Cl AES peak. The uppermost spectrum (100–200 eV) on the right-hand side shows the absence of Cl after a pulse of H_2S which completes the cycle, yielding a growth of a ZnS molecular layer. Oxygen and boron signals originate from the glass substrate.

Tammenmaa et al.[54] have also carried out doping experiments in connection with growth of ZnS via reaction (2), using volatile complexes of Eu, Tb, and Tm. Photoluminescence measurements at room temperature showed that Tb^{+3} ions gave a clear PL spectrum with green emission peaking at a wavelength of 547 nm. Intensity was found to increase with Tb concentration up to 1.5 at. %. In comparison with the yellowish-orange emission (peaking at $\lambda \approx 580$ nm) from Mn^{+2}, the most common activator in ZnS, emission from Tb^{+3} was very small.

The microstructure of ALE samples from Lohja, observed by the TEM technique exhibited no fine-grained region at any thickness.[64] Fig. 24 shows a typical cross section of ZnS layers deposited onto amorphous Al_2O_3. Very pronounced columnar grain growth occurred with many grains extending from the bottom to the top of the layer. Selected area x-ray diffraction curves[56,58] showed that the films had a cubic or hexagonal polytype structure for growth in the temperature range from 300 to 570 K. The specific orientations were (111) for the cubic structure and (00.2) for the hexagonal structure which consisted predominantly of a 2H phase. The hexagonality increased remarkably in the range from 630 to 770 K. The degree of preferred orientation of microcrystallites at $T_{gr} = 770$ K was so high that one-half of the (00.2) poles were aligned within 7° of the substrate normal.

The substrate material was also found to influence the texture. The highest degree of orientation was obtained with films deposited onto a amorphous Ta_2O_5 (or Al_2O_3) buffer layer of thickness of about 50 nm grown on a glass substrate. Insertion of a microcrystalline SnO_2 layer between the glass and the Ta_2O_5 (or Al_2O_3) caused some reduction in the degree of preferred orientation.

The crystallite size varied as a function of film thickness. Typically, for films thicker than 200 nm prepared at $T_{gr} = 770$ K, the length of coherently diffracting domains in the direction normal to the surface ranged from 40 to 120 nm with a size distribution maximum at 100 nm. It is noteworthy that the mean grain diameter parallel to the film plane seen by TEM (Fig. 24) was also about 100 nm. This agreement between x-ray diffraction and TEM suggests that the columnar grains are made up of single crystals mainly of a hexagonal structure with preferential (00.2) orientation obtained at high T_{gr}.

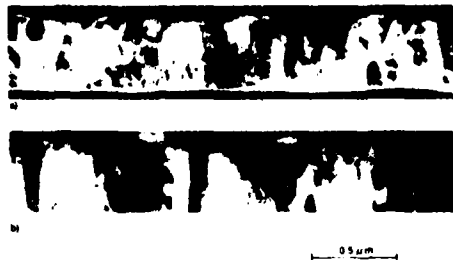ZnS films grown from zinc acetate at $T_{gr} = 560-650$ K

FIG. 24. Transmission electron micrographs of ZnS:Mn films grown on amorphous Al_2O_3 by ALE at Lohja Corp (a) Corning 7059 glass substrate; (b) soda lime glass substrate.
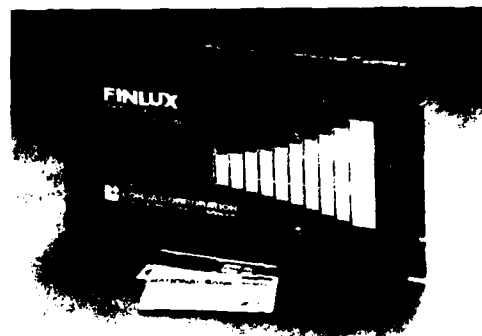

FIG. 25. Half-page matrix display module for personal computers. The light-emitting layer of ZnS:Mn is sandwiched between two dielectric layers of mixed Al_2O_3-TiO_2 grown by ALE. The transparent front electrode is ITO made by sputtering. The back electrode can be either ITO or aluminum. The structure is protected by a passivation layer of Al_2O_3, black printing is applied on top of the passivation layer to increase contrast

exhibited the average crystallite sizes of 40-80 nm, depending on the film thickness.[63] Electroreflectance studies[62] indicated that two crystal phases, cubic and hexagonal, coexist in these films with the cubic structure predominating at the lower end of the T_{gr} range.

It is thus concluded that crystal structure of ZnS films depends both on growth temperature and on source materials. The substrate has also an influence on the specific orientation of crystallites.

The dislocation density in ZnS films grown at 770 K was found[58] to be about 10^{10} cm^{-2}. This is an order of magnitude lower than the dislocation density in ZnS grown by electron beam evaporation.[60]

The ZnS:Mn films used by Lohja in their ac thin-film EL displays (see Fig. 25) exhibit a maximum luminance of 3000 cd/m^2 at 1 kHz. An EL external efficiency of about 2 lm/W obtained at 1 kHz has been observed.[66] At very high frequencies the external efficiency may rise up to 8 lm/W which is probably the highest efficiency attained for active layers of ZnS:Mn grown by any technique. These displays also require the introduction of dielectric layers, e.g., Al_2O_3, again grown by ALE. Uniform pinhole-free deposits of ZnS and dielectric layer materials can be obtained over very large areas—250 × 150 mm^2 glass substrates are routinely used at Lohja.

2. Zinc telluride

ZnTe films grown from elemental Zn and Te exhibit smooth and featureless surfaces. X-ray diffraction measurements revealed that the films tended to crystallize preferentially in the (111) direction.[5] An interesting observation is that in a comparison of x-ray diffraction curves of the films grown in UHV by MBE and ALE as a function of T_{gr}, the ALE-grown films show a weaker temperature dependence of the texture than those grown by MBE. That reasonably close control of stoichiometry was maintained during ALE growth could be deduced from XPS and AES spectra.[4]

3. Oxides

Zinc acetate and water vapor have been used as reactants for growing ZnO.[54,59] The following reaction appeared to hold:

$$Zn(CH_3COO)_2 + H_2O$$
$$\rightarrow ZnO + CH_3COOH \ (560 < T_{gr} < 630 \ K). \quad (3)$$
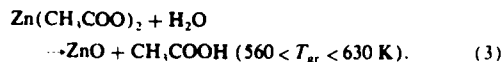
The growth rate was typically 60 nm/h, and thus one-fifth of the growth rate observed in most cases for ZnS. X-ray diffraction revealed that the ZnO films were of rather poor crystallinity. Presumably this was because ZnO is a more refractory material than ZnS, so that the surface mobility of atoms at 600 K would be rather small (see comments at beginning of Sec. IV).

Growth of Ta_2O_5 by ALE variant (ii) has been realized via the reaction

$$2TaCl_5 + 5H_2O \rightarrow Ta_2O_5 + 10HCl \ (T_{gr} \approx 770 \ K). \quad (4)$$
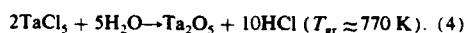
That this exchange reaction in fact occurs has been demonstrated by in situ AES measurements[4] of a substrate which was exposed alternately to vapor pulses of $TaCl_5$ and H_2O. Cl was seen in AES after each pulse of $TaCl_5$ but was always removed by a subsequent pulse of H_2O. Ta_2O_x layers are amorphous (again Ta_2O_5 is a refractory material with a very high melting point). It should be noted that the extremely low vapor pressure of Ta at 770 K would prevent ALE variant (i) being employed.

Amorphous layers of Al_2O_3 are grown from anhydrous $AlCl_3$ and water vapor at $T_{gr} \approx 720$ K. They are pinhole-free and can therefore be used as an ion barrier and dielectric and passivation layers in EL devices. Although Al_2O_3 has a reasonable dielectric strength by itself, essential improvement has been achieved using a mixture of Al_2O_3 and TiO_2, prepared by ALE. SnO_2 films are grown from $SnCl_4$ and water vapor. They are noted as exhibiting some weak x-ray diffraction peaks, and so are not completely amorphous.

Work is also being done at Lohja[67] on indium tin oxide (ITO) used as a transparent conductor in displays. Resistivity of 1.6×10^{-4} Ω cm, with transmission of more than 80% has been reproducibly demonstrated over a large substrate area.

V. THE EXTENSION OF ALE TO OTHER MATERIALS

In principle it should be possible to extend ALE to a wide range of materials, even those in which one of the constituents is involatile, since there appears to be a general family of reactions that might be used for achieving ALE variant (ii). These can be summarized:

Metal halide + H_2O or oxygen→Metal oxide;
Metal halide + H_2S or sulfur vapor→Metal sulfide;
Metal halide + H_2Se or selenium vapor→Metal selenide.

One could well expect that closely related compounds to those discussed in the preceding section ($ZnCl_2$, $AlCl_3$, $SnCl_4$, and $TaCl_5$), should behave in very much the same way, for example: $CdCl_2$, $HgCl_2$, $GaCl_3$, $InCl_3$, $SiCl_4$, $GeCl_4$, $ZrCl_4$, $NbCl_5$, and also other transition metal halides, e.g., $FeCl_3$. In addition, the success of Nishizawa and Bedair et al. in using TMG,[9,11,53] TEG,[9,11] and TMA (Ref. 53) in the

preparation of GaAs and AlAs (Ref. 53) suggests that metalorganics generally might be utilized as metal sources. Some caution may be needed here, however, not so much on account of the toxicity and pyrophoric nature of metalorganics, but with regard to their thermal stability. That must be sufficient to withstand an encounter with the hot substrate without decomposition in order that desorption of physisorbed material would occur.

It is also important to consider the second reaction component. On general thermodynamic grounds oxygen or sulfur will not react with a chemisorbed halide layer at so low a temperature as water vapor or H_2S, since such reaction would require greater free energy for the halogen to be given off as an elemental vapor than as a hydride. Since there is a major drive with electronic materials towards the use of the lowest possible temperature for material preparation, this could favor the use of the hydrides rather than the pure elements. A further important point is that H_2O, H_2S, etc. greatly resemble H_3N, H_3P, H_3As, and, as Nishizawa's work with GaAs has shown, it should be possible for such molecules to react with chemisorbed metal compounds to facilitate ALE growth of nitrides, phosphides, arsenides, etc. The first successful growth of phosphides (InGaP) has already been carried out.[11]

It should also be possible to prepare more complex materials than the relatively simple compounds discussed so far. Ferrites would serve as an example to illustrate the point. Nickel zinc ferrite could in principle be prepared from $NiCl_2$, $ZnCl_2$, and $FeCl_3$ or manganese ferrite from $MnCl_2$ and $FeCl_3$. The magnetic properties of ultrathin films of such materials remain essentially unknown and would warrant attention. It could, for example, be interesting to prepare multilayer structures of ferrites combined with nonmagnetic analogues in order to obtain direct access to effects of strain and "two-dimensionality" on magnetic properties. For development of magnetic properties, layers of good crystal perfection would be required. In order to obtain them ALE would need to be carried out on a substrate held at high temperatures, say, 0.5 of the melting point. In the case of most ferrites this might be 1000 K or more. No experiments on the ALE growth of oxides at such high temperatures has yet been attempted.

Finally the ALE approach has so far been restricted to compounds. It is conceivable that elemental materials, e.g., silicon, could be grown via chemisorption of a monolayer of, say, a chlorosilane from a stream of argon, followed by reduction of the chlorosilane in a pulse of hydrogen.

VI. CONCLUSIONS

Crystal growth in the ALE mode, whether by physical or chemical vapor deposition, is necessarily slow because individual layers of atoms are deposited with a time of the order of one second being required for each layer. Although it seems unlikely that such times could be shortened very significantly there are advantages, e.g., the feasibility of depositing several large-area films simultaneously, which make long growth times acceptable.

Where ALE might offer particularly striking advantages is in the growth of ultrathin epilayers under precise

R79   J. Appl. Phys., Vol. 60, No. 3, 1 August 1986

C. H. L. Goodman and M. V. Pessa   R79

and, almost, automatic control. The technique gives a "growth per cycle" rather than a growth rate, and does so at relatively low temperatures. It therefore should enable heterojunctions with abrupt interfaces, quantum well structures and superlattices to be grown without the need for the complex and costly control systems. Additionally, ALE may provide a vehicle for investigating fundamental aspects of compound semiconductor growth. However, it still remains to be demonstrated that the perfection of structure and control of impurities and stoichiometry required of materials for electronic devices can in fact be achieved.

With regard to polycrystalline and amorphous materials, the ac thin-film EL displays made by the Lohja group have demonstrated unequivocally that ALE can be used to grow highly uniform deposits of good structural integrity both mechanically and dielectrically speaking. These qualities are of importance in many other fields, too. Application to ternary or higher compounds could also prove feasible, and low-dimensional magnetic structures might eventually be fabricated by ALE.

ACKNOWLEDGMENTS

[1]T. Suntola and J. Antson, Finnish Patent No. 52359 (1974) and T. Suntola and J. Antson, US Patent No. 4058430 (1977); T. Suntola, A. Pakkala, and S. Lindfors, US Patent No. 4389973 (1983).

[2]T. Suntola, J. Antson, A. Pakkala, and S. Lindfors, Soc. Information Display (SID'80) Dig., 109 (1980).

[3]M. Pessa, in *Optoelectronic Materials and Devices*, edited by M. A. Herman (PWN—Polish Science Publishing, Warsaw, 1983), p. 217 and in Extended Abstracts of the First Symposium on Atomic Layer Epitaxy, Espoo, Finland, Dec. 13-14, 1984 (unpublished).

[4]M. Pessa, R. Mäkela, and T. Suntola, Appl. Phys. Lett. 38, 131 (1981).

[5]M. Ahonen, M. Pessa, and T. Suntola, Thin Solid Films 65, 301 (1980).

[6]M. Pessa, O. Jylhä, and M. A. Herman, J. Cryst. Growth 67, 255 (1984).

[7]M. A. Herman, O. Jylhä, and M. Pessa, to be published in Crystal Research and Technology (1986); for application of the generalized model of ALE variant (i) to growth of CdTe, see M. A. Herman, M. Vulli, and M. Pessa, J. Cryst. Growth 73, 403 (1985).

[8]T. Pakkanen, M. Lindblad, and V. Nevalainen, in Extended Abstracts of *The First Symposium on Atomic Layer Epitaxy, Espoo, Finland, Dec.* 13-14, 1984 (unpublished).

[9]J. I. Nishizawa, H. Abe, and T. Kurabayashi, J. Electrochem. Soc. 132, 1197 (1985).

[10]A. Usui and H. Sunakawa, The 12th International Symposium on Gallium Arsenide and Related Compound, Karuizawa, Japan, Sept. 23-27, 1985 (unpublished); A. Usui (private communication).

[11]J. I. Nishizawa, *International Conference on Solid State Devices and Materials, Kobe, Extended Abstracts* (Japan Society of Applied Physics, Tokyo, 1984), p. 1.

[12]K. A. Jackson, in *Progress in Solid State Chemistry*, edited by H. Reiss (Pergamon, Oxford, 1967), Vol. 4, Chap. 2, pp. 53-80.

[13]P. Hartman, in *Crystal Growth: An Introduction*, edited by P. Hartman (North-Holland/American Elsevier, Amsterdam/New York, 1973), Chap. 14, pp 366-402.

[14]I. Dawentz, Surf. Sci. 160, 171 (1985).

[15]L. B. Theeten, L. Hollan, and R. Cadoret, in *Crystal Growth and Materials*, edited by E. Kaldis and H. Scheel (North-Holland, Amsterdam, 1977), Chap. 16, pp. 196-235.

[16]D. W. Shaw, *Crystal Growth, Theory and Techniques*, edited by C. H. L. Goodman (Plenum, New York, 1974), Vol. 1, Chap. I, pp. 1-48

[17]C. Engler and W. Lorenz, Surf. Sci. 104, 549 (1981).

[18]J. Korec and M. Heyen, J. Cryst. Growth 60, 297 (1982).

[19]W. Lorenz and C. Engler, Surf. Sci. 114, 607 (1982).

[20]M. Pessa, P. Huttunen, and M. A. Herman, J. Appl. Phys. 54, 6047 (1983).

[21]M. Pessa, O. Jylhä, P. Huttunen, and M. A. Herman, J. Vac. Sci. Technol. A 2, 418 (1984).

[22]M. A. Herman, O. Jylhä, and M. Pessa, J. Cryst. Growth 66, 480 (1984); M. Pessa and O. Jylhä, Appl. Phys. Lett. 45, 646 (1984).

[23]D. L. Smith and V. Y. Pickhardt, J. Appl. Phys. 46, 2367 (1975).

[24]I. Bhat, L.M.G. Sundaram, J. M. Borrego, and S. K. Ghandhi, in Abstracts of 1984 Fall Meeting of Materials Research Society, Boston, Mass. Nov. 26-30, 1984 (unpublished).

[25]M. A. Herman and M. Pessa, J. Appl. Phys. 57, 2671 (1985) and references therein.

[26]J. P. Faurie, A. Million, and J. Piquet, Appl. Phys. Lett. 41, 713 (1982); J. P. Faurier, in Extended Abstracts of The 1984 US Workshop on The Physics and Chemistry of Mercury Cadmium Telluride, San Diego, Ca, May 15-17, 1984 (unpublished).

[27]R. F. C. Farrow, G. R. Jones, G. M. Williams, and I. M. Yong, Appl Phys. Lett. 39, 954 (1981).

[28]R. F. C. Farrow, A. J. Noreika, F. A. Shirland, W. J. Takei, S. Wood, J Greggi, and M. H. Francombe, J. Vac. Sci. Technol. A 2, 527 (1984).

[29]T. H. Myers, Y. Lo, R. N. Bicknell, and J. F. Schetzina, Appl. Phys. Lett 42, 247 (1983).

[30]Y. Lo, R. N. Bicknell, T. H. Myers, and J. F. Schetzina, J Appl. Phys 54, 4238 (1983).

[31]M. Pessa and O. Jylhä (unpublished work).

[32]C. B. Duke, A. Paton, and W K. Ford, Phys. Rev. B 24, 3310 (1981); J Vac. Sci. Technol. 20, 778 (1982).

[33]J. A. Venables, Vacuum 33, 701 (1983); J. A. Venables, G. D. T Spiller, and M. Hanbucken, Rep. Prog. Phys. 47, 399 (1984).

[34]The PL spectra were measured and partly interpreted by B. Monemar at The University of Linköping, Sweden.

[35]K. Nishitani, R. Okhata, and T. Murotani, J. Electron. Mater. 12, 619 (1983).

[36]R. N. Bicknell, R. W. Yanka, N. C. Giles, J. F. Schetzina, T. J. Magee, C. Leung, and K. Kawayoshi, Appl. Phys. Lett 44, 313 (1984).

[37]N. Otsuka, L. A. Kolodziejski, R. L. Gunshor, S. Datta, R. N. Bicknell, and J. F. Schetzina, Appl. Phys. Lett. 46, 860 (1985)

[38]J. J. Dubowski, D. F. Williams, P. B. Sewell, and P. Norman, Appl. Phys Lett. 46, 1081 (1985).

[39]J. T. Cheung, M. Khoshenevisan, and T J. Magee, Appl. Phys. Lett 43, 462 (1983).

[40]P. P. Chow, D. K. Greenlaw, and D. Johnson, J. Vac. Sci. Technol. A 1, 562 (1983)

[41]H. A. Mar, K. T. Chee, and N. Salansky, Appl. Phys. Lett. 44, 898 (1984).

[42]S. Datta, J. K. Furdyna, and R. L. Gunshor, Superlattices and Microstructures 1, 327 (1985)

[43]R. R. Galazka, in *Physics of Semiconductors 1978*, edited by B. L. H. Wilson (Institute of Physics Conf. Ser. No. 43, London, 1979), p. 133.

[44]J. K. Furdyna, J. Appl. Phys. 53, 7637 (1982)

[45]N. B. Brandt and V. V. Moshchalkov, Adv. Phys. 33, 193 (1984).

[46]A. V. Nurmikko, R. L. Gundshor, and L. A. Kolodziejski, J. Quantum Electron (to be published).

[47]M. Dobrowolska, A. M. Witowski, J. K. Furdyna, T. Ichiguchi, H. D Drew, and P. A. Wolff, Phys. Rev. B 29, 6652 (1984).

[48]J. A. Gaj, R. R. Galazka, and M. Nawrochi, Solid State Commun 25, 193 (1978).

[49]J. K. Furdyna and J. Kossut, Superlattices and Microstructures (to be published).

[50]S. P. Kowalczyk, J. T. Cheung, E. A. Kraut, and R. W. Grant, in Proceedings of The 1985 US Workshop on Physics and Chemistry of CdHgTe, San Diego, Oct. 7-10, 1985, p. 143 (unpublished).

[51]L. A. Kolodziejski, T. Sakamoto, R. L. Gunshor, and S. Datta, Appl. Phys. Lett. 44, 799 (1984).

[52]J. I. Nishizawa, private communication and a lecture in The 32nd National Symposium of American Vacuum Society, Houston, TX, Nov 19-22, 1985 (unpublished).

[53]S. M. Bedair, M. A. Tischler, T. Katsuyama, and N. A. El-Masry, Appl. Phys. Lett. 47, 51 (1985).

[54]M. Tammenmaa, T. Koskinen, L. Hiltunen, M. Leskelä, and L. Niinistö,

in Extended Abstracts of The First Symposium on Atomic Layer Epitaxy, Espoo, Finland, Dec. 13–14, 1984 (unpublished).

[55]V. P. Tanninen, M. Oikkonen, and T. Tuomi, Phys. Status Solidi A **67**, 573 (1981).

[56]V. P. Tanninen and T. Tuomi, Thin Solid Films **90**, 339 (1982).

[57]R. Tornqvist, J Appl. Phys. **54**, 4110 (1983).

[58]V. P. Tanninen, M. Oikkonen, and T. Tuomi, Thin Solid Films **109**, 283 (1983).

[59]M Tammenmaa (private communication).

[60]D Thesis, H. Oppolzer, G. Ebbinghaus, and S. Schild, J. Cryst. Growth **63**, 47 (1983).

[61]J. A Lahtinen and T. Tuomi, Acta Polytech. Scand. Appl. Phys. Ser. **138**, 97 (1983).

[62]R. O. Tornqvist, J. Antson, J. Skarp, and V P Tanninen, IEEE Trans. Electron Devices **ED-30**, 468 (1983).

[63]M. Oikkonen, M. Blomberg, T Tuomi, and M Tammenmaa, Thin Solid Films **124**, 317 (1985).

[64]L. E. Tannas, Jr., Electroluminescent Displays, Report 6475 (Aerojet Electro Systems, 1983).

[65]J. A. Lahtinen, A. Lu, T Tuomi, and M. Tammenmaa, J Appl. Phys **58**, 1851 (1985).

[66]T. Suntola, International Symposium Digest, Society of Information Display, New York, April 20–21, 1981 (unpublished)

[67]T Suntola and J Hyvarinen, Annu Rev Mater. Sci. **15**, 177 (1985)

M. A. HERMAN, O. JYLHÄ, M. PESSA

Department of Physics, Tampere University of Technology, Finland

Growth Mechanism in Atomic Layer Epitaxy (I)

Re-evaporation of Cd and Te from CdTe(111) Surfaces Monitored by Auger Electron Spectroscopy

The mechanism of atomic layer epitaxy (ALE) of cadmium telluride has been studied. Auger electron spectroscopy is used to measure the isothermal re-evaporation rates of elemental Cd and Te deposits on the (111)A and (111)B surfaces of CdTe substrates. The results include an observation that the sticking coefficients of Cd and Te are smaller than unity at the growth temperatures typical of CdTe ALE. After desorption the substrates are left partially covered: 35% by a Cd overlayer on the (111)B surface and 72% by Te on the (111)A surface. The re-evaporation rates of Cd and Te experience a drastic change near the substrate-deposit interface. These rates appear two orders of magnitude smaller than those of bulk-like amorphous Cd and Te solids. The activation energies for re-evaporation of the near-interface layer region are estimated to be: 1.5 eV for Te on the (111)A face, 1.0 eV for Te on (111)B and 0.5 eV for Cd on (111)B. It has also been shown that AES can be used to identify the polarity of the CdTe(111) surfaces. The relative difference in peak-to-peak intensity ratios of Cd MNN to Te MNN for (111)A and 111)B is $(11 \pm 2)\%$.

1. Introduction

The atomic layer epitaxy (ALE) method has been developed for fabricating large-area II–VI compound films primarily for production of electroluminescent displays (SUNTOLA, ANTSON; SUNTOLA et al.). Recently, ALE was shown to be applicable to growth of single crystal overlayers of II–VI compounds (PESSA et al. 1983; PESSA; PESSA et al. 1984a; PESSA et al. 1984b; HERMAN et al.) and even GaAs, a III–V compound (NISHIZAWA). ALE is based on chemical reactions in the solid surface of a substrate to which the reactants are alternately transported as neutral molecular vapour pulses or beam bunches. The growth rate and the composition of a layer are controlled by the growth process itself because they are largely independent on excess incident molecules impinging on the surface. Accordingly, no thickness monitoring is needed. The thickness of the layer is determined by counting the number of reaction steps provided that the dose in a reaction step is high enough to yield a full monolayer coverage. ALE is limited to those compounds with vapour pressures of solid phases much lower than the vapour pressures of solid phases of their pure constituents or reacting chemical compounds.

Among II–VI compounds CdTe is of considerable importance for studying the peculiarities of ALE growth because the evaporation rates of elemental Cd and Te are extremely high in comparison with dissociative or molecular evaporation of the CdTe compound at elevated temperatures.

In the present paper we report a comprehensive study of the growth mechanism in ALE of CdTe by using AES to monitor the isothermal desorption rates of the elemental Cd and Te deposits for the (111)A and (111)B surfaces of CdTe substrates.

2. Experimental procedure

Chemisorption and isothermal desorption of the constituent elements play a crucial role in the ALE process. Bearing this in mind we have investigated the ALE growth mechanism by measuring the isothermal desorption of Cd and Te deposits for the polar surfaces of CdTe(111) substrates.

Studying the isothermal desorption is one of the simplest methods to characterize adsorbed layers (CASSUTO). The desorption rate at which the surface coverage diminishes in time may be determined by a gas phase analysis which observes a rise in partial pressure, Δp, due to desorption. A more complex and arduous way of studying desorption is to measure Auger electron spectra for the re-evaporating deposit. The low-energy Auger electrons having a short inelastic mean free path in solids, escape from the surface region and make the AES method a powerful non-destructive tool in analysis of very thin overlayers. Since the ALE mechanism is based on reactions at the surface of a substrate AES is most suitable for providing information about the reaction zone.

The CdTe(111)A and (111)B substrate platelets of the size of 8×8 mm² were cut from unintentionally doped p-type wafers grown by a modified Bridgman method. They were polished mirror shiny chemimechanically and then rinsed in pure methanol and ethanol. Two substrates, one with the (111)A face and the other with the (111)B face were mounted side by side simultaneously on a Mo sample holder so that growth of the overlayers on both surfaces could be carried out under identical conditions. Prior to growth the substrates were cleaned by Ar⁺ ion etching and subsequent annealing at $450-500$ K for several hours. After cleaning no contaminants were observed above the detection limit of AES. Deposition of the Cd and Te films was performed at the pressure of 10^{-7} Pa. The layer thickness was monitored by a quartz crystal oscillator.

Cd and Te were produced as thermal molecular beams from Knudsenlike effusion cells. Three re-evaporation experiments on pure Cd and Te deposits designated as CB 1–3, TA 1–3 and TB 1–3 were carried out. The deposition parameters are given in Table 1. In CB 1–3 and TA 1–3, T_s was 300 K so that re-evaporation of Cd or Te during deposition was negligible. Experiments TB 1–3 were performed at elevated temperatures at which partial re-evaporation took place during deposition.

The substrates covered with deposits were transferred, without breaking the vacuum, into the analysis chamber of a multitechnique electron spectrometer comprising facilities of AES, and other surface-analytical techniques (Fig. 1). The rate of re-evaporation was determined by measuring the peak-to-peak ratio $R(t) = I_{Cd}/I_{Te}$ of differentiated Auger electron lines of the principal Cd $M_{4,5}N_{4,5}N_{4,5}$ (375 eV) and Te $M_{4,5}N_{4,5}N_{4,5}$ (479 eV) transitions as a function of re-evaporation time t. In experiments CB 1–3 and TA 1–3

Table 1

Temperatures and deposition parameters used in Auger re-evaporation experiments

| Experiment	substrate surface	element deposited	original thickness of deposit d_0 (nm)	substrate temperature during deposition T_s (K)	re-evaporation temperature (K)
CB 1	(111)B	Cd	70	300	385 ± 2
CB 2	(111)B	Cd	100	300	425 ± 2
CB 3	(111)B	Cd	200	300	480 ± 2
TA 1	(111)A	Te	40	300	500 ± 2
TA 2	(111)A	Te	70	300	525 ± 2
TA 3	(111)A	Te	50	300	550 ± 2
TB 1	(111)B	Te	10	440 ± 2	440 ± 2
TB 2	(111)B	Te	10	460 ± 2	460 ± 2
TB 3	(111)B	Te	10	500 ± 2	500 ± 2
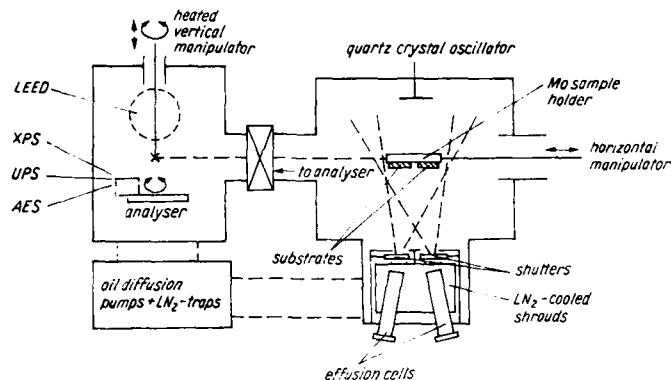
Fig. 1. Layout of the MBE growth chamber incorporated into an ADES-400 electron spectro-
meter

the substrates were heated to a nominal re-evaporation temperature in each case by
putting them in contact with a pre-heated sample holder of the analysis chamber. To
reduce effects of transient thermal conditions on the measurements of re-evaporation
rates, r_{exp}, for the near-interface layers relatively thick Cd and Te films were deposited.
Therefore the only Auger signal detected at the beginning of each experiment was that
of the deposit. As the deposit became thinner, due to desorption, both the Cd MXX and
Te MXX lines appeared in the spectra. By measuring these signals as functions of time at
a stable substrate temperature, r_{exp} could be determined to a reasonable accuracy. The
re-evaporation rates for thick (amorphous) deposits, $r_{a, exp}$, were obtained by dividing the
initial thickness of a deposit by the total time of re-evaporation. Because of the transient
thermal effects the $r_{a, exp}$ values were subject to large errors.

3. Results

The (111)A substrate surface exhibited systematically higher R values did the (111)B
surface. On the average, R 1.75 ± 0.03 and 1.55 ± 0.03 for (111)A and (111)B,
respectively, as deduced from four individual measurements on either substrate.
Figures 2a—2c show the $R(t)$ curves resulting from experiments CB 1—3, TA 1—3
and TB 1—3. Here R denotes an average value of three measurements taken in
rapid succession. The number of monolayers $\Theta(t)$ for a flat surface were calculated
from $R(t)$ by means of a standard computational procedure used in estimating an
attenuation of the Auger signal in solids (SEAH; MEMEO et al.; FADLEY et al.). The
inelastic mean free path λ, of a Cd Auger electron was taken equal to that of a Te
electron but to the dependent upon the overlayer material. According to the analysis
discussed in Appendix we found reasonable to choose $\lambda = 2.4$ nm for a CdTe single
crystal matrix, 1.55 nm for amorphous Te and 1.25 nm for amorphous Cd.

For the stationary surfaces, i.e., for the "plateau" region of $\dot{R}(t)$, the following
coverages Θ_{ave} were obtained:

Θ_{ave} — 0.35 ± 0.15 ML corresponding to R_{ave} 1.64 ± 0.08 for CB 1—3,

Θ_{ave} = 0.72 ± 0.12 ML corresponding to R_{ave} = 1.57 ± 0.08 for TA 1—3,

Θ_{ave} = 0.17 ± 0.12 ML corresponding to R_{ave} = 1.47 ± 0.08 for T5B 1—3.
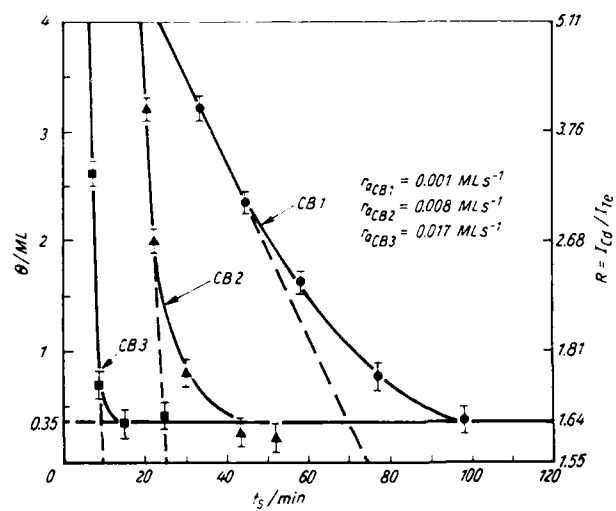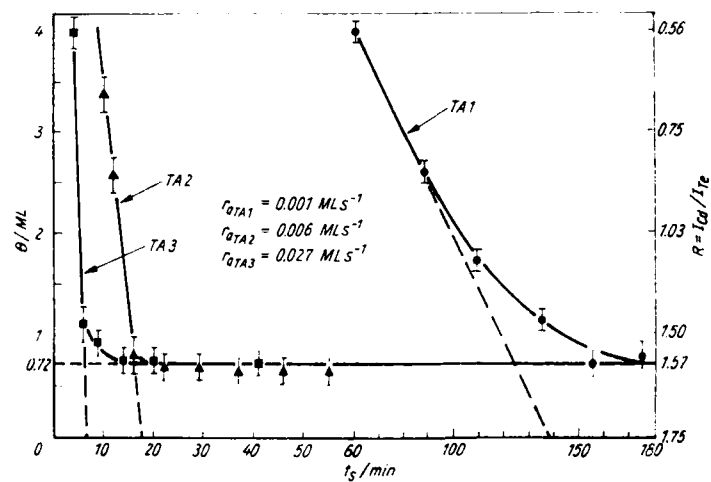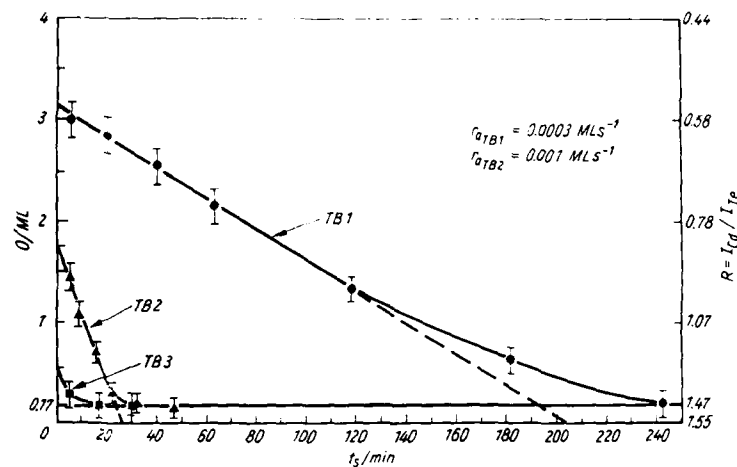
Fig. 2 a

Fig. 2 b

Fig. 2 c

Fig. 2. Re-evaporation of Cd and Te deposits on the CdTe(111) substrates as a function of re-evaporation time. a) Experiments TB 1—3, b) TA 1—3, and c) TB 1—3 (ML monolayers)

It is worth noting that all these final layers are independent on T_s within the range from 385 to 550 K studied. Adsorption of some Te on the (111)B surface (experiments TB 1—3) may be ascribed to a presence of crystal defects capable of trapping the atoms.

We have regarded the (111) surface as a truncated bulk solid. In fact, LEED symmetry appears to be lowered for the real surface which exhibits a p(2 × 2) structure the half-order spots being more clear for the (111)A face. This reconstruction of the top layer may influence adsorption processes and further complicate the growth mechanism of the compound.

The slope parts of the $R(t)$ curves represent re-evaporation of the deposits from a near-interface region extending at least to the AES probing depth of 3–4 ML (exluding the first monolayer on the substrate). The re-evaporation rates r_{exp} for this region are given in Table 2 and Figures 2a—2c. In Figure 3 a general behaviour of film thickness as a function of re-evaporation time has been delineated. Here d_0 denotes the initial thickness, t_A and t_p refer to the onsets of the near-interface region and "plateau" region, respectively. Since t_A could not be directly measured we have used an approximation $t_A = t_p$. This assumption leads to a reduction in $r_{a,exp} = d_0 t_A$. A finite transient time t_h (chosen to be zero in our calculation), during which the substrate reaches its steady state temperature of re-evaporation quoted in Figures 2a to 2c and Table 2. Causes a further reduction in $r_{a,exp}$. With these approximations in t_A and t_h we have estimated $r_{a,exp}$.

In order to obtain more information about re-evaporation of the amorphous bulk-like Cd and Te layers we have calculated theoretical re-evaporation rates $r_{a,theo}$ of these layers. The bulk-like layers desorb freely by Langmuir evaporation. To the best of our knowledge, no simple theory exists for calculating $r_{a,theo}$ according to the Langmuir evaporation which is a non-equilibrium process. Therefore, we have

Table 2

Numerical data of re-evaporation of Cd and Te deposits on the CdTe(111) surfaces. $r_{a,theo}$ is calculated from eqs. (2) and (3). r_{exp} refers to re-evaporation of Cd and Te measured for the near-interface region and $r_{a,exp}$ to that of thick (amorphous) deposits obtained by setting $t_A = t_p$ and $t_h = 0$, see also Figure 4

Experiment	$r_{a,theo}$ (nm s^{-1})	r_{exp} (nm s^{-1})	$r_{a,exp}$ (nm s^{-1})
CB 1	0.02	$3 \cdot 10^{-4}$	0.04
CB 2	0.51	$2 \cdot 10^{-3}$	0.06
CB 3	16.47	$5 \cdot 10^{-3}$	0.67
TA 1	0.05	$3 \cdot 10^{-4}$	$5 \cdot 10^{-3}$
TA 2	0.31	$2 \cdot 10^{-3}$	$5 \cdot 10^{-2}$
TA 3	1.68	$9 \cdot 10^{-3}$	$6 \cdot 10^{-2}$
TB 1	$2.3 \cdot 10^{-4}$	$1 \cdot 10^{-4}$	
TB 2	$1.6 \cdot 10^{-3}$	$3 \cdot 10^{-4}$	
TB 3	0.05		

Fig. 3. Complete re-evaporation curve assumed for re-evaporation of Cd and Te deposits from the CdTe(111) surfaces in experiments CB 1—3 and TA 1—3

estimated $r_{a,theo}$ in a crude approximation by using the Knudsen equation (for an equilibrium process) (HERMAN, CHO)

$$N = 3.51 \cdot 10^{22} \, pa(AT)^{1/2} \tag{1}$$

where N is the number of atoms evaporated per second from a solid surface of an area of a (cm^2) at temperature T(K). A(g) is the atomic weight and p(Torr) the pressure at T. It can be shown that

$$r_{a,theo}(Cd) = 7.144 \cdot 10^5 \, pT^{-1/2} \, (nm/s) \tag{2}$$

and

$$r_{a,theo}(Te) = 10.551 \cdot 10^5 \, pT^{-1/2} \, (nm/s) \tag{3}$$

with the equilibrium vapor pressures obtained from (WEAST)

$$\log p(Cd) = 5693.07 \, T^{-1} + 8.564 \tag{4}$$

and (KUBASCHEWSKI et al.)

$$\log p(Te) = 917.5 T^{-1} + 2.71 \log T + 19.68 . \tag{5}$$

Since the Langmuir evaporation is expected to be faster than Knudsen evaporation $r_{a,theo}$ obtained from Eqs. (2) and (3) is probably smaller than that in a more accurate calculation. A comparison of the values listed in Table 2 reveals that $r_{a,theo}$ is two orders of magnitude larger than r_{exp}. It can also be seen that $r_{a,exp} \approx r_{a,theo}$ for the low-temperature experiment CB 1 (385 K). With increasing temperature, however, the difference between $r_{a,exp}$ and $r_{a,theo}$ becomes large. At 480 K for Cd and 550 K

for Te re-evaporation is so fast that AES is practically incapable of measuring $r_{a,exp}$. It should be emphasized that r_{exp} (taken at stable temperature) is a straightforward measure for the observed parts of $R(t)$. Therefore it is not subject to uncertainties in t_A and t_h.

The activation energy E_a for re-evaporation of Cd and Te of the near-interface region is calculated from the Arrhenius equation

$$r_a = C_0 \exp\left(-E_a/kT\right) \tag{6}$$

where C_0 is a constant. By plotting ln r_{exp} against $1/T$ a straight line is obtained (Fig. 4). From the slopes of these lines one finds $E_a = 0.5$, 1.0 and 1.5 eV for CB 1—3, TB 1—2 and TA 1—3, respectively. The drawing of the straight line for the TB experiment is only guided by two measured points. Therefore, E_a in this case is less accurate than E_a of the other experiments where three measured points determine the slopes of the lines. However, there is no reason to expect that this line would show an exceptional deviation from Eq. (6).
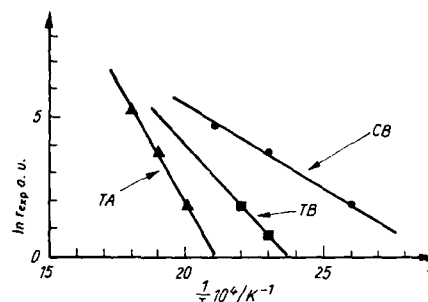
Fig. 4. Temperature dependence of the experimentally determined re-evaporation rates r_{exp} of Cd and Te deposits on CdTe (111) for the near-interface region. The slopes of the lines give the activation energy of re-evaporation E_a. ● $E_a = 0.5$ eV, ▲ $E_a = 1.5$ eV, ■ $E_a = 1.0$ eV

4. Discussion

Surface roughness influences the AES spectra (WU, BUTLER). Among the most remarkable effects is a reduction in intensity of an Auger signal. In the present experiment the chief Auger electrons of Cd and Te have comparable mean free paths. Therefore any intensity variation caused by surface roughness is the same for Cd MNN and Te MNN, and leaves the steady state intensity ratio $R = I_{Cd}/I_{Te}$ unaffected. Despite this fact it is conceivable that morphological effects influence "dynamic" $R(t)$ in the near-interface region. On the basis of the present results it is somewhat hard to distinguish these effects from those caused by a change in bonding strength. The results favour, however, an interpretation of the behavior of $R(t)$ in bonding terms. For example, in experiment TA 3 the thickness of the film deposited was 50 nm. Re-evaporation at 550 K in the "dynamic" $R(t)$ range took about 7 min to reach the first monolayer coverage (and 13 min more in the sub-monolayer evaporation range to yield the steady state value of $R = 1.57$, i.e., $\Theta_{ave} = 0.72$, see Fig. 2b). Using the constant bulk-like re-evaporation rate of 1.68 nm/s for Te (Table 2)

throughout the deposit yields the film thickness of 700 nm, in sharp contrast to the real situation. Similar discrepancies appear in the other cases. Therefore, we interprete the observed trend in $R(t)$ as mainly due to a change in the re-evaporation rate.

5. Conclusions

We have studied re-evaporation of amorphous deposits of Cd and Te from the CdTe(111) surfaces by employing the AES method. It has been found that the re-evaporation rates for the region near the substrate-overlayer interface are two orders of magnitude smaller than those of bulk Cd and Te. The activation energies for re-evaporation of this region are measured to be $E_a = 1.5$ eV for Te on the (111)A substrate, $E_a = 1.0$ eV for Te on (111)B and $E_a = 0.5$ eV for Cd on (111)B. The sticking coefficients of Cd and Te are less than 1. The persistent sub-monolayer coverages are: $\Theta = (0.35 \pm 0.12)$ ML for Cd on (111)B, $\Theta = (0.72 \pm 0.12)$ ML for Te on (111)A and $\Theta = (0.17 \pm 0.12)$ ML for Te on (111)B (the last result is likely to indicate that the density of surface defects is comparatively large after Ar^+ bombarding and annealing).

We have also shown that AES can be used to identify the polarity of the CdTe(111) surfaces. The relative difference in peak-to-peak intensity ratios of Cd MNN to Te MNN for (111)A and (111)B is $(11 \pm 2)\%$.

Appendix

Contributions of successive Cd and Te layers to the total AES signal for a clean (111)B surface of CdTe, the structure of which is shown in Figure A 1a, are given by the following expressions:

$$I_{Cd} = I_{Cd}^{\infty} a_1 (1 - q_1)^{-1} \tag{A1}$$

$$I_{Te} = I_{Te}^{\infty} a_2 (1 - q_2)^{-1} \tag{A2}$$

where

$$a_1 = [1 - \exp(-d_0/2\lambda_{Cd})] \exp(-d/\lambda_{Cd}), \qquad q_1 = \exp(-d_0/\lambda_{Cd})$$

$$a_2 = 1 - \exp(-d_0/2\lambda_{Te}), \qquad q_2 = \exp(-d_0/\lambda_{Te}).$$

Here I_{Cd}^{∞} and I_{Te}^{∞} are the Auger signals from a semi-infinite CdTe crystal, λ_{Cd} and λ_{Te} are the inelastic mean free paths of Cd MNN and Te MNN Auger electrons. Consequently,

$$R_{(111)B} = (I_{Cd}^{\infty}/I_{Te}^{\infty}) \cdot [a_1(1 - q_2)/a_2(1 - q_1)]. \tag{A3}$$

For the (111)A surface

$$R_{(111)A} = (I_{Cd}^{\infty}/I_{Te}^{\infty}) \cdot [a_1(1 - q_2)/a_2(1 - q_1)] \exp[d/(\lambda_{Cd} + \lambda_{Te})]. \tag{A4}$$

From the paper of SZAJMAN et al. (1980) one obtains $\lambda_{Cd} = 1.3 \pm 0.2$ nm and $\lambda_{Te} = 1.4 \pm 0.2$ nm. These values are underestimated when considering a single crystal CdTe matrix where the interatomic spacings are larger than in the amorphous phase, $d_{0,Cd} = d_{0,Te} = 0.374$ nm and 0.324 nm, respectively. If the empirical relations of SEAH and DENCH compiled for inorganic compounds and elemental species are applied to the single crystal matrix and the amorphous pure Cd and Te deposits, then the following λ values are obtained: $\lambda_{Cd} = 3.195$ and $\lambda_{Te} = 3.610$ nm in CdTe, $\lambda_{Cd} = 1.17$ and $\lambda_{Te} = 1.32$ nm in amorphous Cd, and $\lambda_{Cd} = 1.47$ and $\lambda_{Te} = 1.66$ nm in amorphous Te.
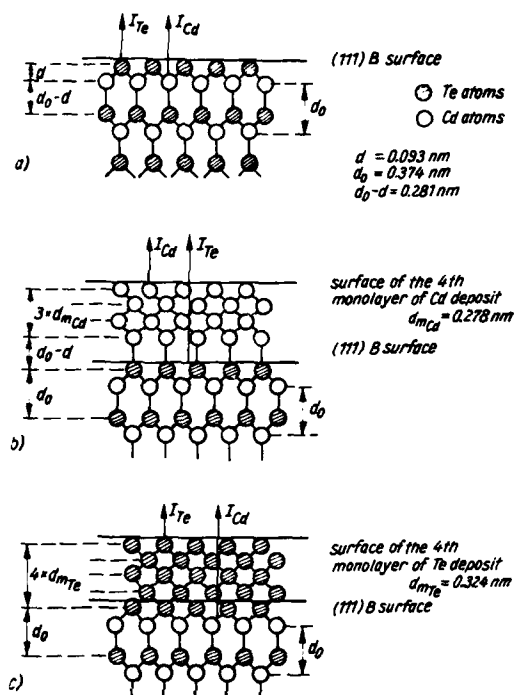
Fig. A1. Schematic illustration of the spatial configuration of Cd and Te atoms in the CdTe(111)B surface of truncated bulk, a) clean substrate surface, b) the substrate covered by 4 ML Cd, c) the substrate covered by 4 ML Te. The first monolayer in b) is bound to the surface with Cd–Te covalent bonds, in c) Te forms weak Te–Te-bonds

The formula of SEAH and DENCH gives a satisfactory experimental agreement in the cases of elemental species but overestimates λ for inorganic compounds (SZAJMAN et al. 1981). In the absence of any better approximation we have taken the average of λ in each case: $\lambda = \lambda_{Cd} = \lambda_{Te} = 2.40$ nm in CdTe, $\lambda = 1.55$ nm for the Cd and Te Auger electrons in amorphous Te, and $\lambda = 1.25$ nm for both the electrons in amorphous Cd.

When the measured values of $R_{(111)A} = 1.75$ and $R_{(111)B} = 1.55$ are inserted into Eqs. (A3) and (A4) we obtain

$$(I_{Cd}^\infty / I_{Te}^\infty)_{A(111)} = 1.683 \quad \text{and} \quad (I_{Cd}^\infty / I_{Te}^\infty)_{(111)B} = 1.611 .$$

Let us consider a layer of Cd on (111)B, Figure A1 b. A general expression for R in this case is

$$R_{(111)B \cdot Cd} = 1.611 \cdot [a_0(1 - q) + a_1]/a_2 \tag{A5}$$

where $q = \exp(-d_0/\lambda) = 0.856$. The terms a_0, a_1 and a_2 depend on the number of monolayers of Cd on (111)B.

For $0 < \Theta < 1$ ML of Cd $a_0 = 0$, $a_1 = 1 - \exp(-d_0/2\lambda)$ and $a_2 = a_1 \cdot \exp[-(d_0 - d)/\lambda]$. Consequently, $R_{(111)B+1ML} = 1.611 \cdot \exp[(d_0 - d)/\lambda] = 1.81$. This means that in the range $1.55 < R_{(111)B} < 1.81 \Theta$ is obtained from

$$\Theta = (R - 1.55)/(1.81 - 1.55) = 3.84 R - 5.96 \tag{A6}$$

up to one monolayer. For $1 < \Theta < 2$ ML of Cd $a_0 = 1 - \exp(-d_{m,Cd}/\lambda) = 0.199$, $a_1 = [1 - \exp(-d_0/2\lambda)](1 - a_0) = 0.060$, $a_2 = a_1 \exp[-(d_0 - d)/\lambda] = 0.053$ and $R_{(111)B+2ML} = 2.68$, for the definition of $d_{m,Cd}$, see Figure A1 b. So, covering this range

$$1.81 < R_{(111)B} < 2.68 \quad \text{and} \quad \Theta = 1 + (1.14 R - 2.08). \tag{A7}$$

Similarly, for $2 < \Theta < 3$ ML and $3 < \Theta < 4$ ML one can derive the equations

$$2.68 < R_{(111)B} < 3.76 \quad \text{with} \quad \Theta = 2 + (0.925 R - 2.48) \tag{A8}$$

for the third monolayer, and

$$3.76 < R_{(111)B} < 5.11 \quad \text{with} \quad \Theta = 3 + (0.74 R - 2.79) \tag{A9}$$

for the fourth monolayer. Beyond $\Theta = 4$ ML R is difficult to measure to a reasonable accuracy because of the short escape depth of the Auger electrons. Figure A1 c shows the atomic configuration used to calculate Θ from R for the Te deposits on the (111)B substrate.

References

CASSUTO, A.: Proceedings of the IX Int. Vac. Congr. and V Int. Conf. on Solid Surfaces, Segovia, J. L. (ed.), Madrid 1983, Invited Speakers Volume, p. 179
CHO, A. Y.: Thin Solid Films 100, 291 (1983)
FADLEY, C. S., BAIRD, R. J., SIEKHAUS, W., NOVAKOV, T., BERGSTROM, A. L.: J. Electron. Spectroscopy Rel. Phen. 4, 93 (1974)
HERMAN, M. A.: Vacuum 32, 555 (1982)
HERMAN, M. A., JYLHÄ, O., PESSA, M.: J. Cryst. Growth 66, 480 (1984)
KUBASCHEWSKI, O., EVANS, E. L., ALCOCK, C. B.: Metallurgical Termochemistry, 4th ed., Oxford 1967, p. 418
MEMEO, R., CICCACCI, F., MARIANI, C., OSSICINI, S.: Thin Solid Films 109, 159 (1983)
NISHIZAWA, J. I.: Int. Conf. on Solid State Devices and Materials, Kobe, Japan, 1984, and J. Electrochem. Soc. 132, 1197 (1985)
PESSA, M., HUTTUNEN, P., HERMAN, M. A.: J. Appl. Physics 54, 6047 (1983)
PESSA, M.: in: Optoelectronic Materials and Devices, p. 217, M. A. HERMAN (ed.), Warsaw 1983 and in: UK Workshop on Atomic Layer Epitaxy, Standard Telecom. Lab., Harlow, England 1985
PESSA, M., JYLHÄ, O., HUTTUNEN, P., HERMAN, M. A.: J. Vac. Sci. Technol. A2, 418 (1984a)
PESSA, M., JYLHÄ, O., HERMAN, M. A.: J. Cryst. Growth 67, 255 (1984b)
SEAH, M. P.: Vacuum 34, 453 (1984)
SEAH, M. P., DENCH, W. A.: Surface Interface Anal. 1, 2 (1979)
SUNTOLA, T., ANTSON, M. J.: U.S. Patent No. 4058430 (1977)

Suntola, T., Antson, M. J., Pakkala, A., Lindfors, S.: Soc. for Information Display SID 80 Digest, 109 (1980)

Szajman, J., Leckey, R. C. G., Liesegang, J., Jenkin, J. G.: J. Electron. Spect. Rel. Phen. 20, 323 (1980)

Szajman, J., Liesegang, J., Jenkin, J. G., Leckey, R. C. G.: J. Electron. Spectr. Rel. Phen. 23, 97 (1981)

Weast, R. C. (ed.): CRC Handbook Chem. Phys. Phys. 60th ed., p. D. 218, Boca Raton 1979

Wu, O. K. T., Butler, E. M.: J. Vac. Sci. Technol. 20, 453 (1982)

Author's addresses:

Dr. M. A. Herman
Institute of Physics, Polish Academy of Sciences
al. Lotników 46
PL-02-668 Warszawa, Poland

Prof. Dr. M. Pessa, O. Jylhä
Department of Physics, Tampere University of Technology
SF-33101 Tampere 10, Finland

Hg$_{1-x}$Cd$_x$Te-Hg$_{1-y}$Cd$_y$Te (0<x,y<1) heterostructures: Properties, epitaxy, and applications

M. A. Herman[a] and M. Pessa

Department of Physics, Tampere University of Technology, P.O. Box 527, SF-33101 Tampere, Finland

This article presents a review of the state of the art of research and development on Hg$_{1-x}$Cd$_x$Te-Hg$_{1-y}$Cd$_y$Te (0<x,y<1) heterostructures important for applications in the modern infrared detection technique. It deals with the fundamental physical properties, epitaxial growth methods, and applications of these structures. The most important experimental results relevant to this subject are described and discussed. Following a short survey of the physical properties of Hg$_{1-x}$Cd$_x$Te, the travelling heater method for growing bulk crystals of Hg$_{1-x}$Cd$_x$Te has been described and compared with the epitaxial growth techniques used to prepare thin films and layered structures of this compound. Some important aspects of substrate preparation procedures related to CdTe wafers have been discussed. Then the most important problems regarding the liquid-phase, vapor-phase, and molecular-beam-epitaxy methods of Hg$_{1-x}$Cd$_x$Te-Hg$_{1-y}$Cd$_y$Te (0<x,y<1) heterostructures have been studied. A comprehensive discussion of technology and the parameters of different heterostructure photodiodes made of Hg$_{1-x}$Cd$_x$Te with electrically passive and electrically active heterointerfaces has been presented. The review is concluded with an overview of research problems relevant to HgTe-CdTe superlattices and the surfaces and heterointerfaces of Hg$_{1-x}$Cd$_x$Te.

TABLE OF CONTENTS

I. INTRODUCTION

Mercury cadmium telluride (Hg$_{1-x}$Cd$_x$Te) is the most important material for infrared detectors and imaging arrays.[1,2] The energy gap of this compound E_g is a function of the mole fraction x of CdTe and the ambient temperature (T). It ranges from -0.300 eV for semimetallic mercury telluride (HgTe) to 1.648 eV for semiconductive cadmium telluride (CdTe) at 4.2 K temperature.[3] The dependence of E_g on composition and temperature may be obtained from several data based on optical and transport measurements.[2]

Hansen, Schmit, and Casselman[3] made a critical analysis of all experimental data concerning $E_g(x,T)$ published in the literature or accumulated in their laboratory, and presented the following empirical expression for $E_g(x,T)$:

$$E_g(x,T) = -0.302 + 1.93x + 5.35 \times 10^{-4}T(1-2x) - 0.810x^2 + 0.832x^3 \text{ (eV)}. \quad (I.1)$$

[a] Permanent address: The Institute of Physics, Polish Academy of Sciences, 02-668 Warsaw, Poland.

This equation has been shown to be valid to a reasonable accuracy (the standard error of estimate is 0.013 eV) throughout the entire composition range and for the temperature interval from 4.2 to 300 K.

Quite recently, Chu, Xu, and Tang[4] published a slightly different formula:

$$E_g(x,T) = -0.295 + 1.87x - 0.28x^2$$
$$+ (6 - 14x + 3x^2)10^{-4}T + 0.35x^4 , \quad (I.2)$$

applicable for the composition range of $0 < x < 0.37$ (plus $x = 1$) and for the temperature interval of $4.2 < T < 300$ K. The energy-gap values given by this formula are a little higher than those predicted by Eq. (I.1). By comparing both expressions for $E_g(x,T)$ with the known magneto-optical experimental data,[5] Chu et al. found that the standard error of estimate for their expression is only 0.008 eV.

The intrinsic carrier concentration $n_i(x,T,E_g)$ of $Hg_{1-x}Cd_xTe$ may be evaluated from fundamental physical parameters of this compound. Using the Kane nonparabolic approximation for band structure, the average value of the heavy hole mass $m_h = 0.433 m_0$, and the formula (I.1) for the energy gap, Hansen and Schmit[6] calculated n_i as a function of composition, temperature, and energy gap. They presented the best-fit expression:

$$n_i = (5.585 - 3.820x + 1.753 \times 10^{-3}T - 1.364 \times 10^{-3}xT)$$
$$\times 10^{14} E_g^{3/4} T^{3/2} \exp(-E_g/2kT) (cm^{-3}) , \quad (I.3)$$

which has been fitted within 1% of the calculated n_i for the compositions $x < 0.7$, temperature range $50 K < T < 300 K$, and the energy gaps $E_g > 0$. Expression (I.3) has been compared to many values of n_i obtained from Hall measurements and it has been quoted to provide an excellent fit to experimental values.[6]

A. Wavelength regions of applications of $Hg_{1-x}Cd_xTe$ photodetectors

The cutoff wavelength λ_{co} of $Hg_{1-x}Cd_xTe$ photodetectors can be selected over a wide range according to Eqs. (I.1) or (I.2). [λ_{co} is defined as the longest detected wavelength at which the photoresponse of the detector has dropped down to 50% of its peak value[1]; it is often approximated by the relationship $\lambda_{co}(\mu m) = 1.24/E_g(eV)$]. The compositions mostly preferred for infrared detection are $x \approx 0.2$, $x \approx 0.31$, and $x \approx 0.39$, because they allow for fabricating detectors operating with the peak wavelengths, respectively, of $\lambda_p \approx 12.5$ μm (at 77 K), $\lambda_p \approx 4.3$ μm (at 125 K), and $\lambda_p \approx 3$ μm (at 200 K).[1] These cover the two transmission "windows" of the atmosphere from 3 to 5 μm, and from 8 to 14 μm. For the latter wavelength region, $Hg_{1-x}Cd_xTe$ is especially desirable over extrinsic detectors, such as doped Ge and Si, as the intrinsic nature of the semiconductor enables them to operate with higher detectivity.

$Hg_{1-x}Cd_xTe$ photodetectors have also great potential for the 1.0–1.7 μm ($x = 0.8$–0.65) wavelength range, exploited for fiber optic communications. Planar avalanche photodiodes with peak responsivity at 1.22 μm and cutoff at 1.25 μm have been shown to operate successfully, exhibiting peak quantum efficiencies as high as 72% at 300 K without any antireflection coating (see Sec. III A 2).

B. Crystallization of $Hg_{1-x}Cd_xTe$ bulk crystals

Until now the $Hg_{1-x}Cd_xTe$ device technology has been restricted to developing bulklike photoconductive and photovoltaic detectors.[7] When fabricating photoconductive detectors, a low carrier concentration of n-type material ($n \approx 10^{14}$ cm^{-3}) of high purity is desirable because its extremely high electron-hole mobility ratio (> 200)[8] results in a high photoconductive gain. When preparing photovoltaic detectors the substrate is usually p-type bulk material, for example, $Hg_{1-x}Cd_xTe$ platelets into which ions are implanted to form the p-n junctions.[9]

Most of the materials for infrared devices have been prepared so far by a controlled solidification of the molten $Hg_{1-x}Cd_xTe$ alloy at a relatively high temperature (1100 K), followed by homogenization annealing (950 K) and low-temperature annealing (600 K) (see Ref. 10 and Chap. 3 in Ref. 1). However, with this preparation technique there are always serious difficulties associated with compositional nonuniformities inherent in the nonequilibrium solidification of the pseudobinary alloy[11] and long annealing times required to restore homogeneity. In order to overcome these problems, application of the travelling heater method (THM) for growing $Hg_{1-x}Cd_xTe$ bulk crystals has been proposed.[12]

In this method (see Fig. 1) a molten solvent zone is made to migrate through a solid homogeneous source (feed) material by the slow movement of the ampoule relative to the
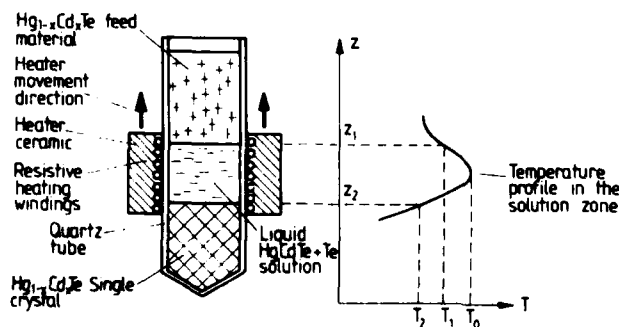

FIG. 1. Principle of the travelling heater method. Geometrical configuration of the loaded ampoule and the heater (left), and the temperature profile in the solvent zone (right). The highest temperature in the zone (T_0) is lower than the melting temperature (T_m) of the $Hg_{1-x}Cd_xTe$ compound.

heater,[13] or vice versa. Matter transport occurs by diffusion and convection across the solvent zone under the influence of the temperature gradient resulting from the movement. In the course of the process, a "pseudo" stationary state is reached. The solvent zone dissolves a solid (the feed material) at the upper hot interface, and deposits in near equilibrium conditions a material of the same composition on the lower growth interface. The crystallization occurs at constant temperature which is lower than the melting temperature of the material. Depending on the desired composition of the grown $Hg_{1-x}Cd_xTe$ crystal, the growth temperature lies in the 800–1000 K range. The growth rate is about 1 μm/min.

Using the THM technique, ingots of 30 mm in diameter and up to 80 mm in length have been grown for different compositions ranging from $x = 0.21$ to $x = 0.70$. The longitudinal homogeneity is found to be better than $\Delta x = \pm 0.02$, and the radial homogeneity better than $\Delta x = \pm 0.002$.[12]

C. Advantages of epitaxy over bulk crystal technology: Heterointerfaces

Despite the progress undoubtedly made in the bulk crystal growth technology, an increasing interest is recently shown towards the growing of $Hg_{1-x}Cd_xTe$ as epitaxial layers and layered structures on high-quality CdTe substrates.[2] Among the growth techniques used, liquid-phase epitaxy (LPE),[14–18] vapor-phase epitaxy (VPE),[19–24] and molecular-beam epitaxy (MBE)[25–30] are the most important. LPE, VPE, and MBE offer, in comparison with the bulk growth techniques, lower growth temperatures, shorter growth times, and, in the case of LPE, much better compositional homogeneity. They allow for growing multiple layers of $Hg_{1-x}Cd_xTe$ with different compositions and doping levels. It is also possible to prepare large-area epilayers not obtained by bulk growth where the quartz-tube cross-section area must be limited to only a few square centimeters to withstand the high pressures at the typical growth temperatures of 1100 K.[1]

In the epitaxial deposition of an overlayer onto a substrate of different materials, a heterointerface is formed. Such a heterointerface is called abrupt or graded according to the distance within which the transition from one material to the other is completed. At an abrupt heterointerface the transition occurs on an atomic scale (≈ 10 nm) while for a

graded junction it takes place over larger distances (1–10 μm).[31] For the $Hg_{1-x}Cd_xTe$ films, semi-insulating CdTe platelets are most frequently used as substrates although $Hg_{1-y}Cd_yTe$ bulk grown wafers have been used, too.[32,33] The $Hg_{1-x}Cd_xTe$ heterointerfaces are graded because of considerable interdiffusion between film and substrate.

At present the understanding of electrical and photoelectrical properties of these heterointerfaces is poor while the technology involved and the structural parameters of $Hg_{1-x}Cd_xTe$ are well known. This somewhat surprising situation is due to the fact that in the infrared detecting devices the $Hg_{1-x}Cd_xTe$ heterojunction acts only as a structural interface between the active $Hg_{1-x}Cd_xTe$ layer and the passive CdTe substrate.[34] It is expected, however, that the electrical and photoelectrical properties of $Hg_{1-x}Cd_xTe$-CdTe junctions and specially those of $Hg_{1-x}Cd_xTe$-$Hg_{1-y}Cd_yTe$ or HgTe-CdTe heterojunctions will be largely applied in the near future to infrared detecting, imaging and processing techniques (see, for example, Bratt[32,33] Migliorato et al.,[35,36] and Smith et al.[37]).

We make an attempt to give here an overview of the area of $Hg_{1-x}Cd_xTe$-$Hg_{1-y}Cd_yTe$ $(0<x,y<1)$ heterostructures. We concentrate on practical aspects of their heteroepitaxy and utilization possibilities in modern infrared technique and, finally, discuss some research problems related to these systems.

II. EPITAXY OF $Hg_{1-x}Cd_xTe$-$Hg_{1-y}Cd_yTe(0<x,y<1)$ HETEROSTRUCTURES

The three growth techniques LPE, VPE, and MBE have proven acceptable for producing thin epitaxial $Hg_{1-x}Cd_xTe$ layers and layered structures with satisfactory device quality (see Refs. 23 and 24 for VPE, and Refs. 27 and 30 for MBE-grown structures), although the best device suited structures are still offered by the LPE technique.[17,18] We limit our discussion to these techniques alone. We only mention in passing that cathodic sputtering[38–40] and laser-assisted deposition and annealing[41–43] have also been used for growing $Hg_{1-x}Cd_xTe$ films.

A. Preparation of CdTe bulk grown substrates

As already noted above, CdTe is usually employed as a substrate for $Hg_{1-x}Cd_xTe$ epilayers because many proper-

TABLE I. Physical parameters of $Hg_{1-x}Cd_xTe$ important for heteroepitaxy on a CdTe substrate.

Chemical composition	Crystal structure	Lattice parameter at 300 K (in nm)	Coefficient of linear expansion per degree at 300 K	Energy band gap at 300 K (eV)
HgTe	Zincblende	$0.64603 + 0.0001$[a]	5×10^{-6}[c]	$-0.141 + 0.013$[c]
$Hg_{0.78}Cd_{0.222}Te$	Zincblende	$0.64658 + 0.00005$[a]	...	$+0.185 + 0.013$[c]
$Hg_{0.584}Cd_{0.416}Te$	Zincblende	$0.64689 + 0.00005$[a]	...	$+0.448 + 0.013$[c]
CdTe	Zincblende	0.6482[b]	5×10^{-6}[d]	$+1.490 + 0.013$[c]

[a] J. P. Schwartz, T. Tung, and R. F. Brebrick, J. Electrochem. Soc. 128, 438 (1982).
[b] A. Ebina and T. Takahashi, J. Cryst. Growth 59, 51 (1982).
[c] G. L. Hansen, J. L. Schmit, and T. N. Casselman, J. Appl. Phys. 53, 7099 (1982).
[d] B. L. Sharma and R. K. Purohit, Semiconductor Heterojunctions (Pergamon, New York, 1974).
[e] D. E. Dalton, J. Cryst. Growth 59, 98 (1982).

ties of these two compounds match very closely,[1,2,44] see Table I, and because it is easier to grow a bulk CdTe crystal than a $Hg_{1-x}Cd_xTe$ or HgTe one. It has been found that the Cd-terminated CdTe(111) surface, called also CdTe(111)A surface, is optimal for growing $Hg_{1-x}Cd_xTe$ by LPE[15,18] and cathodic sputtering[40] while the Te-terminated (111) surface [(111)B] seems most suitable for the MBE technique.[25] The (100) slightly misoriented surface and the (110) precisely oriented surface have been reported to be appropriate for growth by VPE.[19,24] At the moment no well-established conclusion concerning the best orientation of the CdTe substrate in VPE, or in MBE, can be drawn [high-quality $Hg_{1-x}Cd_xTe$ layers have been grown with the aid of VPE also on CdTe(111)A,[23] and with MBE on CdTe(100).[27]]

A standard preparation procedure for CdTe wafers[45] involves cutting of platelets along a crystallographic plane from a bulk crystal, lapping the platelets with wet abrasive, polishing them mechanically with a wet, very fine (1 μm) diamond or alumina powder, followed by cleaning in organic solvents and etching in a 1%–10% bromine-in-methanol solution for a few minutes. Finally, the platelets are immersed in pure methanol, rinsed in ethanol, and dried in nitrogen gas.

New dry[46] and wet[47,48] techniques for polishing CdTe surfaces have been proposed. The dry method is an adaptation of the diamond milling process which is commonly used for polishing aluminum surfaces to precision flatness for large-area infrared optical scanning systems. A CdTe wafer supported by a perforated vacuum fixture is polished with a single diamond edge by cleaving off successively the top layers when the shearing forces produced by the diamond edge are directed along selected crystallographic directions. This method has resulted in very smooth mirrorlike (111)A surfaces with low damage and no chemical contamination beyond surface interaction with the ambient atmosphere. The wet method referred to as "hydroplane polishing" employs the principle of the hydroplane suspension of the samples on a thin layer of etch solution. This differs from chemimechanical polishing in that the samples never come into contact with the polishing pad but are supported by the liquid. As a consequence, mechanical damage is eliminated and the reaction products are removed and fresh etchant is introduced very rapidly. Nomarski interference-contrast photomicrographs and photoluminescence at 77 K[48] have given the evidence that hydroplane polishing with a solution of 20% by volume of ethylene glycol in methanol eliminates the subsurface damage caused by chemimechanical polishing prior to hydroplane polishing. Hydroplane polishing reduces the surface dislocation line density from a value of 10^8–10^{10} cm^{-2} to 10^5–10^6 cm^{-2}, which is characteristic of bulk CdTe.[44]

Crystal imperfections in the surface of a substrate may be reduced by depositing a CdTe "buffer" layer on the substrate. This attempt has been made by applying, for example, the MBE[49–51] and atomic layer epitaxy (ALE)[52] methods. The buffer layers of thickness of typically 50 nm (by ALE) have been found to exhibit remarkably higher structural perfection than that of the original substrate surfaces prepared by chemimechanical polishing.

B. Epitaxy

Epitaxy is a phase-transition process which leads to the formation of single-crystal solids. In epitaxy, the mass transport and surface processes play the major roles. Heat transport which is important in bulk crystal growth has negligibly small influence on epitaxial film growth. An up-to-date survey of the thermodynamics of phase transitions and the main aspects of kinetics relevant to epitaxy has been presented by Stringfellow.[53]

Thermodynamics determines the equilibrium composition of various phases at constant temperature and pressure. Equilibrium is defined as a state of the thermodynamic system where the Gibbs free energy per mole, $G = H - TS$, has its minimum.[54] Here H, T, and S denote enthalpy, temperature, and entropy, respectively. At this G the chemical potential, $\mu_i = \partial G / \partial n_i$, for all the components of the system are equal. If the system is not at equilibrium, the thermodynamic driving force needed to restore equilibrium is the difference in chemical potential, $\Delta\mu_{AB} = \mu_B - \mu_A$, between the nonequilibrium state, $\mu_B = (\Sigma_i \mu_i)_B$ and the equilibrium state, $\mu_A = (\Sigma\mu_i)_A$.

In epitaxy, a nonequilibrium situation is intentionally created to drive the system towards formation of the solid. The maximum amount of solid obtained during epitaxy is equal to the amount of material needed to establish the equilibrium. This amount is thus fundamentally limited by thermodynamics and the total size of the system.

C. LPE of $Hg_{1-x}Cd_xTe$–CdTe heterostructures

The LPE process involves the introduction of a carefully prepared substrate platelet into a supersaturated solution, or into a nearly saturated solution in which supersaturation is created after a short period during which etching may occur.[13] The substrate and the supersaturated solution being in mutual contact represent a thermodynamic system in a nonequilibrium state, what causes the growth of the epitaxial layer on the surface of the substrate. It is necessary to ensure upon growing the layer that the surface is free from any drops of excess solution.

In performing LPE growth it is necessary to know the solid–liquid-phase diagram of the system. The phase diagram can be determined experimentally[55,56] as well as theoretically. In theoretical calculations, the quantities H, S, and G are obtained. The minimum of G for a given temperature determines the equilibrium composition of the constituent phases.

1. Solid–liquid-phase diagram of HgTe-CdTe-Te system

The HgTe and CdTe binary compounds form a continuous range of solid solutions with the zinc-blende structure in which the Hg and Cd atoms are distributed at random over the sites of one sublattice while the Te atoms occupy the sites of the other. The Te-to-metal ratio remains always near unity.

The phase diagram of this material system exhibits the complete range of solid solubility between HgTe and CdTe.[57] The experimental thermodynamic data leading to the phase diagram consist mainly of optical absorption mea-
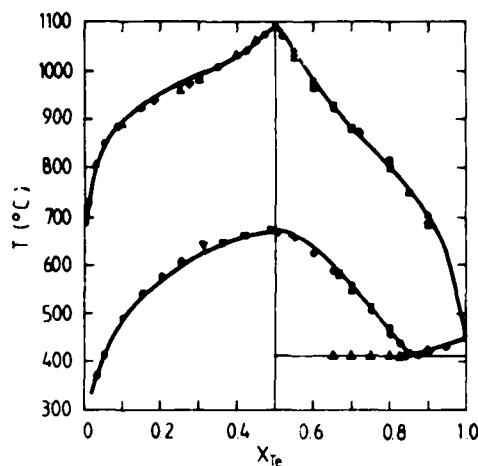
FIG. 2 Liquidus lines for CdTe (upper) and HgTe (lower) binaries.[57] CdTe: squares (Ref. 67), circles (Ref. 68), triangles (Ref. 69), inverted triangles (Ref. 70), diamonds (Ref. 71). HgTe: circles and triangles (Ref. 10), inverted triangles (Ref. 72), squares (Ref. 73).

FIG. 4. Liquid isotherms and solid solution isoconcentration lines plotted according to the GAS theory.[57]

surements of the partial pressures of Hg, Cd, and Te_2[58,59] while theoretical calculations assume various models for the liquid phase.

In the regular associated solution (RAS) model of Jordan, developed for binary compounds,[60,61] CdTe molecules are assumed to be present in the liquid phase and interact with one another and with uncombined Cd and Te atoms.[62] The RAS model was applied to a ternary system by Szapiro,[63] was later reexamined by Brebrick et al.[64,65] and Kelley et al.,[66] and generalized by Tung et al.[57]
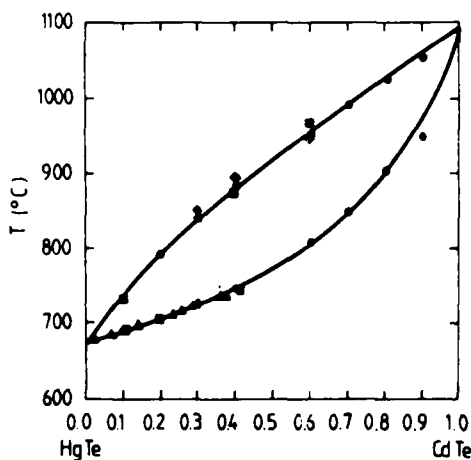

FIG. 3. Liquidus and solidus lines in the HgTe-CdTe pseudobinary section of the Hg-Cd-Te ternary phase diagram[57]; circles (Ref. 74), squares on solidus line (Ref. 59), squares on liquidus line (Ref. 75), diamonds (Ref. 76), triangles (Ref. 10).
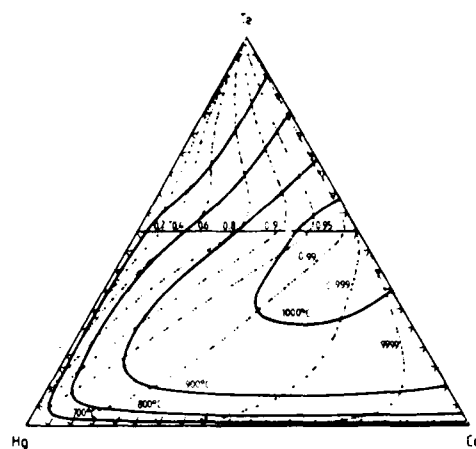
According to the generalized associated solution (GAS) model,[57] the liquid phase is a mixture of five species, viz., Hg, Cd, Te, HgTe, and CdTe. These species interact with one another like in a subregular solution which is assumed to have temperature-dependent interaction coefficients and dissociation constants. In calculating the phase diagram, certain constraints must be placed on the parameters concerning the liquidus equations. With such constraints the thermodynamic properties of the stoichiometric HgTe and CdTe liquids become consistent with the known enthalpies and entropies of formation of solid HgTe and CdTe.

The GAS model appears to be the most successful for predicting the phase diagram of HgTe-CdTe-Te in excellent agreement with the experiments. A detail comparison between the GAS theory and the experiments is presented in Figs. 2 and 3. The calculated results are shown in these figures as solid lines while the experimental data are shown by symbols. Figure 4 shows the liquidus isotherms and solid solution isoconcentration lines over the entire Gibbs composition triangle of the $Hg_{1-x}Cd_x Te$ system. Both sets of lines shown in this figure have been calculated using the GAS theory.[57]

Kikuchi[77,78] has proposed a pseudo lattice-structure model for calculating the solid–liquid-phase diagram of Hg-Cd-Te. This model has been successful in predicting the phase diagram in the Hg and Te corners but has failed to describe the general behavior of the phase diagram.

2. LPE growth

LPE growth of $Hg_{1-x}Cd_x Te$ is defined by (i) the composition of the liquid solution chosen, (ii) the mechanism of bringing the substrate into contact with the melt, and (iii) by the growth mode.[79]

(i) Epilayers of $Hg_{1-x}Cd_x Te$ may be grown from Te-, Hg-, and HgTe-rich solutions[14,17] (Fig. 5). The growth from
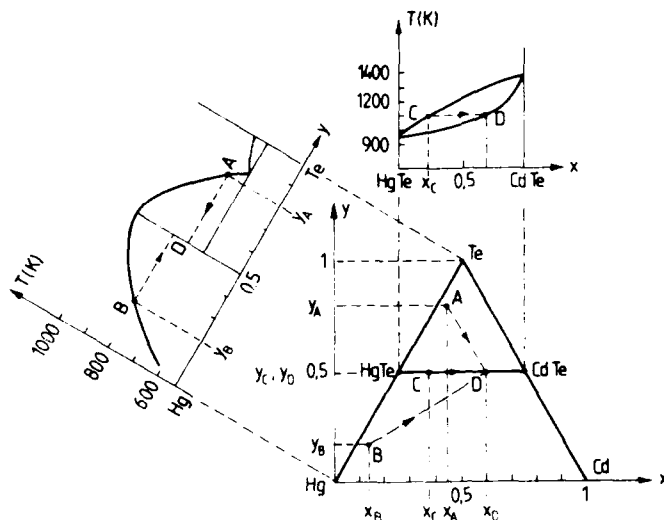
FIG. 5. Schematic representation of the Hg-Cd-Te ternary system with the mixed crystal $Hg_{1-x}Cd_xTe$ represented by the line extending from HgTe ($x=0$) to CdTe ($x=1$) on the Gibbs composition triangle (bottom) Isothermal tie lines may be drawn from points A, B, C to a certain composition ($Hg_{1-D}Cd_{xD}$)Te represented by point D. These tie lines show how the solidus composition at point D grows from the liquidus of a Te-rich solution ($Hg_{1-x}Cd_{xA})_{1-x}Te_{xx}$ of a Hg-rich solution ($Hg_{1-B}Cd_{xB})_{1-B}Te_{xB}$, and from a pseudobinary or HgTe-rich solution ($Hg_{1-C}Cd_{xC-b}Te_{0}$). Solidification processes taking place during LPE are shown by arrows on the Hg-Te binary phase diagram (top left), and on the pseudobinary section of the Hg-Cd-Te ternary phase diagram (top right)

HgTe-rich solutions leads to uniform composition regions of the epilayer but results in graded heterojunctions of about 20 μm wide. This grading is due to the increased interdiffusion of Hg at high substrate temperature required for growth.[80] However, the growth from HgTe-rich solutions has an advantage that it yields easily n- or p-type layers with a variety of carrier concentrations. Growth from Hg-rich solutions results in almost abrupt heterojunctions and the best surface morphology. The compositional uniformity is usually poor due to a depletion of CdTe from the melt. Growth from Te-rich solutions produces layers with excellent compositional uniformity and a relatively narrow interface zone ($\simeq 3$ μm). However, in this case the layers are always p-type with a high carrier concentration of 10^{17} cm^{-3}. Annealing in Hg vapor at 570 K converts the layers to n-type with a carrier concentration of about 10^{15} cm^{-3}.

The conversion process of sample conductivity occurring when annealing the sample in a Hg vapor can be understood by assuming that vacancies in the Hg-Cd sublattice act as ionized acceptors and that vacancies in the Te sublattice act as ionized donors (this assumption is an accepted fact now, see Ref. 81 and Sec. II C 1 in Ref. 2). Annealing of the p type samples after growth in a Hg-atmosphere reduces the metal vacancy concentration to a level below that of residual extrinsic n-type background impurities in the sample, thus converting the conductivity from p type to n type. For epitaxially grown films of thicknesses in the 10–20 μm range, annealing times of one or two days are required.[79] The final carrier concentration obtained using the annealing procedure depends on the level of residual extrinsic impurities in the film.

The role played by vacancies in each of the two $Hg_{1-x}Cd_xTe$ crystal sublattices explains also why the as-grown samples crystallized from Te-rich solutions are always p type and those crystallized from Hg-rich solutions are generally n type.[8,79]

At present there is no consensus as to which one of the growth solutions yields the best quality material in a reproducible way. On the basis of the citation frequency in the literature,[14-18,82-84] growth from Te-rich solutions seems to be employed most often.

(ii) Regarding the mechanism of bringing the liquid solution and the substrate into contact with each other three different approaches have been applied: (a) tipping the melt on and off the substrate,[16,85] (b) dipping the substrate into the melt,[15,86] and (c) sliding the melt on and off the substrate.[14,17,87] Tipping (Fig. 6) may not be suitable for a production-type process.[79] However, it allows performing LPE
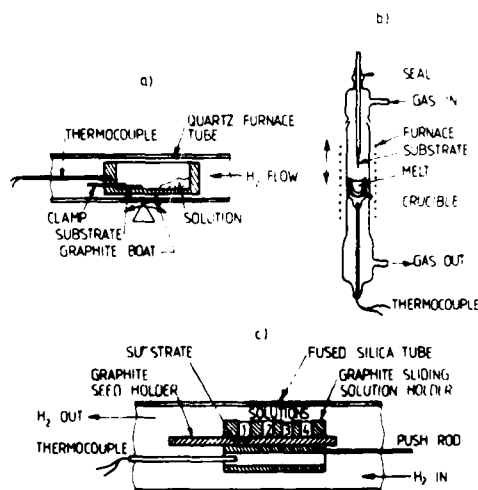

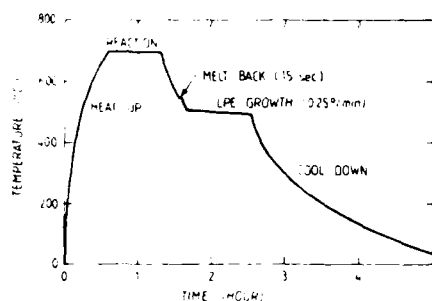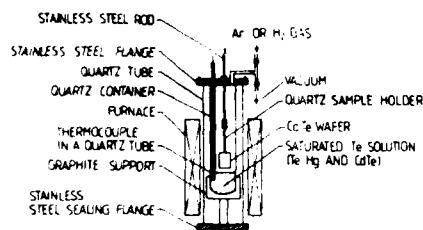FIG. 6. Schematic drawings of LPE growth systems[51]: (a) tipper system,[85] (b) dipper system,[86] and (c) slider system.[87]

FIG 7 Upper panel schematic drawing of the LPE growth system after Wang et al [15]; lower panel temperature profile for LPE growth in this system

in closed evacuated ampoullae.[16] It avoids the loss of Hg and, consequently, results in an accurate control of the Cd segregation for low x values.

Dipping is particularly well suited to the large-scale production of $Hg_{1-x}Cd_xTe$ epilayers. Relatively large melts of 0.1 kg can be used to minimize the melt depletion effects. Therefore, many layers can be grown from the same melt. Melt rotation and agitation are possible which ensure proper melt homogenization before the growth. The substrate can also be rotated to improve the compositional homogeneity in the layers across the entire substrate. Moreover, continuous dipping yields increased efficiency of the process. Multiple slice dipping may also prove feasible in LPE of $Hg_{1-x}Cd_xTe$.

The dipping technique used by Wang et al.[15] under high pressure of Ar and H_2 gas is shown in Fig. 7. This experimental arrangement enables one to fabricate not only $Hg_{1-x}Cd_xTe$ layers in the range of x from 0.17 to 0.4 but also pure CdTe epilayers as well as $Hg_{1-x}Cd_xTe$-CdTe heterostructures for backside-illuminated photodiodes.[83] It seems especially suitable for the production of high-quality epilayers for infrared detecting and imaging devices.

Growth of $Hg_{1-x}Cd_xTe$ epilayers by slider boat LPE in production quantities has not been reported in the literature. Encouraging results have been achieved, however, in research modes of operation.[14,17,84] Uniform layers to within an accuracy of 0.01 mole fraction of CdTe across the layer

and the bulk, except for an interdiffusion zone of thickness of 3 μm, have been obtained.[17,88] Multilayer growth of $Hg_{1-x}Cd_xTe$ with different compositions has also been studied.[14,17]

The slider boat technique allows one to obtain clean and smooth surfaces and multilayer structures in a closely controlled and reproducible manner. Main disadvantage is the long cycle time of the process to form an epilayer and, thus, a limited output even if multisubstrate slider boats are used Other problems are small melt volumes and losses of Hg from the melt. The loss of Hg may be minimized by using an external Hg source placed within the confines of the boat and generating a Hg vapor stream over the growth solution.[85]

(iii) LPE $Hg_{1-x}Cd_xTe$ films can be produced with the aid of isothermal growth, equilibrium (programmed) cooling, and supersaturated cooling.

Growth from a supersaturated solution in the isothermal growth mode is accomplished by cooling the melt down to a temperature below the liquidus temperature (T_l) and subsequently introducing the substrate into the melt. The driving force for epitaxy is provided by supersaturation (supercooling) related to the temperature difference $T_l - T_g$, where T_g is the growth temperature. In an ideal case, the substrate acts as the only region where nucleation takes place.

In equilibrium cooling the substrate and the melt are brought into contact at or slightly above T_l. Growth is accomplished by decreasing the temperature of the melt and the substrate at a uniform rate. As the melt is cooled, the solution concentration exceeds its equilibrium value causing the epilayer formation on the substrate which, again, acts as the only nucleation site.

Finally, growth from a continuously cooled supersaturated solution can be performed. In this case growth is obtained by cooling the melt and the substrate (which are not yet in contact) to a temperature below T_l, introducing the substrate into the melt, and further cooling the melt and substrate at a uniform rate.

The isothermal supersaturation and the programmed cooling growth methods have been compared by means of a computer simulation procedure.[90] The comparison showed that the isothermal supersaturated LPE is superior to the programmed cooling method regarding the uniformity of the epilayer composition. This has also been confirmed by experiments.[91] The isothermal growth also allows for greater variations in the growth rates.

Another approach of isothermal LPE of $Hg_{1-x}Cd_xTe$ is Hg pressure-induced LPE reported by Ruda et al.[92,93] The principle of this method is illustrated in Fig. 8. Growth is performed from Te-rich solutions under strictly isothermal conditions. Growth involves the generation of excess Hg in the vapor from an Hg reservoir. The vapor is incorporated into the solution, thereby providing its effective supersaturation. The contact between the supersaturated solution and the substrate wafer is then established by tipping the apparatus through a small angle, what leads to growth of the epitaxial film. This method enables a precise control of the solid compound composition. It also permits in situ post-growth annealing under controlled Hg pressure.
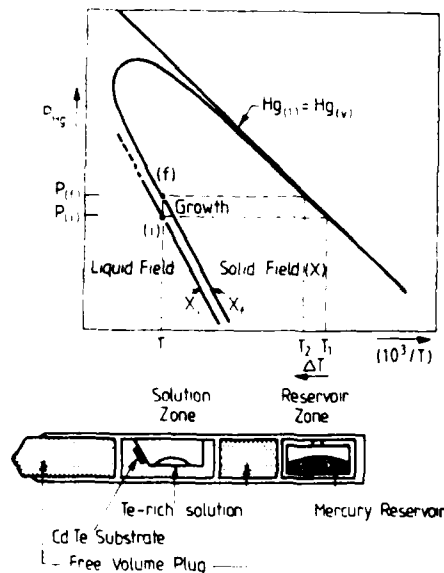
FIG. 8. Schematic diagram of the sealed quartz ampoule for Hg pressure-induced LPE of $Hg_{1-x}Cd_xTe$, and illustration of the growth principle. A temperature increase ΔT of the mercury reservoir causes a supersaturation of the solution (held at constant temperature) leading to growth. x_i is the initial composition at equilibrium T_i, and x_f is the composition of the growing layer.[92]

Liquid-phase electroepitaxy (LPEE) has also been employed for growing $Hg_{1-x}Cd_xTe$ epilayers on CdTe (111)A substrates[94] from a Te-rich solution in an open-tube slider system. In LPEE, an electric current is passed through the interface between the substrate and the melt. Since the substrate is a semiconductor and the solution is a metal, they have different thermoelectric coefficients. Thus, the flow of electric current across their interface is accompanied by absorption or evolution of heat (Peltier effect), depending on the direction of the current. The temperature change at the interface depends on electrical parameters of the substrate, current density, thickness of the substrate, and the growth cell geometry.[95] LPEE has been found to have certain advantages over more conventional LPE.[96] In LPEE the growth velocity and doping are readily controlled by the current density because the driving forces in this process are Peltier effect-induced temperature gradients (solute convection) as well as electric field-induced electromigration and electrotransport of ionized particles in the melt. The surface morphology and defect structure are improved and the interface stability is enhanced.

To summarize, the LPE procedures have made it possible to make large-area $Hg_{1-x}Cd_xTe$ epilayers on CdTe substrates. It has recently[18] become a production-worthy process. Several problems, especially the difficulties in reproducing the films with low carrier concentrations, still remain unsolved. It also seems necessary for many applica-

tions to improve the surface morphology of epilayers to that obtained by LPE at present.

D. VPE of $Hg_{1-x}Cd_xTe$-CdTe heterostructures

Vapor-phase epitaxy refers to the formation of an epitaxial film from a gaseous medium of different or the same chemical composition.[53] The various techniques that have evolved for VPE growth of crystalline materials fall roughly into two categories, depending on whether the species are transported physically or chemically to the deposition zone.

In the physical transport techniques (referred to as physical vapor deposit on (PVD) processes], the compound to be grown is vaporized from a polycrystalline or amorphous source at a high local temperature and subsequently transported down a temperature or pressure gradient and deposited on the substrate in the absence of any chemical change.

In the chemical transport techniques [referred to as chemical vapor deposition (CVD) processes] a condensed phase reacts initially with a transport agent and produces volatile species which, in another region under different conditions, will undergo a chemical reaction to form a condensed phase again. CVD processes require both a source and a transport agent, whereas PVD processes employ only gaseous reactants which are stable at room temperature and require no separate condensed phase.[53]

$Hg_{1-x}Cd_xTe$ films have been grown by both VPE techniques with encouraging results, although the CVD technique seems to be the more perspective one.[24]

1. CVD of $Hg_{1-x}Cd_xTe$-CdTe heterostructures

The selection of a chemical process for epitaxial growth is influenced by a number of factors, such as the availability of sufficiently pure reactants, their compatibility with the substrate and the growth apparatus, and the thermodynamics of the process involved. A thermodynamic analysis is essential not only for finding the optimum growth conditions but also for designing the apparatus.[97] It further provides an important estimate of the extent to which the system tends to deviate from equilibrium. Epitaxial growth must occur under relatively low gas-phase supersaturations so that the partial pressures of reactants do not deviate excessively from those at equilibrium. If the arrival rate of reactant species greatly exceeds the nucleation and lattice incorporation rate at the crystal surface, poor crystal structure will result. High fluxes of reactants increase the probability of misoriented two-dimensional nucleation and yield, in severe cases, polycrystalline layers. In addition, excessive supersaturation may lead to three-dimensional nucleation in the gas phase with the resultant nuclei falling onto the substrate surface to produce misoriented regions within the layers.

Two different growth procedures for the epitaxy of $Hg_{1-x}Cd_xTe$ by CVD have been reported until now. These are the chemical vapor transport process in a closed ampoule using HgI_2 as a transport agent,[19,98] and metalorganic CVD in an open-tube flow system where vapors of $(CH_3)_2Cd$, $(C_2H_5)_2Te$, and Hg in H_2 are used as reactants.[20,24,99,100] In
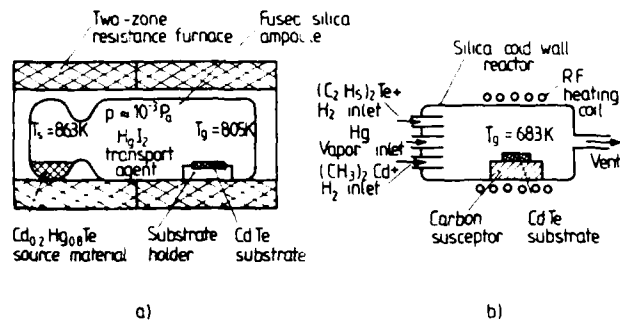
FIG. 9. Sketch of the closed ampoule[19] (a) and open-tube flow[20] (b) CVD systems.

a)   b)

both these cases, single-crystal CcTe platelets have been used as substrates.

In the closed ampoule growth procedure[19] [Fig. 9(a)], $Hg_{0.8}Cd_{0.2}Te$ has been used as a source material. This material and the HgI_2 transport agent were synthesized from high-purity elements[98] and then placed in a pretreated fused silica ampoule. (The substrate was positioned at the tube end opposite to the source.) Growth was performed in a transparent, two-zone tubular resistance furnace made out of fused silica tubing which allowed direct visual observation. The chemical reactions in this system were very complex. Exploratory studies suggested that under these conditions the mass transport was controlled by diffusion of transport species (HgI_2, CdI_2, and Te_2) through the gas phase containing predominantiy Hg vapor. No data indicating the purity (e.g., iodine contamination) or the composition of the $Hg_{1-x}Cd_xTe$ films grown with this technique have been published so far.

In the experiment of metalorganic CVD[20,22,101] vapors of $(CH_3)_2Cd$ and $(C_2H_5)_2Te$ were transported in a H_2 gas stream through an open cold-wall silica tube [Fig. 9(b)] where they reacted on the surface of a CdTe substrate in the presence of a Hg vapor flow. The substrate was placed on a rf-heated carbon susceptor the temperature of which was maintained constant at 683 K. The use of Hg vapor instead of a Hg alkyl was preferred on account of its reduced toxicity compared to the alkyl.[21] A theoretical prediction of the mole fraction of Cd in the epilayer is very difficult on the basis of the input flows of Cd alkyls and Hg vapor because of the complex nature of the transport and pyrolysis (thermal decomposition) phenomena.[20,102] Nevertheless, if one assumes that there is a steady-state growth condition, an analysis of concentrations of the components adjacent to the solid-vapor growth interface can provide a guide to the controlling parameters. The pyrolysis of the reactant alkyls can be deemed a kinetic parameter which is a rate factor controlling the supply of the elements. The incorporation of Cd and Hg into $Hg_{1-x}Cd_xTe$ will then be determined by the concentration of the elements present at the interface and by the thermodynamic properties of the various chemical species. If the growth is performed with only one solid phase and a gas phase, then the thermodynamic system will possess four degrees of freedom on assumption that the input species are $(CH_3)_2Cd$, $(C_2H_5)_2Te$, Hg, and H_2. If the total pressure and

temperature are regarded as independent variables, then the choice of ratios $|Te|/|H|$ and $Cd|/|H|$ should determine the solid composition. This is clear, because for $Hg_{1-x}Cd_xTe$, x is determined by the relation

$$x = \frac{|Cd|}{|Cd| + |Hg|} = \frac{|Cd|}{|Cd| - |(|Te| - |Cd|)} = \frac{|Cd|}{|Te|} . \quad (II.1)$$

The results of experiments in Refs. 20 and 100 indicate that x is a function of substrate temperature. At temperatures below 653 K, the epilayers obtained were essentially CdTe ($x = 1$). As shown below, this temperature was too low for Hg reactions to produce $Hg_{1-x}Cd_xTe$. A similar dependence of x on substrate temperature was also found by Vohl and Wolfe[103] in their VPE study of $Hg_{1-x}Cd_xTe$ grown from the elements. The temperature-dependent behavior of x is related to pyrolysis of the Cd and Te alkyls.[20] $(CH_3)_2Cd$ decomposes more rapidly than $(C_2H_5)_2Te$.[99] The lowest temperature for 100% pyrolysis of $(C_2H_5)_2Te$ is about 723 K while that for $(CH_3)_2Cd$ is about 650 K (at 623 K the yield of Te is found to be only 1% while the yield of Cd is still appreciable). If equivalent flows of $(C_2H_5)_2Te$ and $(CH_3)_2Cd$ in H_2 are pyrolyzed in the presence of a CdTe substrate, the pyrolysis is monitored by the growth rate of a CdTe layer. Hg begins to react with the Te alkyl only above 673 K, producing $Hg_{1-x}Cd_xTe$. This temperature is consistent with the finding that formation of HgTe from the pyrolysis of $(C_2H_5)_2Te$ falls off rapily below 683 K. Clearly, one may now explain the temperature dependence of x in metalorganic CVD. The Cd alkyl reacts with the Te alkyl and thermally decomposes at temperatures below 683 K (down to about 633 K), resulting in the growth of CdTe. An incorporation of Hg into CdTe requires the presence of metallic Te because Hg does not form an adduct with $(C_2H_5)_2Te$. An effective pyrolysis of $(C_2H_5)_2Te$ producing metallic Te occurs at temperatures above 683 K and, thus, places this lower limit for growth temperature of $Hg_{1-x}Cd_xTe$. Reducing the temperature below this value simply progressively increases the proportion of CdTe over HgTe in the layer, as is found experimentally.[20]

The chemical purity of $Hg_{1-x}Cd_xTe$ epitaxial layers grown with the metalorganic CVD method has been investigated by using secondary ion mass spectrometry (SIMS).[22] These investigations have revealed a significant impurity concentration enhancement of a number of elements (Li, Na,

K, Al, Ga, In, and Mn) at the $Hg_{1-x}Cd_x$ Te-CdTe heterointerface. The magnitude of this enhancement effect has been measured but the origin of the effect has not been found.

Hall mobility measurements performed recently on n-type $Hg_{0.83}Cd_{0.17}$ Te layers grown with the MOCVD technique[24] have confirmed the applicability of this technique for growing device-quality layers. The electron mobility of 2.45×10^5 cm^2/V s at 77 K reported for samples with a carrier concentration of 3.8×10^{15} cm^{-3} is comparable to the values characteristic of the best n-type layers grown by LPE and post-growth annealed in a Hg atmosphere.[93]

2. PVD of $Hg_{1-x}Cd_x$ Te-CdTe heterostructures

The PVD growth technique employs the evaporation of the source material (HgTe or HgCdTe), the pressure gradient-induced transport of the vapor to the CdTe substrate, condensation on the substrate surface, diffusion of the transferred atoms into the substrate, and diffusion of Cd atoms from the substrate into the growing layer. The CdTe substrate and the source material are typically placed at a short distance from each other in a sealed quartz ampoule that is heated under isothermal conditions.[104,105] Epitaxial growth proceeds because the partial pressures of Hg, Cd, and Te exceed the dissociation pressures of $Hg_{1-x}Cd_x$ Te layers.[106-109]

A given value of x can be obtained by selecting the proper source composition and the growth temperature. Then x increases with increasing temperature. The layers grown at lower temperature are strongly p type, while at higher growth temperatures the layers become n type in the as-grown state.[105]

At the optimum growth temperature the mobility of the charge carriers reaches its maximum value and the carrier concentration passes through a minimum. Electron mobilities as high as 3.4×10^5 cm^2/V s at 77 K for $Hg_{0.84}Cd_{0.16}$ Te samples with electron concentration $n = 10^{15}$ cm^{-3} have been reported.[105]

A modification of isothermal PVD growth has been presented by Becla et al.,[110] who introduced a pure Hg source into the sealed ampoule in a second thermal zone, thus reducing the number of parameters controlling the epitaxial growth of $Hg_{1-x}Cd_x$ Te layers on CdTe substrates to only two; i.e., to the source-substrate temperature (growth temperature) and the temperature of the Hg source. It has been shown that isothermal growth under a controlled Hg vapor pressure (two-thermal zone configuration) permits a convenient and precise control of the composition, the type of conductivity, and the mobility of carriers of the $Hg_{1-x}Cd_x$ Te layers. It also ensures a perfect surface morphology of the layers.

Although the closed-tube isothermal PVD technique yields $Hg_{1-x}Cd_x$ Te layers with excellent electrical properties and perfect surface morphology, it may limit the throughput of the growth processes for manufacturing purposes because of the need for sealing the growth ampoules. However, Shin and Pasko[23] recently developed an open-tube isothermal PVD method which seems to be able to overcome this disadvantage and produces device-quality $Hg_{1-x}Cd_x$ Te $(0.2 < x < 0.35)$ epitaxial layers on CdTe sub-

strates. Photovoltaic infrared detectors with a cutoff wavelength of 4.1 μm at 77 K were fabricated on those layers. Their performance was comparable with those obtained for such devices when fabricating on LPE $Hg_{1-x}Cd_x$ Te layers.

E. MBE of $Hg_{1-x}Cd_x$ Te-CdTe heterostructures

Molecular beam epitaxy[111-113] is an epitaxial growth process by which thin layers of different compounds crystallize via reactions between thermal-energy molecular or atomic beams of the constituent elements and a substrate surface which is maintained at an elevated temperature in ultrahigh vacuum. Characteristics of $Hg_{1-x}Cd_x$ Te MBE are distinguished from those of LPE and VPE in many ways:

(i) MBE growth has a relatively low rate of typically 1 μm/h;

(ii) a low growth temperature (373–493 K);

(iii) the ability of abrupt cessation or initiation of growth, as mechanical shutters for each effusion source of the constituent elements can be used;

(iv) a smoothing of the surface of the growing crystal on an atomic scale;

(v) the facility for in situ analysis.

As a result of these favorable features, MBE provides $Hg_{1-x}Cd_x$ Te epilayers and HgTe-CdTe superlattice structures at a device-quality level.[27-30]

The basic process of MBE growth is schematically illustrated in Fig. 10. The molecular beams are generated under ultrahigh vacuum conditions from Knudsen-type effusion cells,[114,115] whose temperatures are accurately controlled. Intensities of the projected beams are determined by the temperatures of the effusion cells. Choosing appropriately the substrate and cell temperatures, epitaxial films with desired chemical compositions can be obtained. Operation of the shutters permits a rapid changing of the beam species for abrupt alteration of the composition and doping. The uniformity in the film composition and crystal structure depends on the uniformities of the molecular beams across the substrate.

Although a number of CdTe epilayers have been prepared by MBE on various substrates since 1975,[116,117] the
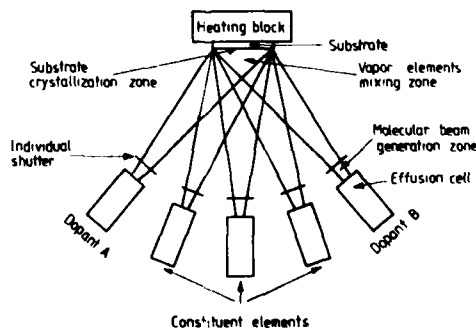

FIG. 10. Illustration of the essential elements of a MBE system for fabricating doped ternary compounds. The three zones where the main physical phenomena of MBE occur are indicated.[114]

first homoepitaxial growth of these layers on CdTe substrates was reported not until 1981.[18] Soon after this, Faurie et al. and Chow et al.[25,26,28,119] succeeded in preparing epitaxial $Hg_{1-x}Cd_xTe$ films as well as multilayer structures consisting of a series of alternate layers of CdTe and HgTe.[120] Faurie and Million[119] grew the epilayers using CdTe (111)B as substrates which were maintained at 373–393 K. Crystal structure was reasonably good for the film thicknesses smaller than 1 μm but became poor for thicker films. Carrier mobilities were low due to a short mean free path of electron scattering (about 100 nm) caused by microtwins in the layers. Crystal structure could be improved by post-growth anneal for about 10 h at 573 K,[25] an effect indicative of too low growth temperature. Since the sticking coefficient of Hg decreases as temperature is increased, a metallic Hg vapor source rather than a HgTe compound source[26] was preferred to yield a sufficiently high flux of Hg. The Hg cell was transferable and was introduced into the growth chamber only during the actual deposition in order to reduce the pressure in the growth chamber. With such a cell the Hg flux of 10^{18} atoms $cm^{-2} s^{-1}$ could be maintained for several hours at the growth temperature of 453 K. These epilayers were n type, exhibiting low carrier concentration and high electron Hall mobilities, 1.7×10^4 cm^2 V^{-1} s^{-1} at 300 K and 1.85×10^5 cm^2 V^{-1} s^{-1} at 77 K. These results are close to the best values obtained by other growth methods.[26] Epilayers of p type obtained by growing the films at high temperature or at a reduced Hg flux have also shown satisfactory electrical properties.[121]

The theory of MBE growth of $Hg_{1-x}Cd_xTe$-CdTe heterostructures is still in its infancy. Preliminary considerations[122] have shown, however, that the growth rate R of the $Hg_{1-x}Cd_xTe$ epilayer is given by the ratio of the number of Te atoms sticking in the growing surface to the number of atoms per cm^3 present in the HgCdTe alloy, N,

$$R = \frac{2k_{Te_2} F_{Te_2}}{N}. \tag{II.2}$$

The alloy composition x is determined by the relative incorporation rates of Hg and Cd atoms into the crystal. Thus x may be expressed as

$$x = \frac{k_{Cd} F_{Cd}}{(k_{Hg} F_{Hg} - F_{Hg}^S) + k_{Cd} F_{Cd}} = \frac{2k_{Cd} F_{Cd}}{k_{Te_2} F_{Te_2}}. \tag{II.3}$$

It is assumed that at the growing interface the relation

$$(k_{Hg} F_{Hg} - F_{Hg}^S) + k_{Cd} F_{Cd} = \frac{k_{Te_2} F_{Te_2}}{2} \tag{II.4}$$

is satisfied (the factor of 2 accounts for the fact that tellurium evaporates as a dimer). Here F_{Hg}^S is the flux of the Hg atoms lost from the surface of the HgCdTe layer on sublimation; F_{Hg}, F_{Cd}, and F_{Te_2} are the elemental beam fluxes from the effusion cells; and k_{Hg}, k_{Cd}, and k_{Te_2} are the respective sticking coefficients of these elements on the substrate surface. The Hg flux required to grow a given alloy composition for a fixed substrate temperature and growth rate can be calculated from the formula

$$F_{Hg} = \frac{xF_{Hg}^S + (1-x) k_{Cd} F_{Cd}}{k_{Hg}}, \tag{II.5}$$

provided that the sticking coefficients, which are determined by the thermal energy of the substrate surface and by chemical attachment kinetics, are known.

It can be concluded that the growth rate of MBE $Hg_{1-x}Cd_xTe$ is determined primarily by the Te$_2$ flux and secondarily by the Cd flux plus the amount of the Hg flux necessary to equal the Te$_2$ flux. It is also clear from Eq. (II.3) that the x value is determined by the Cd/Te flux ratio, similarly to the case of MOCVD. However, according to other authors (Faurie, private communication) experiments show that the Hg/Te ratio also has an influence on the x value.

We complete this section by noting that at least one more technique may be worth trying in attempts to fabricate $Hg_{1-x}Cd_xTe$. This technique is atomic layer epitaxy.[52] Many high-quality II-VI compound films, for example, single-crystal CdTe and semimagnetic $Cd_{1-x}Mn_xTe$,[123,124] have already been grown by ALE. To the best of our knowledge, no attempt has yet been made to grow $Hg_{1-x}Cd_xTe$.

F. Epitaxy of HgTe-CdTe superlattices

The HgTe-CdTe superlattice consisting alternately of HgTe and CdTe layes, repeated several times, is a limiting case of a multiheterostructure of $Hg_{1-x}Cd_xTe$-CdTe (with $x = 0$). For example, HgTe-CdTe superlattices with 18-nm HgTe layers and 4-nm CdTe layers, repeated 100 times, have been grown using MBE.[27,120,125] MBE is well suited for growing superlattices because (i) growth temperature is low and, therefore, serious interdiffusion is avoided; this fact ensures the required abruptness of heterointerfaces in the superlattice; and (ii) MBE HgTe and CdTe layers of the superlattice possess sufficiently high structural perfection[126] and may still be improved in the near future.[30]

SIMS and Auger depth profiling measurements of HgTe-CdTe[27,125] have revealed that this periodic structure consists of distinct layers of HgTe and CdTe with an interdiffusion depth of only 40–50 Å which, in fact, represents a limit of depth resolution of the profiling methods used. A minimal Hg interdiffusion has been evidenced also by using optical reflectance measurements.[125]

RHEED (reflected high-energy electron diffraction) investigations have shown[120] that the growth temperature plays an important role in MBE of the HgTe-CdTe superlattices. Like for single epitaxial layers, as the substrate temperature is increased, e.g., from 390 to 473 K, a crystal perfection improvement occurs for both CdTe and HgTe layers. However, below 473 K the epitaxy occurs with more difficulty for CdTe than for HgTe, and the HgTe crystal quality seems better than the CdTe.

So far, HgTe-CdTe superlattices have been grown on CdTe(111) substrates by using three different effusion cells. Elemental Hg and Te have been used as sources to grow HgTe layers and a single CdTe source to grow CdTe. The deposition rate for both CdTe and HgTe layers has been held constant at about 2 monolayers/s. The highest crystal quality has been obtained at the growth temperature of 473 K.
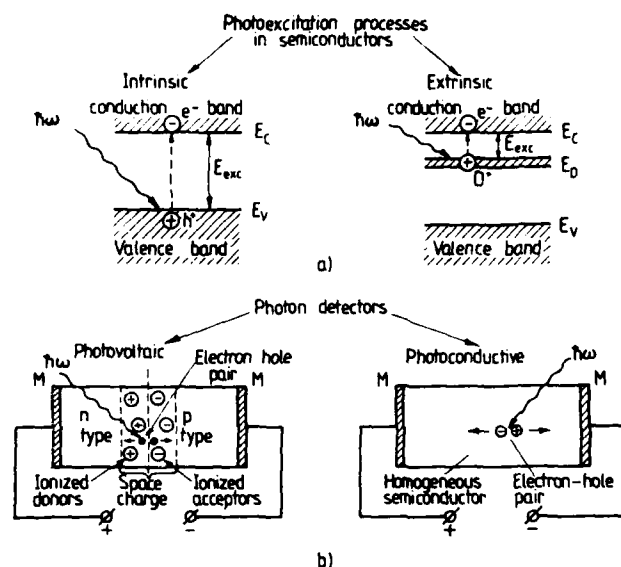
FIG. 11. Photoexcitation processes (a) and principles of photon detectors (b).

III. APPLICATIONS OF Hg₁₋ₓCdₓTe-Hg₁₋ᵧCdᵧTe HETEROSTRUCTURES IN THE INFRARED DETECTION TECHNIQUE

Photovoltaic and photoconductive effects in semiconductors are widely used for detecting infrared radiation. A schematic illustration of photoexcitation processes and the principles of photovoltaic and photoconductive detectors are shown in Fig. 11. When cooled down to low temperature these detectors offer very high detectivities.[127] Thermal imaging, space surveillance, detection of high-bit rate optical fiber communication signals, and other commercial, medical, and military applications have become possible with the $Hg_{1-x}Cd_xTe$ material in a broad wavelength region from 0.9 to 30 μm and beyond. Owing to many interesting properties of $Hg_{1-x}Cd_xTe$, a variety of detectors can be fabricated for operation in the photovoltaic and photoconductive modes. Also, several types of infrared-sensitive metal-insulator-semiconductor (MIS) devices including charge coupled devices (CCDs), charge injection devices (CIDs), and metal-oxide-semiconductor field-effect transistors (MOSFETs) have been made by using $Hg_{1-x}Cd_xTe$.[1]

A. Photodiodes with passive Hg₁₋ₓCdₓTe heterointerfaces

Significant advances in device performance have been achieved by incorporating the p-n homojunction consisting of $Hg_{1-x}Cd_xTe$ into a heterostructure configuration formed in contact with CdTe. This configuration has made it possible to use the backside illumination mode of photodiodes with improved quantum efficiency and reduction in noise.[128]

A variety of methods has been used to construct the p-n junctions in $Hg_{1-x}Cd_xTe$. Both n-on-p and p-on-n junc-

tions have been formed. Junction formation techniques include ion implantation of donors and acceptors,[9,129] high-energy proton bombardment, diffusion of donors and acceptors,[80,130] in-diffusion and out-diffusion of Hg, creation of p-type surface layers on n-type material by intense pulsed laser radiation, and in situ cosputtering of donors and acceptors.[1] It appears that the ion implantation and Hg in-diffusion are the most significant techniques for preparing high-performance infrared photodiodes.

An aim in designing an infrared detector is to provide efficient illumination of the absorbing material by only those photons which have their energy within the desired spectral band.[128] Frontside illumination of the detector is a relatively simple conventional method. In frontside illumination the photon absorption takes place near the surface layer of the p-n junction [Fig. 12(a)]. Unfortunately, recombination of carriers at the surface appreciably reduces the quantum efficiency of this structure, in particular, at high photon energies with large absorption coefficients. Reliability and efficiency of device performance are improved if a wide-gap semiconductor film (e.g., CdTe) is deposited onto the bulk photoabsorbing material [Fig. 12(b)]. Now absorption of the desired radiation begins in the bulk. If the recombination rate at the heterointerface is lower than that in the surface of the bulk material, the device efficiency is increased relative to the p-n junction structure [Fig. 12(a)] mentioned above. A backside illumination configuration [Fig. 12(c)] is a further improvement in design. The optically active area is now located behind a wide-gap semiconductor substrate which acts as spectral filter for incident radiation. In this case, filtering is independent of the angle of incidence and can be performed at the detector temperature. A reduction in the volume of the absorbing narrow-gap semiconductor leads to reduction in the noise of the detector. A sophisticated het-
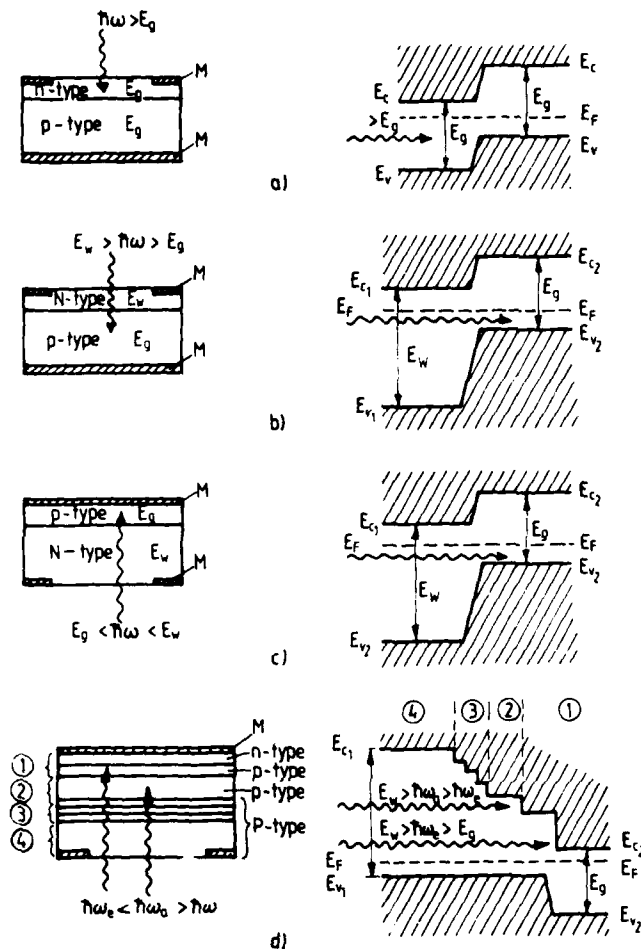
FIG. 12. Schematic illustrations of different photodiode structures designed to achieve optical illumination of the active layer with energy gap $E_g < h\nu$. (a) Conventional frontside illumination, (b) frontside illumination through a wide band-gap layer with $E_w > E_g$, (c) backside illumination through a wide band-gap substrate, (d) backside illumination with spectral filtering in an multilayer heterostructure.[128]

erostructure photodetector is illustrated in Fig. 12(d). Filtering is performed by a set of step-graded buffer layers and a thick filter layer which forms an interface with the absorbing active layer of the p-n junction. The main role of the buffer layers is the matching of the lattice parameters between the substrate and the filter layer to diminish the interface recombination processes. It is also possible in this detector to place the heterointerface directly in the p-n junction region. This configuration would maximize the quantum efficiency of the diode at high-modulation frequencies because photon detection may take place, at sufficiently high reverse bias, within the depletion region of the heterojunction.

In the infrared detecting technique using discrete diodes heterostructures with backside illumination promises the highest performance level accessible today. As illustrative examples, we discuss next two different $Hg_{1-x}Cd_x$Te-CdTe heterostructure photodiodes.

1. Mosaic of mesa photodiodes

First, a backside illuminated mesa-type diode grown by LPE[34] is shown in Fig. 13. This structure is prepared as a part of a mosaic of separately supplied mesa diodes which
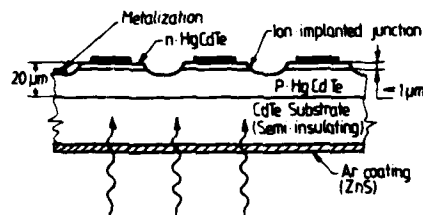

FIG. 13. Construction of a mesa-type $Hg_{1-x}Cd_x$Te-CdTe heterostructure photodiode mosaic.[34]

A)

A)

B)

B)
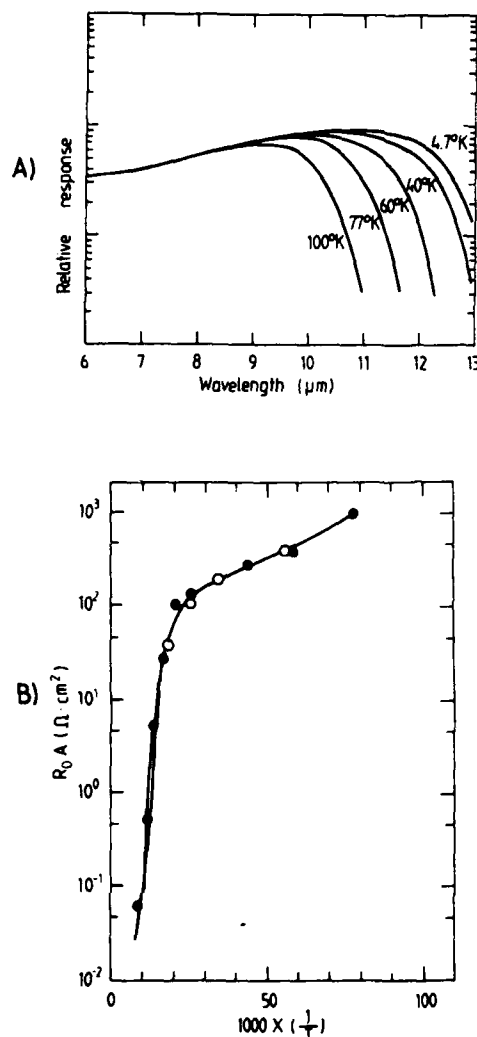
FIG. 14. (a) Temperature variation of the mesa-type diode spectral response, and (b) a RA product vs $1/T$ data for $\lambda_{co} \simeq 11$ μm at 77 K.[14]

are all deposited onto a common CdTe substrate. The temperature variation of the spectral response and the resistance area (RA) product-versus-$1/T$ plot of these diodes are displayed in Fig. 14.

For the mesa mosaic device, a p-type $Hg_{0.79}Cd_{0.21}Te$ epilayer of an area of 12×20 mm^2 was deposited from a saturated Te solution onto a CdTe (111)A substrate. The epilayer showed an acceptor carrier concentration on the order of 5×10^{16} cm^{-3} and a Hall mobility of the majority carriers of 400 cm^2 V^{-1} s^{-1} at 77 K. Upon growing the epilayer, the mesa devices were fabricated by boron ion implan-
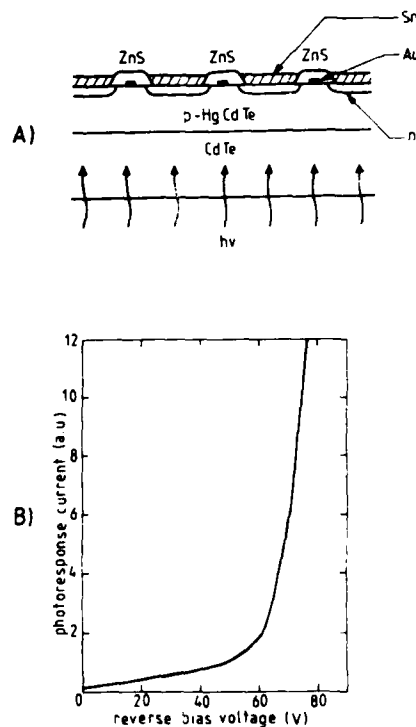
tation into the surface region of the layer. This measure produced a p-n junction at the depth of about 0.75 μm below the surface. Then, a standard photolithographic technique was used for delineating the active areas of the individual elements of the mosaic. Ohmic contacts were deposited onto the top of the active areas, indium for the n region and gold for the p region. Gold wires were attached to the detectors and the mounting header with the aid of a thermocompression bonding technique. The header was a framelike fixture that facilitated illumination from the substrate side.

Quantum efficiency of the individual diodes without any antireflection coating was found to be about 40%. The current of these diodes was dominated by surface-related leakage at temperatures below 77 K. The $1/f$ noise knee occurred at 10 Hz for zero-biased diodes which is substantially less than the corresponding value for the photoconductors of $Hg_{0.8}Cd_{0.2}Te$. The spectral spread of the diodes was only 0.3 μm over the entire area of the wafer, giving evidence of the high uniformity of $Hg_{0.79}Cd_{0.21}Te$ layers.

2. Planar avalanche photodiode

The second example concerns planar $Hg_{1-x}Cd_xTe$ avalanche photodiodes.[131,132] These diodes are of particular

interest when preparing fiber optical communication systems. Although III-V alloys are used frequently for optical detectors[133] in the wavelength range from 1.0 to 1.7 μm, $Hg_{1-x}Cd_xTe$ alloys with $x = 0.80–0.65$ have the potential for application in this wavelength region. In essence, the $Hg_{1-x}Cd_xTe$-CdTe heterostructures have several fundamental physical properties which are very suitable for near-infrared source and detector applications. There are little[134-136] lattice mismatch problems with these structures over the whole 1.0–1.7 μm range. Also, $Hg_{1-x}Cd_xTe$ has high absorption coefficients for high quantum efficiency and low intrinsic carrier concentrations for low detector noise.

A backside-illuminated avalanche photodiode of $Hg_{1-x}Cd_xTe$-CdTe is shown in Fig. 15(a).[131] It is grown by a vertical dipping LPE Method.[15] The $Hg_{1-x}Cd_xTe$ epilayers, approximately 10 μm thick, were grown on an undoped CdTe (111)A substrate from Te-rich solutions. The n-p junction was formed by boron-ion implantation. Lithographic techniques were used during the diode processing, with electron-beam-evaporated ZnS layers as passivation coatings. Ohmic contacts into the n region were made by evaporated tin. Ohmic contacts into the p region were made by depositing a gold grid for reducing the spreading resistance along the thin p layer. The current-voltage characteristics of one of the highest gain diodes are shown in Fig. 15(b). Avalanche gains as high as 15 were observed with 1.06-μm Nd-yttrium aluminum garnet laser illumination. Quantum efficiencies were 50% and 72% at 1.06 and 122 μm, respectively. The doping profile near the p-n junction was abrupt, with a background acceptor concentration of 2×10^{15} cm^{-3}.

The two heterostructure photodiodes described above illustrate the application of passive $Hg_{1-x}Cd_xTe$-CdTe heterojunctions in the infrared detecting technique. This application is based on the wide-gap optical window effect and, in fact, needs no knowledge about the physics of the heterojunction for descripton of the electrical and photodetecting parameters of the diodes. The situation is quite different in the case of indium-diffused $Hg_{1-x}Cd_xTe$-CdTe photodiodes[35,36] and the $Hg_{1-x}Cd_xTe$-$Hg_{1-y}Cd_yTe$ photodiodes,[32,33] where the energy band profiles at the interface are of great importance in defining the technical parameters.

B. Photodiodes with active $Hg_{1-x}Cd_xTe$ heterointerfaces

As mentioned earlier, the present day $Hg_{1-x}Cd_xTe$ heterostructures are characterized by graded gap heterointerfaces resulting from interdiffusion of the Hg and Cd atoms.

Under certain conditions, the potential barriers characteristic of abrupt heterojunctions can also be formed for the graded gap heterostructures. These barriers are related to anisotype (p-n or n-p) heterojunctions generating free carrier depletion layers. The shape of the potential barrier of such a heterointerface depends on the location and the width of the p-n junction as well as on the widths of the depletion layer and the graded transition region.[13]

Two kinds of $Hg_{1-x}Cd_xTe$ heterostructure photodiodes with characteristics depending on the potential barriers at the heterointerfaces have been investigated so far.

In the indium-diffused photodiode,[35] where electron diffusion in the p-type $Hg_{1-x}Cd_xTe$ substrate is the dominant conduction mechanism, carriers recombination at the $Hg_{1-x}Cd_xTe$-CdTe interface and carriers transport through this interface are of less importance. However, in the $Hg_{1-x}Cd_xTe$-$Hg_{1-y}Cd_yTe$ photodiode,[32] transport of photogenerated carriers through the heterointerface is dominating the photodiode characteristics. We will discuss both these photodiodes next.

1. $Hg_{1-x}Cd_xTe$-CdTe indium-diffused photodiode

The $Hg_{1-x}Cd_xTe$-CdTe heterostructures of indium-diffused photodiodes (Fig. 16) have been prepared with the aid of MBE by depositing high-resistivity CdTe epilayers (200–500 nm) onto bulk p-type $Hg_{0.705}Cd_{0.295}Te$ substrate platelets. The p-n junctions were produced by diffusion of In into the platelets through the insulating CdTe epilayers from indium dots which were evaporated on the top of these layers. CdTe prevents Hg loss from the substrates during diffusion. It also provides a good electrical passivation of the surface of the diode. These photodiodes operate in the range from 0.9 to 5.2 μm with the peak current responsivity of 3 A/W.[35] The interfaces are depleted of both majority and minority carriers so that surface leakage currents are minimized while the minority carrier lifetimes in the substrate
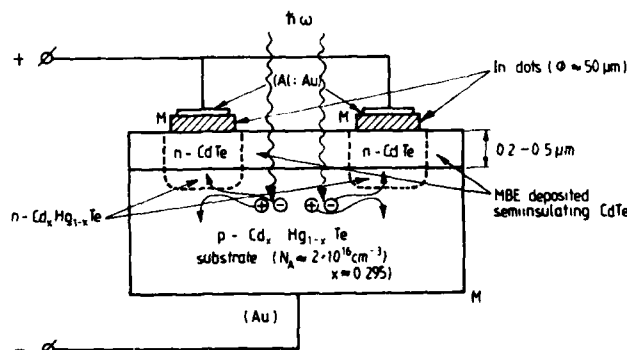

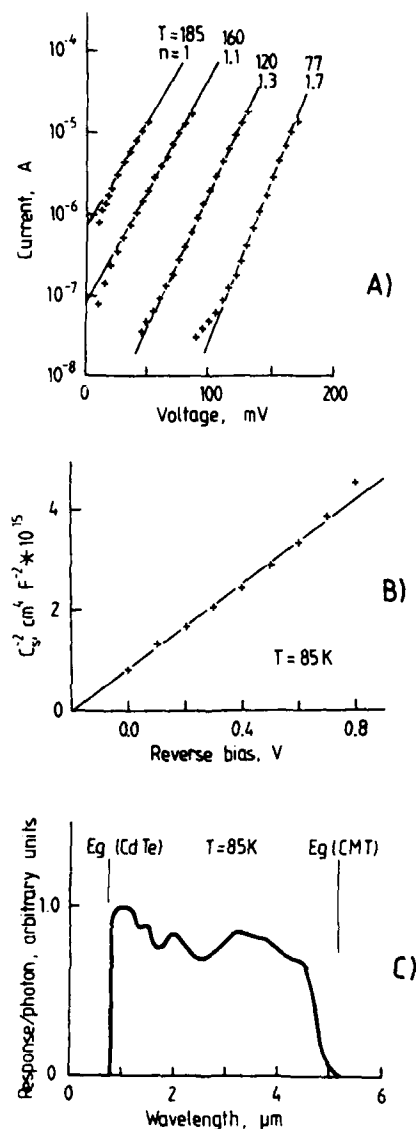FIG. 16. Cross section of the CdTe-$Hg_{1-x}Cd_xTe$ indium-diffused photodiode.[35]

A)

B)

C)

FIG. 17 Experimental characteristics for the CdTe-Hg₁₋ₓCdₓTe indium-diffused photodiode [11] (a) Forward I-V characteristics at 77, 120, 160, and 185 K. The ideality parameter n is also indicated at each temperature. Nominal junction area is equal to 2×10^{-3} cm² (b) C-V characteristic for a junction area of 1×10^{-3} cm² (c) 85 K spectral response

remain unaffected. These properties are obtained by properly choosing the p-$Hg_{1-x}Cd_xTe$-n-CdTe heterojunction band-edge profiles.

Each indium dot was contacted through a sputtered 50-μm-wide Al/Au strip starting from the dot center and end-

ing in a large area pad to which a wire could be easily bonded. The Al and Au were deposited in sequence to avoid oxidation of the Al surface. In this structure, the CdTe film provided the isolation between the Al contact and the substrate (the resistivity was higher than $10^9 \Omega$ and insensitive to heat treatment up to 430 K). The diodes were produced by diffusion using the In dots as sources. The diffusion was performed in 95% N_2/54% H_2 atmosphere at temperatures between 353 and 433 K for 15 min–24 h. The best results were obtained with the samples having 500-nm-thick CdTe films and having a 15-h heat treatment at 373 K. Finally, ohmic contacts with the aid of electroplated Au were made.

These heterojunction diodes were characterized by their dark I-V and C-V curves and by the spectral response curve. The I-V characteristics are described by

$$I = I_0 \exp(qV/nkT - 1) \qquad (III 1)$$

at all temperatures for currents above 10^{-7} A. A set of I-V curves are shown in Fig. 17(a). The "ideality parameter" n in Eq. (III.1) varies from 1.0 at 180 K to 1.7 at 77 K. This behavior of n indicates that the dominant conduction mechanism is diffusion at temperatures above 160 K, while generation-recombination in the depletion region plays an increasingly important role at lower temperatures. There is an evidence of the presence of a third conduction mechanism in these I-V characteristics at 120 and 77 K for currents lower than 10^{-7} A, where a deviation from the exponential behavior begins to take place. The excess current causing this deviation is nearly independent of temperature and may be attributed to a tunneling mechanism. This effect limits the 77 K zero-bias RA product of the described diode to a value of 100 Ω cm². Since no dependence of the 77 K RA product on the diode area A has been found, it is likely that the leakage mechanism is tunneling across the junction region, rather than at the diode perimeter.

The C-V characteristic of the indium-diffused diode exhibits a linear dependence of C^{-2} vs V, as shown in Fig. 17(b). From the intercept and the slope of the best-fit straight line, a built-in voltage of 0.2 V and an impurity concentration of 2×10^{15} cm^{-3} can be deduced. This built-in voltage is consistent with the one expected for a junction formed in the $Hg_{1-x}Cd_xTe$ substrate. It also indicates that the band-edge profile over the diffused p-n junction exhibits no potential barrier; i.e., the conduction-band spike is quenched (see Sec. III C for discussion of the band-edge profile at the junction)

The indium-diffused photodiodes operate as photovoltaic detectors. Photons with energy smaller than the CdTe band gap and incident outside the In dots are transmitted through the CdTe layer. They generate electron-hole pairs only in the $Hg_{1-x}Cd_xTe$ substrate. The photon generated minority electrons diffuse laterally toward the p-n junctions where they are collected (see Fig. 16). No current can flow through the $Hg_{1-x}Cd_xTe$-CdTe heterojunctions existing between the neighboring In-diffused regions because the band-edge profiles of these junctions are of a "funnel" type (CdTe without In donors is semi-insulating). The spectral response at 85 K of these diodes is displayed in Fig. 17(c). The short-wavelength cutoff is due to light absorption in CdTe, which does not produce any significant photocurrent due to the much shorter diffusion length. The long-wave-

length cutoff is caused by inadequate absorption in the $Hg_{1-x}Cd_x$ Te substrate. The response shows the modulation due to multiple interference in the CdTe layer.

It can be concluded[35] that the dominant conduction mechanism in the indium-diffused diodes described above is electron diffusion in the p-$Hg_{1-x}Cd_x$ Te substrate. However, the characteristics of these photodiodes are controlled as well by the properties of the substrate material as by the potential barriers formed in the diodes (i.e., by the junction fabrication process). The diffusion of extrinsic dopants through the $CdTe$-$Hg_{1-x}Cd_x$ Te heterojunction is a useful effect regarding the production of p-n homojunctions in $Hg_{1-x}Cd_x$ Te photodetectors.

2. $Hg_{1-x}Cd_x Te$-$Hg_{1-y}Cd_y Te$ heterojunction photodiode

The photodiode heterostructure was formed by LPE deposition of a 2-μm layer of n-type wide-gap $Hg_{0.67}Cd_{0.33}$ Te onto a bulk-grown p-type narrow-gap $Hg_{0.78}Cd_{0.22}$ Te substrate. With this heterostructure, mesa-type (compare Fig. 13) photodiodes were fabricated by standard photolithographic processes.[32] With the infrared radiation incident on the photodiode from the epilayer side, the shorter wavelengths will be absorbed in the wide-gap n-type layer whereas the longer wavelengths will be transmitted through to the underlying p-type region and thus be absorbed very near the p-n heterojunction. Minority carriers (electrons) generated at the junction may then be collected efficiently, provided that no potential barrier exists at the heterointerface.

The properties of these heterojunction photodiodes were investigated by measurements of I-V and C-V characteristics (77 K), relative spectral response (77 K), and SIMS.[32] These measurements revealed that the LPE-grown heterostructures (growth temperatures ranging from 620 to 720 K) were graded with a transition region width of the order of only 0.4–0.8 μm. The depletion layer at the p-n junction was found to have a width of about 0.3–0.4 μm. The location of the depletion layer within the graded transition region was found to have a strong effect on electrical and optical properties of the heterojunction photodiode. If the depletion layer is near the center or toward the wide-gap side of the transition region, a potential barrier is formed which inhibits the flow of electrons originating from the p-type

material across the heterojunction. This results in photodiodes with a high RA product but a poor minority carrier collection efficiency. When the depletion layer is located near the narrow-gap side of the heterojunction, the potential barrier goes away and normal photodiode characteristics are observed. A control of the location of the depletion layer was achieved by adequate doping the n-type layer with indium (the In concentration for a normal photodiode mode of operation was about 5–10 times the acceptor concentration in the p-type substrate).

In order to explain the observed experimental results, theoretical energy band diagram of the anisotype $Hg_{1-x}Cd_x$ Te-$Hg_{1-y}Cd_y$ Te heterojunctions were calculated.[32] To this end, the graded gap model of the $Hg_{1-x}Cd_x$ Te-CdTe heterojunction, developed by Migliorato and White[36] (see Sec. III C), has been used. Computer simulations related to these heterojunctions have also been performed.[33]

It is believed that the $Hg_{1-x}Cd_x$ Te-$Hg_{1-y}Cd_y$ Te heterojunction photodiodes should exhibit better exploitation characteristics than p-n homojunction or passive heterojunction photodiodes constructed with this material system. This is because (i) the backside (wide-gap material-side) illumination mode is combined here with the p-n junction photovoltaic effect, and (ii) the lattice mismatch, which is responsible for the presence of localized interface energy states (carrier recombination centers)[31,135] is not much larger than in homojunctions, and much less than in $Hg_{1-x}Cd_x$ Te-CdTe heterojunctions.

C. Heterojunction band-edge profile

The band-edge profile formed between two dissimilar lattice-matched semiconductors having different band gaps exhibits discontinuities in the valence-band maximum and conduction-band minimum at the heterojunction. The sum of these discontinuities, ΔE_v and ΔE_c, is equal to the energy difference between the two band gaps ΔE_g. For calculating the band-edge discontinuities, several approaches have been proposed,[137] ranging from simple phenomenological models to fully self-consistent microscopic computations. A model based on an "electron affinity rule" put forth by Anderson[31,138,139] is perhaps the most widely used method. The conduction band-edge and valence band-edge discontinui-
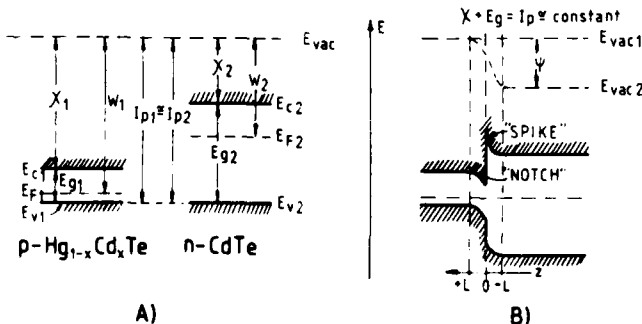
FIG. 18. Equilibrium energy bands before (a) and after (b) the formation of an abrupt p-n heterojunction for p-$Hg_{1-x}Cd_x$ Te-n-CdTe. The common anion rule, $I_{p_1} \simeq I_{p_2}$, has been used for both diagrams (a) and (b).

ties are determined by the difference in electron affinities, χ_1 and χ_2, between the two materials:

$$\Delta E_c = \chi_1 - \chi_2 \tag{III.2}$$

and

$$\Delta E_v = \Delta E_g - (\chi_1 - \chi_2) \tag{III.3}$$

CdTe and HgTe possess very similar ionization potentials ($I_p = 5.8-6.2$ eV for CdTe[140,141] and 5.9 eV for HgTe[141]). In essence, this is the "common anion rule" which states that I_p is dependent on the anion species alone.[142,143] ΔE_v between CdTe and $Hg_{1-x}Cd_x$Te is given by[144]

$$\Delta E_v = I_{p1} - I_{p2} \simeq 0 \tag{III.4}$$

for any x value (I_{p1} and I_{p2} are the ionization potentials for the ternary and binary compounds, respectively; see also Fig. 18). Faurie[126] has found a discontinuity of 40–50 meV in ΔE_v for the $Hg_{0.8}Cd_{0.2}$Te-CdTe heterojunction in qualitative agreement with Eq. (III.4). Therefore, the electron affinities of $Hg_{1-x}Cd_x$Te for each x are not needed. Because $\Delta E_c \simeq \Delta E_g$, according to Eqs. (III.2) and (III.3), the band-gap dependence on x given by Eq. (I.1) will suffice for an estimate of ΔE_c.

Numerical calculations of the equilibrium band-edge profiles for p-$Hg_{1-x}Cd_x$Te-n-CdTe have been perfomed by Migliorato and White,[36] who used Anderson's model and the common anion rule. Their calculation shows the presence of a large spike in the band-edge profile at the interface (see Fig 18). Such a spike prevents an efficient photovoltaic operation by acting as a potential barrier to the minority carrier flow. The barrier can be quenched by grading the junction and doping the CdTe layer in a proper way. With the spike quenched, the junction possesses a conduction band-edge profile suitable for photovoltaic operation.

For the graded p-$Hg_{1-x}Cd_x$Te heterojunction, the band-edge profile may be expressed in terms of position in the z direction (growth direction). This concept of position-dependent band structure with a simultaneous ignorance of the apparent variations of the carrier lifetime and mobility in the heterojunction has been proposed already in 1967[145,146] and is still used in the theory of heterojunction.[147] By choosing the vacuum level E_{vac} at $z = L$ to be a reference level with zero energy, and on the assumption that the electrostatic built-in potential Ψ is zero at $z = L$ (Fig. 18), one obtains

$$E_c(z) = -\Psi(z) - \chi(z) \tag{III.5}$$

and

$$E_v(z) = -\Psi(z) - \chi(z) - E_g(z) . \tag{III.6}$$

From the common anion rule we have

$$\chi + E_g = I_p \simeq const .$$

To calculate the actual band-edge profile, one has to solve the Poisson's equation

$$(1/q)\frac{d}{dz}\left(\epsilon \frac{d\Psi}{dz}\right) = N_A - N_D + n - p . \tag{III.7}$$

Here N_A and N_D are the acceptor and donor concentrations, and n and p the concentrations of free electrons and holes, respectively,

$$n = N_c \exp[-(E_c - E_F)/kT] \tag{III.8}$$

and

$$p = N_v \exp[(E_v - E_F)/kT] . \tag{III.9}$$

N_c and N_v are the effective mass conduction and valence band densities of states, and $E_F = -W(L)$ is the Fermi energy relative to E_{vac}. The boundary conditions can be written as

$$\Psi(-L) - \Psi(L) = W(L) - W(-L) = \Delta W$$

and

$$\left(\frac{d\Psi}{dz}\right)_{z=-L} = \left(\frac{d\Psi}{dz}\right)_{z=-L} = 0.$$

The composition and doping are assumed to vary as

$$x = x(L) + \tfrac{1}{2}[x(-L) - x(L)]\,\mathrm{erfc}(z/C)$$

and

$$N = N(L) + \tfrac{1}{2}[N(-L) - N(L)]\,\mathrm{erfc}(z/B) ,$$

where $N = N_D - N_A$; C and B denote characteristic lengths of the composition profile and the doping profile, respectively. The composition (doping) suffers a change from 80% to 20% of the total change in x (or N), as z goes from position $-C$ to $+C$ (or from $-B$ to $+B$).

For the graded heterojunction where an n-type CdTe layer is deposited onto a p-type $Hg_{1-x}Cd_x$Te substrate, the following parameters may be substituted into Eq. (III.7):

$$N_c = 4.831 \times 10^{15} T^{3/2} m_e^{*3/2} ,$$

$$N_v = 2.033 \times 10^{15} T^{3/2} ,$$

$$m_e^* = (1.093 - 0.296x + 4.42 \times 10^{-4} T) \times 7.063 \times 10^{-2} E_g ,$$

$$\epsilon = (20 - 9.4x)\epsilon_0 .$$

The results of the calculation are shown in Fig. 19. It can be seen that the valence band-edge profile exhibits no extrema. Maxima and minima occur only for the conduction band-edge profile for which E_c is a function of position z. At small values of C the band profile bears a close resemblance to the shape of an abrupt interface because an interfacial spike emerges with a depletion region on the n side (CdTe) and an inversion region on the p side. At large C, the band profile appears to be quite complicated. Namely, (i) the spike is quenched for $C = 0.14$ μm and $N_D = 5 \times 10^{16}$ cm^{-3} on the CdTe side, (ii) the inversion region disappears on the p-$Hg_{1-x}Cd_x$Te side while the interfacial maximum persists and, in fact, is still seen at $C = 0.21$ μm and $N_D = 5 \times 10^{16}$ cm^{-3} (in CdTe), and (iii) the "funnel"-shaped profile is found at the interface on the n side at $C = 0.21$ μm and $N_D = 5 \times 10^{15}$ cm^{-3}. Calculations show[36] that for a donor density $N_D > 10^{18}$ cm^{-1} in CdTe, the graded region length ($\simeq 2C$) of 40 nm would be large enough to yield the correct photodiode band-edge profile.

Similar small lengths are adequate also for generating the "funnel"-shaped surface passivation profiles. A comparison with the calculated 40-nm interdiffusion length with that observed in the grown $Hg_{1-x}Cd_x$Te-CdTe heterojunctions indicates that designing the junctions with desired band-edge profile is feasible.

N_D	N_A	B	C
(cm^{-3})	(cm^{-3})	(μm)	(μm)
$5\cdot10^{16}$	$1\cdot10^{16}$	0.03	0.03
$5\cdot10^{16}$	$1\cdot10^{16}$	0.03	0.07
$5\cdot10^{16}$	$1\cdot10^{16}$	0.03	0.14
$5\cdot10^{16}$	$1\cdot10^{16}$	0.03	0.21
$5\cdot10^{15}$	$1\cdot10^{16}$	0.03	0.07
$5\cdot10^{15}$	$1\cdot10^{16}$	0.03	0.21

ENERGY BAND PROFILES

p-Hg$_{1-x}$Cd$_x$Te   n-CdTe

E (eV)

2.4

$Eg_1 \cong 0.2$eV $E_B \cong 0.8$eV E_{C_2} E_F

$Eg_2 \cong 1.6$eV E_{V_2}

0

Z (μm)

0.4   0.2   0   -0.2   -0.4

$E_B \cong 0.3$eV

$E_B \cong 0$eV

$E_B \cong 0.1$eV

$E_B \cong 0.7$eV

"Funnel" shaped profile
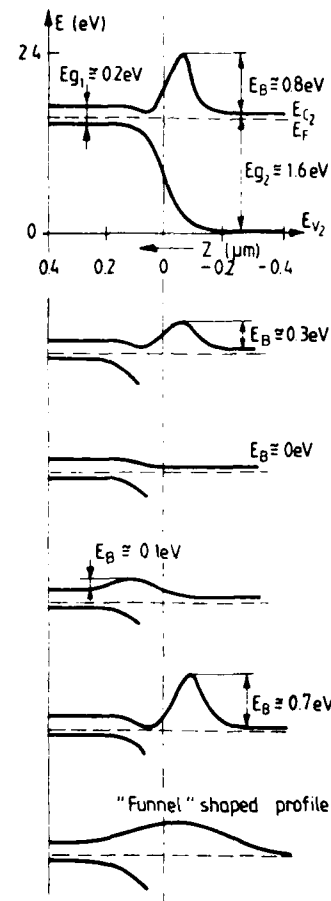
FIG. 19. Calculated band-edge profiles of p-Hg$_{1-x}$Cd$_x$Te-n-CdTe graded heterojunctions (with $x = 0.2$) for different doping levels and composition profiles.[36]

IV. RESEARCH PROBLEMS AND DEVELOPMENT PROSPECTS

A. Electronic structure versus "macroscopic" properties

1. Bulk features

The present day understanding of the Hg$_{1-x}$Cd$_x$Te-CdTe heterostructures and electronic and optoelectronic processes is far from complete. The strong dependence of many physical properties of these heterostructures as well as the Hg$_{1-x}$Cd$_x$Te epilayers on the growth conditions and growth techniques, and the peculiar vulnerability of the Hg$_{1-x}$Cd$_x$Te films to stress induced by a misfit in lattice parameters at the interface are the most intriguing problems.

A systematic study by electrolyte electroreflectance measurements[148] shows that many peculiarities of Hg$_{1-x}$Cd$_x$Te are related to instability of the HgTe lattice

upon alloying with Cd. The instability, in turn, may be associated with the electronic structure of Hg$_{1-x}$Cd$_x$Te. Angle-resolved photoemission measurements[149] which probe individual electronic bands throughout the entire valence-band region and k space in the reduced Brillouin zone have revealed that the photoelectron signals arising from low-lying mainly metal s-electron derived states in the energy range from -4 to -6 eV below the valence-band maximum correlate separately with Hg and Cd of Hg$_{1-x}$Cd$_x$Te (Fig. 20). In the atomic states, the valence s electrons of Hg (6s^2) are bound 1.4 eV more strongly than the valence 5s^2 electrons of Cd. The fact that these electrons give distinct contributions to photemission from Hg$_{1-x}$Cd$_x$Te indicates that the difference in atomic Hg and Cd potentials remains in the alloy. It appears possible[149] that this difference in the binding energy (the "s-shift") is responsible for many "macroscopic" effects observed in Hg$_{1-x}$Cd$_x$Te. Spicer et al.[149] have suggested
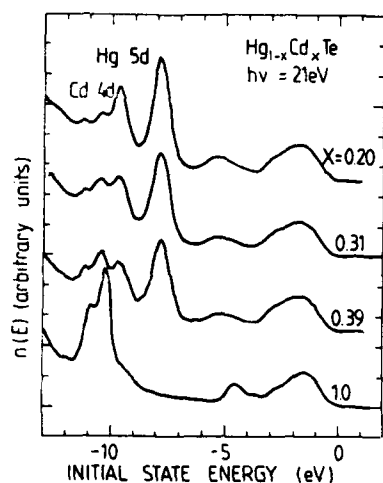
FIG. 20. Angle-resolved photoemission spectra ($hv = 21$ eV, $\Theta = 0°$) for $Hg_{1-x}Cd_xTe$ bulk crystals. Note the shift of the Cd 4d lines with the addition of Hg.
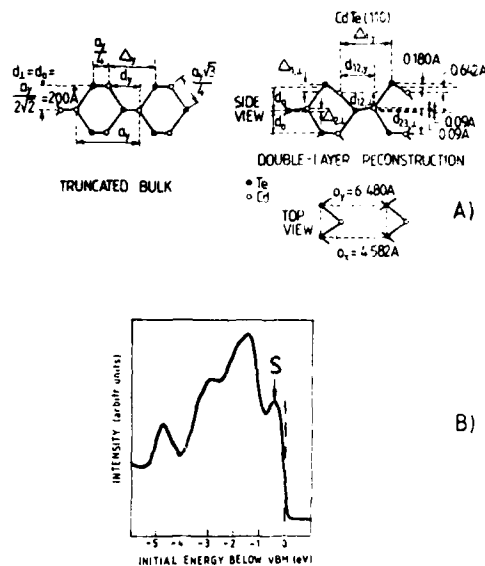

FIG. 21. (a) Atomic geometry of a CdTe crystal for the truncated bulk face (left side) and the relaxed surface in double-layer reconstruction (right side) according to Ref. 151. This rearrangement moves the filled and empty surface states out of the band gap, for example, in CdTe, ZnSe, and GaAs and probably also in $Hg_{1-x}Cd_xTe$. (b) Angle-resolved photoemission ($hv = 21$ eV, $\Theta = 0°$) from a high-quality CdTe (110) overlayer grown by the ALE method revealing the presence of an occupied surface state (surface resonance, labeled S) at the energy of 0.3 eV below the valence band maximum.[140]

that it is actually a necessary condition for any compound semiconductor system whose band gap drops from a large value to zero as the composition is changed. It is likely that the s shift causes high electron mobility in $Hg_{1-x}Cd_xTe$ and the difficulties experienced with growth and mechanical properties. It was also found that the Cd 4d-derived states tend to move to higher binding energy with addition of Hg. This direction of the shift suggests that Cd becomes more ionic, as the Hg content increases, and reflects a relative ease of involving the more loosely bound Cd electrons in bond formation. As the Cd content decreases, therefore, the Cd-Te bond strength increases. Conversely, the Hg-Te bond is likely to be weaker in $Hg_{1-x}Cd_xTe$ than in pure HgTe, where the heat of atomization is 30% smaller than that of CdTe. As a consequence, one expects an easier formation of metallic vacancies in HgTe than in CdTe, in qualitative agreement with experience.

The different bond strengths of Hg-Te and Cd-Te may be expected to cause clustering effects in the alloy. Infrared lattice vibration reflection spectra of $Hg_{1-x}Cd_xTe$ by Kozyrev et al.[150] can be accounted for by assuming an occurrence of the short-range clustering of the cations around Te. Kozyrev et al. observed that a good fit of the experimental and calculated reflectivity spectra could be obtained if they chose the clustering parameter β to be 0.6. Since β is zero for a random distribution and one for a complete clustering, the $Hg_{1-x}Cd_x$ sublattice cannot be deemed, on the basis of this work, an ideal substitutionally disordered alloy.

2. Surface features

Fundamental studies of electronic structure of the surface and interfaces of $Hg_{1-x}Cd_xTe$ are in their infancy However major developments made in the understanding of

the surfaces and interfaces of closely related III-V compound semiconductors, for which much information is available about the intrinsic surface states (surface resonances) as well as the mechanisms of formation of Schottky barriers and MOS/MIS interface states, provide an important starting point for the work on $Hg_{1-x}Cd_xTe$. The results obtained for the III-Vs may be applied to the II-VIs to a large extent because the surface of II-VIs and III-Vs of equal crystal structure exhibit many similar properties (provided that the band gaps are similar). For example, the nonpolar (110) surfaces of GaAs, ZnSe, and CdTe are relaxed in the same fashion.[151] The surface electronic structure is also known to be similar for these compounds.[152-154] A striking common feature in electronic structure of the (110) surface is that the intrinsic surface states associated with anion-derived dangling bonds are moved out of the band-gap region by the rearrangement of the surface atoms. It is interesting to note in this context that the predicted surface state (surface resonance) has been found recently in epitaxially grown CdTe (110) overlayers.[140] A summary of the atomic geometry of the CdTe (110) surface and a photoemission valence-band spectrum showing the surface resonance is presented in Fig. 21. We are tempted to believe that surface relaxation and surface resonances are also characteristics of $Hg_{1-x}Cd_xTe$ (110).

B. Surfaces and interfaces

The stability of the $Hg_{1-x}Cd_xTe$ alloy surface is of fundamental interest. We have already mentioned that the Hg-Te bond energy is 30% smaller than the Cd-Te bond energy in the bulk of the alloy. Although this is a bulk property, it is also critical to the understanding of surfaces and interfaces. There has been considerable concern as to the stability of the $Hg_{1-x}Cd_xTe$ surface against room-temperature evaporation of Hg. Nitz et al.[156] have reported changes in the surface composition with time at room and elevated temperatures for $Hg_{0.8}Cd_{0.2}Te$ samples prepared by scraping the surface in vacuum or by ion bombarding. They found a loss of 25% of Hg at the surface in 3 h at 290 K. This observation lends support to the proposals by Nimtz et al.[157] and Micklethwaite and Redden[158] that the changes observed in electrical parameters and conduction type in $Hg_{1-x}Cd_xTe$ samples stored open under room-temperature conditions for periods of 3–13 years are caused by out-diffusion and evaporation of Hg. Recent studies by Silberman et al.[159] indicate that perturbations to the surface such as oxidation and sputtering have a remarkable effect on surface composition. They found no evidence of a Hg loss in vacuum-cleaved samples for periods of 5–20 h. Although these experiments cannot be used to assert the stability of the samples for periods of years, due to the short period of observation, they clearly document that the quality of the surface is the key factor determining compositional stability.

The preferential sputtering of Hg from the surface under ion bombardment has been firmly established.[156,159,160–163] Even low doses of electrons are found to induce desorption of Hg.[156,162,163] Cadmium enrichment has been noted to accompany Hg loss for the sputtered and scraped surface.[156,161,162] Sputtering causes deviations from the stoichiometry also for the HgTe surface but leaves the CdTe surface unreconstructed of stoichiometric composition. Thus, the analysis and extraction of atomic concentration profiles of the $Hg_{1-x}Cd_xTe$ layers and interfaces by using conventional Auger electron spectroscopy (AES) in conjunction with ion bombardment are complicated by nonstoichiometric sputter erosion of the materials.

Sputtering yields for individual elements Cd, Te, and Hg have been discussed in Ref. 156. Effects of different etching techniques on surface composition have been studied using XPS[161,164–166] and electroreflectance spectroscopy.[167] The standard bromine-methanol chemical etching damages the surfaces to a depth of about 60 nm depleting them in Cd and leaving them covered with thin activated Te-rich layers which are quickly contaminated with oxygen and carbon when exposed to laboratory atmosphere.[167] The Hg-to-Te content near the surface depends on details of the etch procedure.[166]

The lattice defects in undoped and Cu- or In-doped $Hg_{1-x}Cd_xTe$ bulk crystals have been investigated by Vydyanath et al.[168–170] The interface transitional zone defects and misfit dislocations in LPE-grown $Hg_{1-x}Cd_xTe$-CdTe heterostructures have been studied by Magee and Woolhouse.[171]

Despite the fact that a collection of experimental data concerning the defects behavior in $Hg_{1-x}Cd_xTe$ crystals, or

in $Hg_{1-x}Cd_xTe$-CdTe already exists a number of unsolved problems still remain to be investigated. It is worth noting that the most important feature of the $Hg_{1-x}Cd_xTe$-CdTe heterostructure system is connected with the fact that the interface and bulk properties of the ternary compound cannot be treated as two separate entities. The strong effect of bulk imperfections and the rapid communication of defects between bulk and interface or surface must be properly taken into account in any investigation or technological process. This is principally the result of the weak Hg-Te bond in $Hg_{1-x}Cd_xTe$ and it can be seen as a great technological difficulty encountered when fabricating IR detecting devices.

Although $Hg_{1-x}Cd_xTe$-CdTe heterostructures have been used until now with success only in discrete IR detecting devices it is reasonable to expect that the advantages of these structures will be in the future applications for producing complicated integrated focal planes for IR imaging technique which are presently made out of $Hg_{1-x}Cd_xTe$ platelets cut from bulk crystals.[7,172]

C. HgTe-CdTe heterojunctions and superlattices

The heterojunctions consisting of HgTe (a semimetallic compound) epitaxially grown on CdTe may have a number of applications. They can afford higher Schottky barriers than those obtained by depositing an elemental metal onto CdTe.[173] They can also provide some insight into the mechanism of Schottky barrier formation. Since HgTe and CdTe are similar in their chemistry and physical structure the study of this heterojunction system provides a rather ideal Schottky barrier structure which is free of the structural and chemical complexities found in most metal-semiconductor contacts.[174]

Perhaps the most interesting and perspective applications are, however, related to HgTe-CdTe superlattices. Such superlattices potentially offer inherent advantages over $Hg_{1-x}Cd_xTe$-CdTe structures as IR detector materials. Namely, (i) the fractional uncertainty in layer thickness and composition of the alloy permissible in the superlattice is
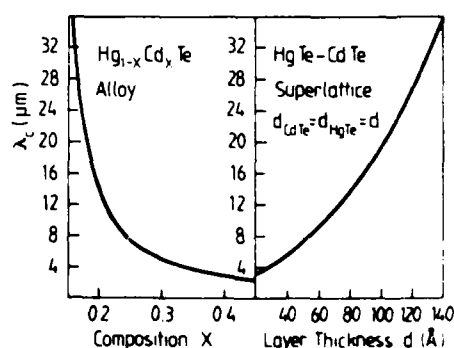

FIG. 22. Cutoff wavelength as a function of alloy composition (left panel) for the $Hg_{1-x}Cd_xTe$ alloy and cutoff wavelength as a function of layer thickness (right panel) for the HgTe-CdTe superlattice with equally thick HgTe and CdTe layers.[175]

greater than that in the ternary system for fixed band-gap tolerance requirements; (ii) the calculated tunneling currents in the superlattice are found to be much smaller than in the alloy of the same band gap, and (iii) p-side diffusion currents in the superlattice are expected to be smaller than in the alloy of the same band gap.[175] The calculated cutoff wavelengths for superlattices with equal HgTe and CdTe layer thicknesses are compared in Fig. 22 with those of the alloy.[175] It can be seen that a large part of the IR spectrum is sampled by the superlattice without going to extremely thin layer spacings, which is difficult to fabricate. For example, for the cutoff wavelength of $\lambda = 12$ μm, a layer thickness of 7.3 nm is sufficient. Although thicker layers could be grown at present the results of Refs. 27 and 125 are very encouraging and suggest that the difficulties associated with growing HgTe-CdTe can be solved.

Measurements of electronic properties of HgTe-CdTe superlattices using a far-infrared magnetoabsorption technique[176] at low temperature (1.6 K) have shown that these superlattices with geometrical and compositional parameters described in Ref. 120 are quasi zero-energy gap semiconductors, displaying electronic properties which are found neither in bulk HgTe and CdTe crystals nor in $Hg_{1-x}Cd_xTe$ ternary alloys. For example, at low magnetic fields the electron effective mass in the plane of the layers is strongly nonparabolic and much lighter than in bulk HgTe.

V. CONCLUDING REMARKS

$Hg_{1-x}Cd_xTe$ is a semiconducting alloy with a band gap that can be selected in the range from 0 to 1.5 eV at room temperature by varying the mole fraction of CdTe. The variable band-gap aspect and high electron mobilities make this material nearly ideal for infrared device applications. The need for large-area $Hg_{1-x}Cd_xTe$ material of good crystalline quality for detectors and advanced focal plane arrays has prompted research in thin-film structures of $Hg_{1-x}Cd_xTe$. The advantages of the backside-illuminated operation mode of the infrared photovoltaic detectors and the encouraging theoretical forecasts concerning superlattices as structures for infrared detectors have given rise to growing interest toward heterostructures of this material system.

We have presented the state of the art of the physical and technological knowledge of semiconductor $Hg_{1-x}Cd_xTe\text{-}Hg_{1-y}Cd_yTe$ $(0 < x, y < 1)$ heterostructures. For these structures, CdTe or $Hg_{1-x}Cd_xTe$ wafers cut from bulk grown crystals are normally used as substrates. The most promising crystallization method for growing these crystals seems to be at present the travelling heater method. For preparation of high-quality substrate surfaces, acceptable for epitaxy, the "hydroplane polishing" method, which leads to the lowest surface dislocation density, may be used. However, only a buffer layer epitaxially grown on the "hydroplane polished" surface is able to produce the final quality of the substrate required for epitaxy of $Hg_{1-x}Cd_xTe$.

As evidenced in this review, three growth techniques, namely, LPE, VPE, and MBE have proven acceptable for producing device-quality $Hg_{1-x}Cd_xTe\text{-}Hg_{1-y}Cd_yTe$ heterostructures. Cathodic sputtering and laser-assisted depo-

sition and annealing have also indicated encouraging results in epitaxy of these layered systems.

The understanding of electrical and photoelectrical properties of the constituent heterointerfaces of these structures is still poor, while the technology involved and the structural parameters of the interfaces are known much better. As discussed above, some good results related to the photodetectors with active $Hg_{1-x}Cd_xTe$ heterointerfaces as well as to HgTe-CdTe superlattices predict that the electrical and photoelectrical properties of the $Hg_{1-x}Cd_xTe\text{-}Hg_{1-y}Cd_yTe$ $(0 < x, y < 1)$ heterostructures will be largely applied in the near future to infrared detecting, imaging and processing techniques. To this end, however, the following fundamental research problems relevant to these heterointerfaces should be solved:

(i) how to control the peculiar vulnerability of $Hg_{1-x}Cd_xTe$ films to stress induced by a misfit in the lattice parameters at the heterointerface;

(ii) how to enhance the physical and chemical stability of the $Hg_{1-x}Cd_xTe$ alloy surface;

(iii) how the physical space-quantized effects in superlattices could be applied to device structures; and

(iv) how to optimize the device preparation processes (metallization, passivation, bonding, etc.) in order to save the heterostructures used in a device from changing their physical parameters.

ACKNOWLEDGMENTS

[1]R. K. Willardson and A. C. Beer (editors), in *Semiconductors and Semimetals—Mercury Cadmium Telluride*, Vol. 18 (Academic, New York, 1981).
[2]R. Dornhaus and G. Nimtz, in *Narrow Gap Semiconductors*, Vol. 98 in *Springer Tracts in Modern Physics* (Springer, Berlin, 1983), p. 119.
[3]G. L. Hansen, J. L. Schmit, and T. N. Casselman, J. Appl. Phys. 53, 7099 (1982).
[4]J. Chu, S. Xu, and D. Tang, Appl. Phys. Lett. 43, 1064 (1983).
[5]Y. Guldner, C. Rigaux, A. Mycielski, and Y. Couder, Phys. Status Solidi B 81, 615 (1977); 82, 149 (1977).
[6]G. L. Hansen and J. L. Schmit, J. Appl. Phys. 54, 1639 (1983)
[7]D. E. Charlton, J. Cryst. Growth 59, 98 (1982).
[8]D. L. Smith, J. Appl. Phys. 53, 7051 (1982).
[9]A. Kolodny and I. Kidron, IEEE Trans. Electron. Devices ED-27, 37 (1980).
[10]T. C. Harman, in *Physics and Chemistry of II-VI Compounds*, edited by M. Aven and J. S. Prener (Wiley, New York, 1967), p. 784.
[11]B. E. Bartlet, P. Capper, J. E. Harris, and M. J. T. Quelch, J. Crystal Growth 46, 623 (1979).
[12]R. Triboulet, T. Nguyen Duy, and A. Durand, The 1984 U. S. Workshop on the Physics and Chemistry of HgCdTe, San Diego, California, 1984, Extended Abstracts, p. 43.
[13]D. Elwell and H. J. Scheel, *Crystal Growth from High-Temperature Solutions* (Academic, New York, 1975), p. 307.
[14]J. E. Bowers, J. L. Schmit, C. J. Speerschneider, and R. B. Maciolek, IEEE Trans. Electron Devices ED-27, 24 (1980).

[15]C. C. Wang, S. H. Shin, M. Chu, M. Lanir, and A. H. B. Vanderwyck, J. Electrochem. Soc. **127**, 175 (1980)

[16]J. A. Mroczkowski and H. R. Vydyanath, J. Electrochem. Soc. **128**, 655 (1981)

[17]R. A. Wood and R. J. Hager, J. Vac. Sci. Technol. A **1**, 1608 (1983).

[18]D. D. Edwall, E. R. Gertner, and W. E. Tennant, J. Appl. Phys. **55**, 1453 (1984).

[19]H. Wiedemeier and A. E. Uzpurvis, J. Electrochem. Soc. **130**, 252 (1983).

[20]J. B. Mullin and S. J. C. Irvine, J. Vac. Sci. Technol. **21**, 178 (1982).

[21]J. B. Mullin and S. J. C. Irvine, J. Phys. D **14**, L149 (1981).

[22]J. B. Mullin, S. J. C. Irvine, A. Royle, J. Tunnicliffe, G. Blackmore, and R. Holland, J. Vac. Sci. Technol. A **1**, 1612 (1983).

[23]S. H. Shin and J. G. Pasko, Appl. Phys. Lett. **44**, 423 (1984).

[24]S. K. Ghandi and I. Bhat, Appl. Phys. Lett. **44**, 779 (1984).

[25]J. P. Faurie, A. Million, and G. Jacquier, Thin Solid Films **90**, 107 (1982).

[26]J. P. Faurie and A. Million, Appl. Phys. **41**, 264 (1982).

[27]J. P. Faurie, A. Million, R. Boch, and J. L. Tissot, J. Vac. Sci. Technol. A **1**, 1593 (1983).

[28]P. P. Chow, D. K. Greenlaw, and D. Johnson, J. Vac. Sci. Technol. A **1**, 562 (1983).

[29]J. P. Faurie, The 1984 U. S. Workshop on the Physics and Chemistry of HgCdTe, San Diego, California, 1984, Extended Abstracts, p. 1.

[30]R. F. C Farrow, The 1984 U. S. Workshop on the Physics and Chemistry of HgCdTe, San Diego, California, 1984, Extended Abstracts, p. 5.

[31]B. L. Sharma and R. K. Purohit, *Semiconductor Heterojunctions* (Pergamon, New York, 1974).

[32]P. R. Bratt, J. Vac. Sci. Technol. A **1**, 1687 (1983).

[33]P. R. Bratt and T. N. Casselman, The 1984 U. S. Workshop on the Physics and Chemistry of HgCdTe, San Diego, California, 1984, Extended Abstracts, p. 209.

[34]C. C. Wang, M. Chu, S. H. Shin, W. E. Tennant, J. T. Cheung, M. Lanir, A. H. B. Vanderwyck, G. M. Williams, L. O. Bubulac, and R. J. Eisel, IEEE Trans. Electron Devices ED-27, 154 (1980).

[35]P. Migliorato, R. F. C. Farrow, A. B. Dean, and G. M. Williams, Infrared Phys. **22**, 331 (1982).

[36]P. Migliorato and A. M. White, Solid State Electron. **26**, 65 (1983).

[37]D. L. Smith, T. C. McGill, and J. N. Schulman, Appl. Phys. Lett. **43**, 180 (1983).

[38]R. Roussille, R. Boch, M. Dupuy, and G. Rolland, in *Physics of Narrow Gap Semiconductors*, edited by E. Gornik, H. Heinrich, and L. Palmetshofen (Springer, Berlin, 1982), p. 86, 39; R. Roussille, J. Cryst. Growth **56**, 101 (1982).

[39]R. Roussille, S. Guillot, and G. Lefeuvre, J. Cryst. Growth **59**, 130 (1982); R. Roussille, D. Amingual, R. Boch, G. L. Destifanis, and J. L. Tissot, Appl. Phys. Lett. **44**, 679 (1984).

[40]J. T. Cheung and D. T. Cheung, J. Vac. Sci. Technol. **21**, 182 (1982).

[41]J. T. Cheung, Appl. Phys. Lett. **43**, 255 (1983).

[42]J. T. Cheung and T. Magee, J. Vac. Sci. Technol. A **1**, 1604 (1983).

[43]K. Zanio, in *Semiconductors and Semimetals, Vol. 13: Cadmium Telluride* (Academic, New York, 1978).

[44]J. G. Werthen, A. L. Fahrenbruch, R. H. Bube, and J. C. Zesch, J. Appl. Phys. **54**, 2750 (1983).

[45]J. A. Mroczkowski, J. Electrochem. Soc. **128**, 2688 (1981).

[46]J. V. Gormley, M. J. Manfra, and A. R. Calawa, Rev. Sci. Instrum. **52**, 1256 (1981).

[47]T. H. Myers, J. F. Schetzina, S. T. Edwards, and A. F. Schreiner, J. Appl. Phys. **54**, 4232 (1983).

[48]R. F. C. Farrow, A. J. Noreika, F. A. Shirland, W. J. Takei, and M. H. Francombe, Proceedings of the Ninth International Vacuum Congress and Fifth International Conference on Solid Surfaces, Madrid, 1983 [J. Vac. Sci. Technol. A **2**, 527 (1984)].

[49]T. H. Myers, J. F. Schetzina, T. J. Magee, and R. D. Ormond, J. Vac. Sci. Technol. A **1**, 1598 (1983).

[50]R. N. Bicknell, T. H. Myers, and J. F. Schetzina, J. Vac. Sci. Technol. A **2**, 423 (1984).

[51]For ALE, see T. Suntola, U. S. Patent No 4058430(1977), and M. Pessa, in *Optoelectronic Materials and Devices*, edited by M. A. Herman (Polish Sci. Publ., Warsaw, 1983), p. 217, for ALE CdTe single crystal films, see M. Pessa, P. Huttunen, and M. A. Herman, J. Appl. Phys. **54**, 6047 (1983); M. Pessa, O. Jylha, P. Huttunen, and M. A. Herman, J. Vac. Sci. Technol. A **2**, 418 (1984); M. Pessa, O. Jylha, and M. A. Herman, J. Cryst. Growth **67**, 255 (1984).

[52]G. B. Stringfellow, Rept. Prog. Phys. **45**, 469 (1982).

[53]R. A. Swalin, *Thermodynamics of Solids*, 2nd ed. (Wiley, New York, 1972).

[54]A. M. Alper, *Phase Diagrams: Materials Science and Technology* (Academic, New York, 1970).

[55]A. Reisman, *Phase Equilibria* (Academic, New York, 1970).

[56]T. Tung, C. H. Su, P. K. Liao, and R. F. Brebrick, J. Vac. Sci. Technol. **21**, 117 (1982).

[57]J. P. Schwartz, T. Tung, and R. F. Brebrick, J. Electrochem. Soc. **128**, 438 (1981).

[58]T. Tung, L. Golonka, and R. F. Brebrick, J. Electrochem. Soc. **128**, 451 (1981).

[59]A. S. Jordan, Metall. Trans. **1**, 239 (1970).

[60]A. S. Jordan, in *Calculation of Phase Diagrams and Thermochemistry of Alloy Phases*, edited by Y. A. Chang and J. F. Smith (The Metallurgical Society of AIME, Warrendale, 1979), p. 100.

[61]E. A. Guggenheim, *Mixtures* (Oxford University, Oxford, 1952).

[62]S. Szapiro, J. Electron. Mater. **5**, 223 (1976).

[63]R. F. Brebrick, T. Tung, C. H. Su, and P. K. Liao, J. Electrochem. Soc. **128**, 1595 (1981).

[64]T. Tung, L. Golonka, and R. F. Brebrick, J. Electrochem. Soc. **128**, 1601 (1981).

[65]J. D. Kelley, B. G. Martin, F. R. Szofran, and S. L. Lechoczky, J. Electrochem. Soc. **129**, 2360 (1982).

[66]J. Steininger, A. J. Strauss, and R. F. Brebrick, J. Electrochem. Soc. **117**, 1305 (1970).

[67]M. R. Lorenz, J. Phys. Chem. Solids **23**, 939 (1962).

[68]B. M. Kulwicki, Ph.D. dissertation, University of Michigan, 1963.

[69]R. F. Brebrick, J. Electrochem. Soc. **118**, 2014 (1971).

[70]D. DeNobel, Phillips Res. Rept. **14**, 361 (1959).

[71]R. F. Brebrick and A. J. Strauss, J. Phys. Chem. Solids **26**, 989 (1965).

[72]T. C. Harman, J. Electron. Mater. **9**, 945 (1980).

[73]A. Lehoczky and F. Szofran, J. Electron. Mater. **10**, 1131 (1981).

[74]J. Blair and R. Newnham, *Metallurgy of Elemental and Compound Semiconductors* (Interscience, New York, 1961), p. 393.

[75]J. Steininger, J. Electron. Mater. **5**, 299 (1976).

[76]R. Kikuchi, J. Vac. Sci. Technol. **21**, 129 (1982).

[77]R. Kikuchi, Physica **103 B**, 41 (1981).

[78]C. A. Castro and R. Korenstein, SPIE **317** (Integrated Optics and Millimeter and Microwave Integrated Circuits) 262 (1981).

[79]M. Brown and A. F. W. Willoughby, J. Cryst. Growth **59**, 27 (1982).

[80]C. H. Su, P. K. Liao, and R. F. Brebrick, J. Electron. Mater. **12**, 771 (1983).

[81]T. C. Harman, J. Electron. Mater. **8**, 191 (1979).

[82]M. Lanir, C. C. Wang, and A. H. B. Vanderwyck, Appl. Phys. Lett. **34**, 50 (1979).

[83]J. L. Schmit and J. E. Bowers, Appl. Phys. Lett. **35**, 457 (1979).

[84]H. Nelson, RCA Rev. **24**, 603 (1963).

[85]H. Rupprecht, in *Gallium Arsenide*, Inst. Phys. Conf. Ser. No. 3, edited by J. Frankel (Institute of Physics, Bristol, 1967), p. 57.

[86]M. B. Panish, I. Hayashi, and S. Sumski, IEEE J. Quantum Electron. QE-5, 210 (1969).

[87]T. C. Harman, J. Electron. Mater. **9**, 945 (1980).

[88]T. C. Harman, J. Electron. Mater. **10**, 1069 (1981).

[89]D. W. Shaw, J. Cryst. Growth **62**, 247 (1983).

[90]V. I. Ivanov-Omskii, V. K. Ogorodnikov, and V. D. Rozumnyi, Phys. Status Solidi A **76**, 71 (1983).

[91]H. Ruda, P. Becla, J. Lagowski, and H. C. Gatos, J. Electrochem. Soc. **130**, 228 (1983).

[92]H. Ruda, L. Jedral, J. Lagowski, and H. Gatos, J. Electrochem. Soc. **131**, 1159 (1984).

[93]L. Jedral, H. Ruda, P. Becla, J. Lagowski, and H. C. Gatos, J. Electrochem. Soc. **130**, 1614 (1983).

[94]T. Bryskiewicz, in *Semiconductor Optoelectronics*, edited by M. A. Herman (Wiley, New York, 1980), p. 187.

[95]T. Bryskiewicz, J. Lagowski, and H. C. Gatos, J. Appl. Phys. **51**, 988 (1980)

[96]D. W. Shaw, in *Epitaxial Growth*, edited by J. W. Mathews (Academic, New York, 1975), p. 89.

[97]H. Wiedemeier and D. Chandra, Z. Anorg. Allg. Chem. **488**, 137 (1982).

[98]J. B. Mullin, S. J. Irvine, and D. J. Ashen, J. Cryst. Growth **55**, 92 (1981).

[99]W. E. Hoke and R. Traczewski, J. Appl. Phys. **54**, 5087 (1983).

[100]J. L. Schmit, The 1984 U. S. Workshop on the Physics and Chemistry of HgCdTe, San Diego, California, 1984, Extended Abstracts, p. 25.

[101]T. F. Kuech and J. O. McCaldin, J. Electrochem. Soc. **128**, 1142 (1981).

[102]P. Vohl and C. M. Wolfe, J. Electron. Mater. **7**, 659 (1978).

[103]P. Becla, J. Lagowski, H. C. Gatos, and H. Ruda, J. Electrochem. Soc. **128**, 1171 (1981).

[105]P. Becla, J. Lagowski, and H. C. Gatos, J. Electrochem. Soc. 129, 1103 (1982).

[106]G. Cohen-Solal, Y. Marfaing, and F. Bailly, Rev. Phys. Appl. 1, 11 (1966).

[97]D. N. Tufte and E. L. Stelzer, J. Appl. Phys. 40, 4559 (1969).

[98]E. Bailly, L. Svob, G. Cohen-Solal, and R. Triboulet, J. Appl. Phys. 46, 4244 (1975).

[107]L. Svob, Y. Marfaing, R. Triboulet, F. Bailly, and G. Cohen-Solal, J. Appl. Phys. 46, 4251 (1975).

[110]P. Becla, J. Lagowski, H. C. Gatos, and L. Jedral, J. Electrochem. Soc. 129, 2855 (1982).

[111]K. Ploog, in *Crystals—Growth, Properties and Applications*, edited by H. C. Freyhardt (Springer, Berlin, 1980), Vol. 3, p. 73.

[112]A. Y. Cho, Thin Solid Films 100, 291 (1983).

[113]Y. Ota, Thin Solid Films 106, 3 (1983).

[114]M. A. Herman, Vacuum 32, 555 (1982).

[115]M. Knudsen, Ann. Phys. 4, 28, 75, 999 (1909).

[116]L. Smith and V. Y. Pickhardt, J. Appl. Phys. 46, 2366 (1975).

[117]K. Ueda, J. Cryst. Growth 31, 333 (1975).

[118]J. P. Faurie and A. Million, J. Cryst. Growth 54, 577 (1981).

[119]J. P. Faurie and A. Million, J. Cryst. Growth 54, 582 (1981).

[120]J. P. Faurie, A. Million, and J. Piaguet, Appl. Phys. Lett. 41, 713 (1982).

[121]J. P. Faurie, A. Million, and J. Piaguet, J. Cryst. Growth 59, 10 (1982).

[122]C. J. Summers, E. L. Meeks, and N. W. Cox, J. Vac. Sci. Technol. B 2, 224 (1984).

[123]M. Pessa and O. Jylhä, Appl. Phys. Lett. 45, 646 (1984).

[124]M. A. Herman, O. Jylhä, and M. Pessa, J. Cryst. Growth 66, 480 (1984).

[125]P. P. Chow and D. Johnson, The 1984 U.S. Workshop on the Physics and Chemistry of HgCdTe, San Diego, California, 1984, Extended Abstracts, p. 9

[126]P. Faurie (private communication).

[127]D. Long, in *Optical and Infrared Detectors*, edited by R. J. Keyes, in Topics in Applied Physics, Vol. 19 (Springer, Berlin, 1977), p. 101.

[128]J. T. Longo, D. T. Cheung, A. M. Andrews, C. C. Wang, and J. M. Tracy, IEEE Trans. Electron. Devices ED-25, 213 (1978).

[129]G. Bahir and R. Kalish, J. Appl. Phys. 54, 3129 (1983).

[130]P. Capper, J. Cryst. Growth 57, 280 (1982).

[131]S. H. Shin, J. G. Pasko, H. D. Law, and D. T. Cheung, Appl. Phys. Lett. 40, 965 (1982).

[132]M. Chu, S. H. Shin, H. D. Law, and D. T. Cheung, Appl. Phys. Lett. 37, 318 (1980).

[133]H. D. Law, K. Nakano, and L. R. Tomasetta, IEEE J. Quantum Electron. QE-15, 549 (1979).

[134]Y. Nemirovsky, S. Margalit, E. Finkman, Y. Shacham-Damand, and I. Kidron J. Electron. Mater. 11, 133 (1982).

[135]R. B. Schoolar, J. Vac. Sci. Technol. A 2, 77 (1984).

[136]T. W. James and R. E. Stoller, Appl. Phys. Lett. 44, 56 (1984).

[137]J. Pollmann and A. Mazur, Thin Solid Films 104, 257 (1983).

[138]R. L. Anderson, Solid State Electron. 5, 341 (1962).

[139]A. G. Milnes and D. L. Feucht, *Heterojunctions and Metal Semiconductor Junctions* (Academic, New York, 1972).

[140]M. Pessa, P. Huttunen, and M. A. Herman, J. Appl. Phys. 54, 6047 (1983).

[141]N. J. Shevchik, J. Tejeda, M. Cardona, and D. W. Langer, Phys. Status Solidi B 59, 87 (1973).

[142]O. McCaldin, T. C. McGill, and G. A. Mead, Phys. Rev. Lett. 36, 56 (1976).

[143]F. Casula and A. Kisiel, Nuovo Cimento B 39, 470 (1977).

[144]A. Harrison, J. Vac. Sci. Technol. 14, 1016 (1977).

[145]L. J. van Ruyven and F. E. Williams, Am. J. Phys. 35, 705 (1967).

[146]L. J. van Ruyven, Annu. Rev. Mater. Sci. 2, 501 (1972).

[147]A. Chatterjee and A. H. Marshak, Solid State Electron. 26, 59 (1983).

[148]P. M. Raccah, The 1983 U.S. Workshop on the Physics and Chemistry of HgCdTe, Dallas, Texas, 1983, Extended Abstracts, p. 1; P. M. Raccah and U. Lee, J. Vac. Sci. Technol. A 1, 1587 (1983).

[149]W. E. Spicer, J. A. Silberman, P. Morgen, I. Lindau, J. A. Wilson, A. B. Chen, and A. Sher, Phys. Rev. Lett. 49, 948 (1982); J. A. Silberman, P. Morgen, I. Lindau, W. E. Spicer, and J. A. Wilson, J. Vac. Sci. Technol. 21, 142 (1982); W. E. Spicer, J. A. Silberman, P. Morgen, I. Lindau, and J. A. Wilson, J. Vac. Sci. Technol. 21, 149 (1982).

[150]S. P. Kozyrev, L. K. Vodopyanov, and R. Triboulet, Solid State Commun. 45, 383 (1983).

[151]C. B. Duke, A. Paton, and W. K. Ford, Phys. Rev. B 24, 3310 (1981); J. Vac. Sci. Technol. 20, 773 (1982).

[152]C. Calandra, F. Manghi, and C. M. Bertoni, J. Phys. C 10, 1911 (1977).

[153]T. Takahashi and A. Ebina, Appl. Surf. Sci. 11/12, 268 (1982); A. Ebina, T. Unno, Y. Suda, H. Koinuma, and T. Takahashi, J. Vac. Sci. Technol. 19, 301 (1981).

[154]J. Jaroszynski, T. Dietl, M. Sawicki, and E. Janik, Proceedings of the 16th International Conference on Semiconductors, Montpelier, 1983

[155]J. Jaroszynski, T. Dietl, M. Sawicki, and E. Janik, Physica B 117, (1983).

[156]H. M. Nitz, O. Ganschow, U. Kaiser, L. Wiedeman, and A. Benninghoven, Surf. Sci. 104, 365 (1982).

[157]G. Nimtz, B. Schlicht, and R. Dornhaus, Appl. Phys. Lett. 34, 490 (1979).

[158]W. F. H. Wicklethwaite and R. F. Redden, Appl. Phys. Lett. 36, (1980).

[159]J. A. Silberman, P. Morgen, I. Lindau, and W. E. Spicer, J. Vac. Sci. Technol. 21, 154 (1982).

[160]P. Morgen, J. Silberman, I. Lindau, W. E. Spicer, and J. A. Wilson, J. Cryst. Growth 11, 161 (1982).

[161]U. Solzbach and H. J. Richter, Surf. Sci. 97, 191 (1980).

[162]T. S. Sun, S. P. Buchner, and N. E. Byer, J. Vac. Sci. Technol. 17, 1067 (1980).

[163]G. D. Davis, T. S. Sun, S. P. Buchner, and N. E. Byer, J. Vac. Sci. Technol. 19, 472 (1981).

[164]B. K. Janousek and R. C. Carscallen, J. Vac. Sci. Technol. 21, 442 (1982).

[165]S. P. Kowalczyk and J. T. Cheung, J. Vac. Sci. Technol. 18, 944 (1981).

[166]D. R. Rhiger and R. E. Kvaas, J. Vac. Sci. Technol. 21, 168 (1982).

[167]A. Lastras-Martinez, U. Lee, J. Zehnder, and P. M. Raccah, J. Vac. Sci. Technol. 21, 157 (1982).

[168]H. R. Vydyanath, J. Electrochem. Soc. 128, 2609 (1981).

[169]H. R. Vydyanath, J. Electrochem. Soc. 128, 2619 (1981).

[170]H. R. Vydyanath, J. C. Donovan, and D. A. Nelson, J. Electrochem. Soc. 128, 2625 (1981).

[171]T. J. Magee and G. R. Woolhouse, The 1983 U.S. Workshop on the Physics and Chemistry of HgCdTe, Dallas, Texas, 1983, Extended Abstracts, p. 71.

[172]R. A. Chapman, S. R. Borrello, A. Simmons, J. D. Beck, A. J. Lewis, M. A. Kinch, J. Hynecek, and G. G. Roberts, IEEE Trans. Electron Devices ED-27, 134 (1980).

[173]T. F. Kuech and J. O. McCaldin, J. Appl. Phys. 53, 3121 (1982).

[174]L. J. Brillson, J. Phys. Chem. Solids 44, 703 (1983).

[175]D. L. Smith, T. C. McGill, and J. N. Schulman, Appl. Phys. Lett. 43, 18 (1983).

[176]Y. Guldner, G. Bastard, J. P. Vieren, M. Voos, J. P. Faurie, and A. Million, Phys. Rev. Lett. 51, 907 (1983).

END

DATE
FILMED

1-87

DTIC